Preformulation and Metabolic Studies
On
Novel Aminoalkylpyridine Anticonvulsants

Tse Kai Kong, B.Sc. (Hons)
(謝 繼 江)

Department of Pharmacy
Faculty of Medicine
The Chinese University of Hong Kong

August 1998

ABSTRACT

40 million people worldwide suffer from epilepsy. Despite the availability of a large number of anticonvulsants, up to 30 % of patients are still refractory to treatment. Identification of the pharmacophore of triazoline has led to the development of the hydrophobic and lipid soluble novel aminoalkylpyridine (AAP) anticonvulsants, of which the *N*-[4-(chlorophenyl)]-1-[4-(pyridyl)]ethylamine (*p*-Cl AAP) has been shown to possess the highest anti-epileptic activity. However the mechanism of its action, and its pharmacokinetic and metabolic fate have not been fully understood. The aims of the present study are to study preformulation parameters of this novel of aminoalkylpyridine anticonvulsant and to investigate its metabolic and pharmacokinetic fate in laboratory animal.

The physicochemical properties (preformulation parameters) of five structurally related aminoalkylpyridines, naimly *p*-F, *p*-Cl, *p*-Br, *p*-CH_3, *m*-CF_3 AAPs, have been studied, including partition coefficient, aqueous solubility, and thermal behaviour. The *p*-F, *p*-Cl, *p*-Br and *p*-CH_3 AAPs exhibited partition coefficients which were statistically indistinguishable within experimental errors. The relatively low partition coefficient of *m*-CF_3 AAP (37.23 ± 1.2) may be attributed to the increased ionization of the *m*-CF_3 substituted aniline leading to a larger fraction of the compound being partitioned in the aqueous phase. The solubilities of AAPs depended on the substituent on the benzene ring and decreased in the order: *p*-F > *p*-CH_3 > *p*-Cl > *p*-Br > *m*-CF_3. The enthalpy of solution (ΔH^s) of three halogen-substituted AAPs showed no statistically significant difference while the *p*-CH_3 AAP had the lowest ΔH^s (20.24 ± 1.1 kJ/mol) and *m*-CF_3 AAP had the highest ΔH^s (34.76 ± 1.8 kJ/mol). The enthalpy of fusion, ΔH^f of the AAPs are similar in magnitude to ΔH^s (being lower by 1-6 kJ/mol), suggesting that the aqueous solubilities of the AAPs are governed predominantly by solute-solute interaction in the solid state. Thermogravimetric

analysis and differential scanning calorimeteric studies on AAPs demonstrated that these compounds do not contain any solvent of crystallization and are relatively thermostable.

A sensitive and specific high performance liquid chromatographic (HPLC) assay for *p*-Cl AAP and its putative metabolites in rat urine has been developed and fully validated. HPLC analysis of *p*-Cl AAP in rat blood has also been developed.

Preliminary pharmacokinetic studies were performed in conscious rats after intravenous administration of *p*-Cl AAP. The elimination half-life was reasonable (5.0 hour) and the clearance was extensive (1779.4 ml/hr). The volume of distribution was high (12.71 L/kg) indicating extensive extravascular distribution. The area under curve (AUC) was 11.84 $\mu g/ml\ hr^{-1}$.

Six novel metabolites were detected following intraperitoneal administration of *p*-Cl AAP to conscious rats. LC/MS analysis revealed that these metabolites have the following possible chemical structures: *N*-[4-(2-hydroxychlorophenyl)]-1-[4-(2,6-dihydroxypyridyl)]ethylamine, *N*-[4-(chlorophenyl)]-1-hydroxy-1-[4-(pyridyl)]ethylamine, 2-[4-(chlorophenyl)]amino-2-[4-(2,6-dihydroxypyridyl)]ethanoic acid, *N*-[4-(chlorophenyl)]-1-[4-(pyridyl *N*-oxide)]ethylamine, *N*-[4-(chlorophenyl)]-1-[4-(2-hydroxypyridyl)]ethylamine and 2-[4-(chlorophenyl)]amino-2-[4-(pyridyl)]ethanal. Although the proposed biologically active metabolite, β-amino alcohol of *p*-Cl AAP, has not been identified in the present study, its further biotransformed metabolites, such as amino aldehyde and amino acid have been found. The results suggested that the proposed metabolic pathway may have an important learning on its anti-epileptic effect.

Trace amounts of the *p*-Cl AAP were found in the 0-24h urine of control and phenobarbitone-pretreated rats (0.28 ± 0.07% and 0.18 ± 0.002%). This suggests that most of the *p*-Cl AAP was either metabolized or retained inside the body. It was found that pretreatment with phenobarbitone significantly increases urinary excretion

of all identified metabolites except for 2-[4-(chlorophenyl)]amino-2-[4-(2,6-dihydroxypyridyl)]ethanoic acid and 2-[4-(chlorophenyl)]amino-2-[4-(pyridyl)]ethanal. This suggests that phenobarbitone induced the enzyme system responsible for the metabolism of *p*-Cl AAP in rats.

摘要

全世界超過四億人患有癲癇症。雖然坊間有很多抗癲癇藥，但三成以上患者的病程仍難以控制。確認出三唑啉的藥效團，從而發展出疏水和脂溶的新抗癲癇藥——氨基烷基吡啶。其中以*N*-[4-(氯苯基)]-1-[4-(吡啶基)]乙胺顯示出最高的抗癲癇效用。但是它的作用機制、藥物動力學和代謝的資料仍未充份明白。這類新的抗癲癇藥的準方劑設計特點、在實驗老鼠中的藥物動力學和代謝情況將爲本研究的範圍。

五種結構相關的氨基烷基吡啶的物理化學特質(準方劑設計特點)研究，包括它們的分配系數、水溶性和對熱度的表現。在實驗誤差中，對氟、對氯、對溴和對甲基氨基烷基吡啶的分配系數，在統計層面上沒有差異。而間三氟甲基氨基烷基吡啶的系數卻相對地爲最小(37.23±1.2)，可能因爲在苯胺中的間三氟甲基取代基的電離作用較其他的取代基爲高，因而引致較多的化合物分配於水溶態中。氨基烷基吡啶的水溶度，亦受著苯環的取代基影響，其次序爲：對氟 > 對甲基 > 對氯 > 對溴 > 間三氟甲基。三種鹵素取代的氨基烷基吡啶的溶解作用熱函轉變在統計上沒有分別，對甲基氨基烷基吡啶的最小，每一摩爾爲20.24±1.1千焦耳；而間三氟甲基則爲最高，每一摩爾爲34.76±1.8千焦耳。它們熔融和溶解作用的熱函，在熱量上亦差距不大(只有每一摩爾一至六千焦耳)。由此推論出它們的水溶度，主要是受著固體狀態中溶質與溶質的相互作用影響。氨基烷基吡啶的熱重量分析和微分掃描量熱的學習則顯示

出它們比較耐熱，而且並沒有與溶劑產生結晶作用。

本研究發展了一個敏感和獨特，專爲分析和確認老鼠尿液中的對氯氨基烷基吡啶和其推定代謝物之高效液項分析法，並且全面將它確認爲有效。

爲初步探研對氯氨基烷基吡啶的藥物動力學，它將以靜脈注射方式注射到清醒的老鼠上。此藥的半衰期頗長(五小時)，而清除率則很大(每小時一千六百九十九點一一毫升)。它的分佈體積很大(十二點二六公升)，反影出有很廣泛的體內外分佈，而藥時曲線下面積則爲每小時每毫升十一點七七微克。

腹腔注射對氯氨基烷基吡啶到清醒的老鼠，因而探測到六種新的代謝物。透過液體色層分析/質譜分析，它們的化學結構推論爲：*N*-[4-(2-羥氯苯基)]-1-[4-(2,6-雙羥吡啶基)] 乙胺、*N*-[4-(氯苯基)]-1-羥-1-[4-(吡啶基)] 乙胺、2-[4(氯苯基)] 氨基-2-[4-(2,6-雙羥吡啶基)] 乙酸、*N*-[4-(2-氯苯基)]-1-[4-(吡啶基-*N*-氧化物)] 乙胺、*N*-[4-(氯苯基)]-1-[4-(2-羥吡啶基)] 乙胺和2-[4-(氯苯基)] 氨基-2-[4-(吡啶基)] 乙醛。雖然並沒有直接發現構思中的β-氨基醇，但它的繼後轉變代謝物，例如氨基醛和氨基酸卻被發現，這結果顯示出的代謝路線卻和這藥的抗癲癇作用有關。

不論曾接受與非接受苯巴比妥注射的老鼠，在二十四小時內的尿液中，只探測到小量的對氯氨基烷基吡啶(佔注射分量的 0.28±0.07 和 0.18±0.002 %)。可能因爲大部份的對氯氨基烷基已經代謝了，又或遺留在身體裏。

在接受了苯巴比妥的老鼠尿液中，除了2-[4(氯苯基)]氨基-2-[4-(2,6-雙羥吡啶基)]乙酸和2-[4-(氯苯基)]氨基-2-[4-(吡啶基)]乙醛，其他的代謝物均有顯著增加。可能因爲苯巴比妥可能誘發負責對氯氨基烷基吡啶的代謝之酶系統功能。

ACKNOWLEDGEMENTS

I would like to take this opportunity to thank my supervisors, Prof. Albert H.L. Chow and Prof. Ge Lin for their guidance and expert advice during this research project. I would also want to thank Prof. L.A. Damani for his help and advice, and Prof. P.K. Kadaba for the gift of aminoalkylpyridines and triazolines.

I would like to thank Ms. Cheng, the Chinese Medicinal Material Research Centre for performance of HPLC/MS analysis.

I am grateful to the Research Grant Council (RGC) of Hong Kong for the award of a grant to undertake this work.

Finally thanks are also due to my parents and sisters for their support and encouragement.

CONTENTS

LIST OF FIGURES

LISTS OF TABLES

ABBREVIATIONS

AUC	Area Under Curve
AAP	Aminoalkylpyridine
AZI	Aziridine
β-AA	β-amino alcohol
C_{max}	Maximum concentration
CL	Clearance
C.V.	Coefficient of variation
DSC	Differential Scanning Calorimetry
ΔH^f	Enthalpy change of fusion
ΔH^s	Enthalpy change of solution
ΔS^f	Entropy change of fusion
i.v.	Intravenous
i.p.	Intraperitoneal
K°_w	Partition Coefficient
TIC	Total ion current
Vd	Volume of Distribution

Chapter One

Introduction

1 INTRODUCTION

1.1 Definition and Prevalence of Epilepsy

The word "epilepsy" is derived from a Greek word meaning "to take hold of". Epilepsy is not a disease but a chronic disorder of intermittent and recurrent disorganized electrical activity in the brain, which causes a fit or seizure. Seizures are characterized most commonly by impairment of motor activity (a convulsion) or consciousness. The type of seizure depends upon the part of the brain where the abnormal electrical discharge arises. Many varieties of epileptic seizures occur, and frequency and form of attacks vary greatly from person to person. Since the definitions of epilepsy and the types of seizures are numerous, a specific classification system is being promoted by the International League Against Epilepsy. The International Classification of Epilepsy Seizures has been adopted by the medical community and is gradually replacing outdated seizures terminology including "grand mal" and "petit mal". The new classification scheme describes seizures as being of two major types, viz: "partial" and "generalized", defined respectively as excessive electrical discharge being limited to one area of the brain and that involving the whole brain. It further divides each of these categories into simple partial, complex-partial, absence, tonic-clonic, and other types.

With regard to the prevalence of epilepsy, there are no geographical, racial or social class boundaries. Anyone can be affected by seizures. Epilepsy can occur in both sexes of any age, especially infancy, childhood, adolescence and old age. According to the data from the World Health Organization (Fact sheets N165, June 1997), up to 5% of the world's population may have a single seizure at some time in

their lives. The prevalence of a disorder is the proportion of a population with that disorder at a given point in time. The mean prevalence of active epilepsy (i.e. continuing seizures or the need for treatment) from many studies around the world is approximately 7 per 1000 of the general population. Thus, 40 million people in the world have epilepsy at any one time. This may be an underestimate as some studies in developing countries (Colombia, Ecuador, Liberia, Nigeria, Panama, Tanzania and Venezuela) suggest a prevalence of more than 10 per 1000. The lifetime prevalence of epilepsy, i.e. the number of people presently in the world who have epilepsy now or have had it in the past (e.g. childhood) or will get it in the future (e.g. old age), rises to approximately 100 million people. 85% of the people affected by epilepsy live in developing countries where the great majority has little or no access to treatment. Recent studies in both developed and developing countries have shown that up to 70% of newly diagnosed children and adults with epilepsy can be successfully treated (complete control of seizures for several years) with anti-epileptic drugs. After two to five years of successful treatment, drugs can be withdrawn in about 70% of children and 60% of adults without relapses. However, up to 30% of patients may not respond to drug therapy.

1.2 Neurophysiology and Pathophysiology of Epilepsy

The normal neuronal resting membrane potential results from the maintenance of an intracellular electrolyte concentration that is high in K^+ and low in Na^+ relative to the extracellular fluid concentration. With excitatory postsynaptic depolarization sufficient to generate an action potential, Na^+ moves intracellularly and K^+ flows out. During repolarization, Na^+ extrusion is coupled with K^+ uptake and the utilization of

ATP to reestablish the membrane potential. Inhibitory postsynaptic potentials hyperpolarize the neuron and an action potential is not generated. Depolarization of the presynaptic ending is associated with release of neurochemical transmitters that are specific for the neuron involved. Acetylcholine, γ-amino butyric acid (GABA), norepinephrine, dopamine, 5-hydroxytryptamine, glycine, and glutamic acid may be neurotransmitters in the brain or spinal cord. Any events that alter the synthesis, release, sensitivity to, or inactivation of neurotransmitters affect the excitation or inhibition mediated by the compound. Such inhibitors normally act by promoting chloride uptake into the neuron using the chloride ionophore membrane pump; this increases membrane potential and so stabilizes it.

Epileptic seizures indicate a functional impairment of neuronal activity. Within nervous tissue, information is sent via action potentials, which are transmitted across synapses from neuron to neuron. There is normally directionality of the impulses and specific patterns of transmission determined by anatomic and functional connections. The electrochemical activity of the brain produces potential differences that can be measured by electroencephalography (EEG). In a patient with epilepsy, the EEG is abnormal, the characteristic wave forms being altered by the appearance of spikes of electrical activity. The type of EEG activity seen in epilepsy is known as the spike wave. The spike activity is considered to be the summated, synchronized electrical activity of a group of disordered neurons at an epileptogenic focus, which is known as a paroxysmal depolarization shift (PDS). When cells at the seizure focus fire, they normally excite inhibitory interneurons, which release GABA. This inhibitory neurotransmitter causes the focus to turn off and also inhibits the surrounding cells. When seizure activity does occur, some mechanisms seem to

override the surrounding inhibition and decrease the degree of hyperpolarization that usually occurs after the PDS.

Excitatory amino acids may also play an important role in epilepsy. Hayashi reported that sodium glutamate and aspartate, when applied topically onto the cerebral cortex of dogs and primates, induced clonic convulsions (Hayashi, 1952). Endogenous excitatory amino acids include glutamate, aspartate, L-homocysteate, L-homocysteine sulphinate and quinolinic acid. All these compounds elicit epileptic seizures after either systemic injection or focal injection directly into the brain (Johnston, 1973; Stone and Javid, 1983). Thus there exists two opposite but complementary strategies for tackling the epilepsy. The first and widely used method is to enhance the function of inhibitory compounds (Meldrum, 1984). The alternate method is by impairing the excitatory amino acids using excitatory amino acid antagonists.

1.3 Drugs Currently Used in the Treatment of Epilepsy

Phenobarbital was first reported to be a clinically effective anticonvulsant in the early 19th century (Hauptman, 1912). To this day it remains one of the major anticonvulsant drugs. It has the widest spectrum of activity in different seizure patterns, and many anticonvulsant drugs are structural derivatives of this barbiturate, for example, mephobarbital, eterobarb and deoxybarbiturate (primidone).

Primidone, a 2-deoxybarbiturate, is a polar compound that is well absorbed and distributed. It was reported to be clinically effective as an anticonvulsant (Handley and Stewart, 1952) and possessed anticonvulsant activity against various experimental models of epilepsy (Baumel *et al.*, 1973). It appeared to exert its action

by reducing sustained high-frequency repetitive firing of action potentials through delaying the recovery of sodium channels from activation.

Phenytoin, which can also be considered as a structural analogue of phenobarbital, has also been shown to be effective against seizures (Merritt and Putnam, 1938). It can produce a selective blockade of high-frequency repetitive neuronal firing by binding to sodium channels. It also blocks the voltage-dependent calcium channels. Phenytoin has been reported to depress excitatory transmission by both pre- and post-synaptic mechanisms. Since it does not have the sedative properties of barbiturates, it was considered to be less toxic than phenobarbital. However, this is certainly not the case, and the wide range of toxic effects of phenytoin has been reemphasized (Glaser, 1972). The toxic effects may be related to its dose-dependent kinetics (Gerber *et al.*, 1971), individual variations in metabolism (Andreasen *et al.*, 1973), drug interactions (Hansen *et al.*, 1966; Brennan *et al.*, 1970; Christiansen and Dam, 1973) and chronic side-effects (Buchthal and Svensmark, 1960).

Valproate was subsequently demonstrated to have a broad spectrum of anticonvulsant activity in a wide variety of animal seizure models (Chapman *et at.*, 1982; Loscher, 1988). Its mode of action is similar to those of phenytoin and primidone mentioned above. However, valproate is only weakly protective against seizures induced by excitatory amino acids (Chapman *et al.*, 1982; Ferrendelli *et al.*, 1989). In addition, the drug causes motor toxicity in animals at doses that are close to those required to protect against seizures. For the maximal electroshock test, the protective index is only 1.6 compared to a value of 6.9 for phenytoin (Swinyard *et al.*, 1989).

Several acetylurea compounds have been used as anticonvulsants, as have other structurally related derivatives. The prototype drug, phenylacetylurea, has significant efficacy for preventing generalized tonic and/or clonic seizures, absence seizures, and many partial seizures. Unfortunately, it is also one of the most toxic anticonvulsant drugs.

Carbamazepine is another major anticonvulsant with significant efficacy for preventing partial seizures and for generalized tonic and/or clonic seizures (Julien and Hollister, 1975). Carbamazepine is an iminostilbene derivative and as such represents a new chemical class of anticonvulsants. However, the conformation of the compound is quite similar to that of the barbiturates and hydantoins. It has a similar spectrum of anticonvulsant activity to phenytoin in animal seizure models. Its mode of action is similar to phenytoin in that it inhibits voltage-dependent sodium channels. Interaction with adenosine receptors (Lewin and Bleck, 1977) may also be involved but not for the phenytoin. Toxicity with carbamazepine is relatively minor. The most serious effect is its ability to suppress bone marrow function and possibly to produce an aplastic anemia which may be fatal. Sulfonamides (developed in 1959), benzodiazepines (developed in 1970) and dipropylacetic acid (developed in 1973) are also commonly used anticonvulsants.

Recently, a number of new anticonvulsants have become available. Five promising ones include vigabatrin (Lippert *et al.*, 1977), gabapentin (Bartoszyk *et al.*, 1986), felbamate (Swinyard *et al.*, 1986), lamotrigine (Miller *et al.*, 1986) and oxcarbazepine (Jensen *et al.*, 1991). Lamotrigine and vigabatrin, being more frequently prescribed, are discussed below.

Lamotrigine is effective as an adjunct agent in the treatment of complex and simple partial seizures with or without secondary generalization. It has a favourable pharmacokinetic profile, including a long half-life, low serum protein binding, and lack of mixed-function oxidase enzyme induction (Gilman, 1995). Adverse effects are primarily related to the central nervous system, the most common ones being dizziness, diplopia, ataxia, and somnolence. However, the occurrence of rash can limit its use.

The GABA analog vigabatrin is a specific, enzyme-activated inhibitor of the GABA catabolic enzyme, GABA-T. Vigabatrin becomes covalently linked to GABA-T at its active site and thereby causes an irreversible inhibition of the enzyme (Lippert *et al.*, 1977). Since transamination by GABA-T represents the only important pathway for catabolism of brain GABA, the irreversible inhibition of GABA-T by vigabatrin results in a prolonged elevation in brain GABA levels (Jung et al., 1977). The anticonvulsant effect of vigabatrin is related to its inhibitory effect of the GABA-T. However, in mice, rats, dogs, and perhaps monkeys, vigabatrin produces a dose-related microvacuolization of the outer lamellar sheaths of myelinated axons, an effect referred to as "intramyelinic edema" (Butler *et al.*, 1987; Butler, 1989; Graham, 1989).

In general, there are three ways for tackling epilepsy through drug therapy. The present anticonvulsants may target non-synaptic, pre-synaptic or post-synaptic action on neurotransmission.

The non-synaptic action involves reduction of sustained repetitive firing of action potentials due to opening of voltage-dependent sodium channels (McLean and MacDonald, 1981; McLean and MacDonald, 1982; MacDonald and McLean, 1982).

It is thought that some drugs, for example, phenytoin, carbamazepine and felbamate, slow the recovery of these channels thus producing a frequency-dependent block on sodium ion transport and a subsequent decrease in transport of the impulse along the axon.

As an example for the pre-synaptic action of anticonvulsants, lamotrigine acts at voltage-dependent sodium channels resulting in decreased presynaptic release of glutamate (Leach *et al.*, 1986). An inhibitory pre-synaptic role has been postulated for valproate. Certainly valproate produces an increase in total brain GABA concentration (Godin *et al.*, 1969) which is only partly explained by a decrease in post-synaptic metabolism and it is proposed that it may exert its effect by activation of GABA synthesis pre-synaptically (Loscher, 1981).

The post-synaptic inhibition of neurotransmission can act either through the enhancement of the inhibitory mechanisms of GABA or other amino acid inhibitors, or through the direct reduction of excitatory mechanisms. Vigabatrin was developed as an enzyme-activated, irreversible inhibitor of GABA transaminase, the primary degradative enzyme of GABA; by decreasing the catabolism of GABA, it increases the inhibitory action of GABA. Phenobarbitone is the only anticonvulsant that has been shown to enhance GABA action and shows a reduction in excitatory mechanism, namely, an antagonism of glutamate responses.

1.4 Triazolines and Aminoalkylpyridines as a New Class of Potential Antiepileptic Drugs

Recently, the 1,2,3-triazolines have assumed considerable importance as a new class of potential anticonvulsant drugs (Kadaba, 1984a). This new class of

anticonvulsants was first discovered by Wolff in 1912 during the studies on the action of organic azides on quinones (Wolff, 1912).

Triazolines are normally prepared by the 1,3-cycloaddition of diazomethane to Schiff Bases in dioxane solution, in the presence of water (Kadaba, 1988; Kadaba *et al.*, 1984b). The unique ring system of triazolines is a five-membered ring which contains three nitrogen, two carbon atoms and a double bond (Figure 1.1).

The unique ring system of triazolines is different from those of the conventional anticonvulsant drugs in that most of them possess a dicarboximide (ureylene) -CO-NH-CO- and/or ureide (-NH-CO-NH-) (Kadaba *et al.*, 1996) functional group as in barbiturates, hydantoins, succinimides, and oxazolidinediones or the structurally related primidones. The absence of the dicarboximide group, which contributes to the inherent hypnotic and sedative activity of the barbiturates and related compounds, is expected to reduce the toxic effects of triazolines.

Triazolines were evaluated for anticonvulsant activity (Kadaba, 1984a) using the maximal electroshock seizure (MES) test and the subcutaneous pentylenetetrazol (Metrazol) seizure threshold (scMet) test (Porter *et al.*, 1984). In addition, CNS toxicity was determined (Kadaba, 1984a) using rotorod ataxia test (Dunham and Miya, 1957). The dose that elicits an anticonvulsant response in 50% of the animals (ED_{50}), the median minimal neurotoxic dose (TD_{50}), the dose that causes death in 50% of the animals in 24 hours (LD_{50}) and the dose at which 50% of the animals lost their righting reflex (i.e., the median hypnotic dose, HD_{50}) were determined. The representative triazoline, [1-(4-chlorophenyl)-5-(4-pyridyl)-Δ^2-1,2,3-triazoline], coded ADD17014 (Figure 1.1), has successfully advanced through all phases of preclinical

testing, including 14- and 30-day dose-range finding studies, in the NINDS-sponsored Antiepileptic Drug Development (ADD) Program (Porter *et al.*, 1984).

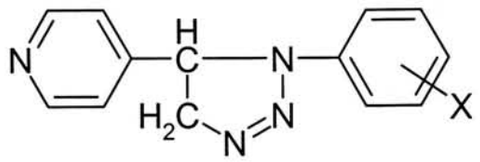

Figure 1.1 Structure of triazoline. The *p*-Cl substituted triazoline is registered as ADD17014.

The ratio of effective dose to toxic dose is an important consideration in the search for new drugs, and the ED_{50}/TD_{50} values, defined as the protective index (PI), for ADD17014 by the MES and s.c.Met. tests are 0.23 and 0.40 respectively. The oral ED_{50}/i.p ED_{50} ratio is taken as a measure of the oral activity and a value of less than 4 is regarded as adequate. The oral ED_{50}/i.p ED_{50} values for ADD17014 as determined by the rotorod, MES and s.c.Met. tests are 0.62, 1.13 and 3.50 respectively, indicating adequate absorption of the drug in mice after oral administration.

Investigations on the metabolism (Figure 1.2) and pharmacology of ADD17014, suggest that this novel anticonvulsant functions as a "prodrug" and exerts its anticonvulsant activity by impairing excitatory amino acid (EAA) L-glutamate neurotransmission via a unique "dual-action" mechanism (Kadaba *et al.*, 1996). While an active β-amino alcohol metabolite from the parent prodrug acts as an *N*-methyl-D-aspartate (NMDA)/MK-801 receptor blocker or the glutamate antagonist, the parent ADD17014 impairs the presynaptic release of L-glutamate. *In vivo* and *in vitro*

pharmacological studies of ADD17014 and its metabolites indicated that the β-amino alcohol (Figure 1.2) was the active species which inhibited the specific binding of [^{3}H]MK-801 to the MK-801 site (by 56% at 10 μM), suggesting ADD17014 acts as a prodrug. In addition, ADD17014 significantly decreased Ca^{2+}-dependent, K^+-evoked L-Glutamate release (by 83% at 100 μM) and the Cl^- channel activity (by 50-63%), a useful membrane action that reduces the excessive L-Glutamate release during epileptic seizures. ADD17014 and its metabolite, β-amino alcohol, together effectively impair both pre- and post-synaptic EAA neurotransmission.

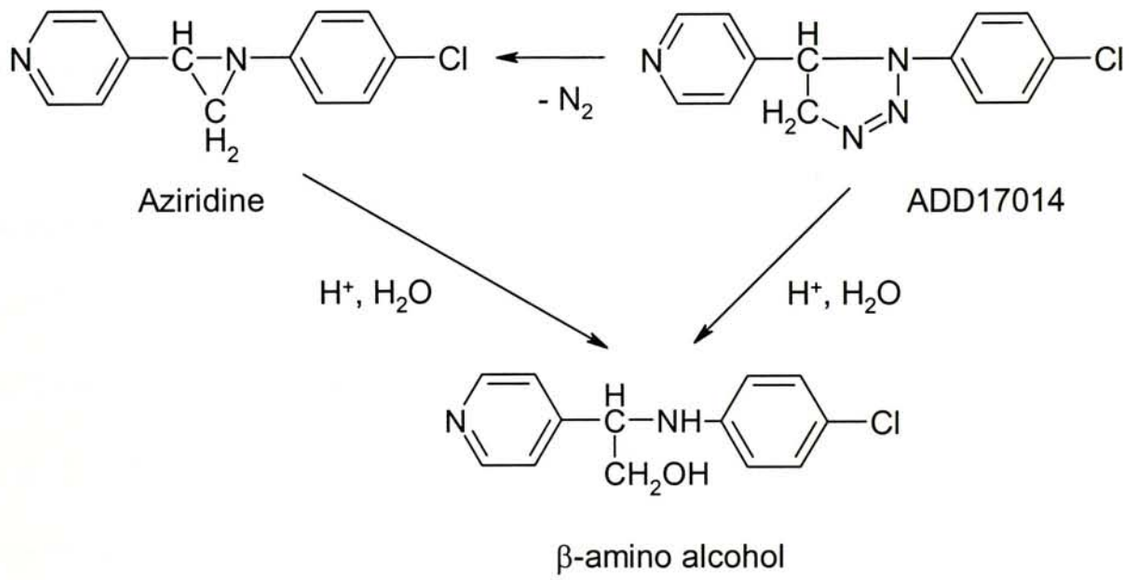

Figure 1.2 Metabolism of ADD17014.

A careful inspection of the structure of triazoline ADD17014 and its potential metabolites reveals the presence of a common "structure-element" comprising an

'open' "two-carbon-one-nitrogen" framework with the pyridyl and phenyl substituent groups incorporated onto the respective carbon and nitrogen atoms (Deshmukh and Kadaba, 1993). This 'open' structure probably constitutes the primary nucleus of the "hidden" pharmacophore of ADD17014, and is present in the aziridine an the β-amino alcohol metabolites. However, being non-lipophilic, the β-amino alcohol cannot cross the blood brain barrier (BBB) and hence fails to demonstrate the seizure protection in both MES and s.c.Met tests in mice (Kadaba, 1990). On the other hand, aziridine, though a prodrug per se and having lipophilicity very similar to that of the parent ADD17014, shows no activity at any of the receptor sites mentioned in above section.

Apparently, the "open flexible" structure of the pharmacophore nucleus is a prerequisite for activity at postsynaptic receptor sites; the closed ring structures in the triazoline and aziridine impart a certain degree of rigidity to the pharmacophore nucleus and prevent it from attaining the proper configuration for receptor interaction. Indeed, the open-chain form of the aziridine gives rise to the aminoalkylpyridine (AAP) structure; it contains the open flexible pharmacophore element of the β-amino alcohol and bears a remarkable structural relationship to the β-amino alcohol as the respective "deoxy-analogue".

Elucidation of the hidden pharmacophore nucleus of the ADD17014 prodrug leads to the logical and directed evolution of the hydrophobic, lipid soluble AAPs, in which the hydroxymethyl group of the β-amino alcohol is replaced by a non-polar methyl-moiety. The AAPs constitute a unique class of the 1,2,3-triazoline metabolite analogues; unlike the hydrophilic amino alcohol metabolite, these hydrophobic metabolite analogues are potent, orally active anticonvulsants.

1.5 Chemical Synthesis of Aminoalkylpyridines

The structures of the ADD17014 pharmacophore and *p*-Cl AAP are shown in Figure 1.3. AAP is synthesized in a two-step reaction (Figure 1.4). 4-acetylpyridine is condensed with a substituted aniline to yield the respective ketimine. Molecular sieves are used to trap the water molecules formed during the reaction; their presence is essential for the successful completion of the reaction leading to a reasonably good product yield. The ketimine thus formed is then reduced by sodium borohydride in refluxing ethanol.

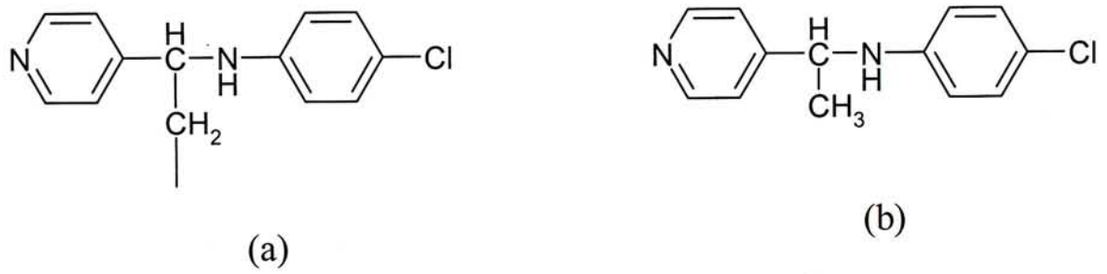

Figure 1.3 Pharmacophore of ADD17014 (a) and structure of *p*-Cl AAP (b).

The reaction mixture is cooled, treated with dilute hydrochloric acid to decompose excess sodium borohydride and then basified with 10% sodium hydroxide solution, to obtain the AAP. The compound is recrystallized from acetone-petroleum ether or t-butyl methyl ether-petroleum ether mixture to give yields ranging from 50-80%.

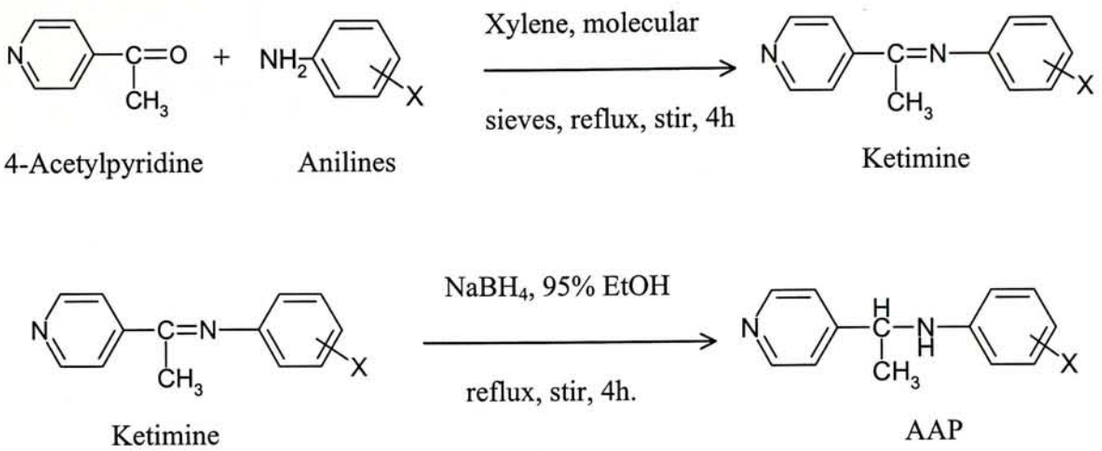

Figure 1.4 Synthesis of aminoalkylpyridines.

1.6 Metabolism of Aminoalkylpyridines

Figure 1.5 shows the potential metabolic pathway of AAPs. AAP is thought to be metabolized to β-amino alcohol that functions as a glutamate antagonist and may further oxidize to α-amino acid. AAP may transform into hydroxylamine, which may further metabolize to nitrone. AAP may also oxidize to *N*-oxide or carbinolamine. The latter may cleave to 4-acetylpyridine and aniline. The resulting metabolites may undergo further phase II transformation.

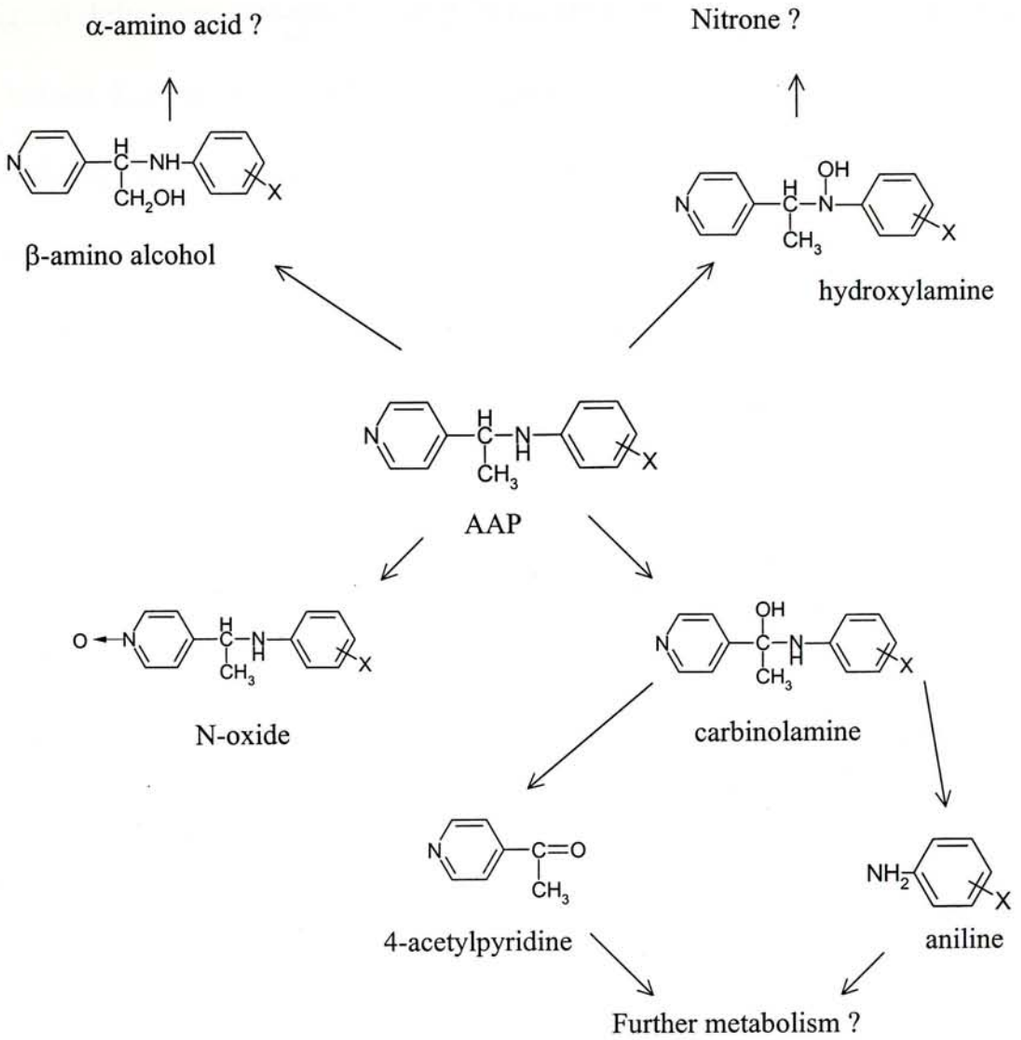

Figure 1.5 Potential metabolic pathway of aminoalkylpyridines.

1.7 Anticonvulsant Activities of Aminoalkylpyridines

It has been demonstrated that the AAPs afford seizure protection in both mice and rats, although their activity by the oral route far exceeds that observed by the i.p. route. They are highly effective in a dose-dependent fashion in the MES test (Deshmukh and Kadaba, 1993). In contrast to i.p. administered compounds, the protective effects of orally administered AAPs reach a peak more slowly and are sustained for up to 4h or longer. Similarly, the doses causing motor impairment are also substantially higher in rat, p.o. than in mouse, i.p. and no apparent signs of

neurological deficit are observed up to 500 mg/kg in the rat, which is well reflected in the P.I. values. For the *p*-Cl AAP, the ED_{50}(MES) and TD_{50} in mouse i.p. are 53.7 and 160.1 mg/kg respectively and the P.I. value is 3.0. In the case of p.o. administration to the rat, the ED_{50}(MES) is 22.9 mg/kg and P.I. value is greater than 20.5.

As the triazoline pharmacophore is an integral part of the AAPs, the latter may act by a similar mechanism to glutamate antagonists. Indeed preliminary receptor displacement and release studies using *p*-Cl AAP indicate that the ability of the triazoline structure to impair presynaptic glutamate release is fully retained or better in this compound (74% at 50 μM and 80% at 100 μM), as with the postsynaptic activity of the β-amino alcohol, albeit at a different site; the *p*-Cl AAP compound weakly displaces [^{3}H] DTG, a ligand highly specific for the σ-receptor (50% at 10 μM concentration) and shows no affinity for the NMDA/PCP sites (Deshmukh and Kadaba, 1992). It indicates that anticonvulsant action of *p*-Cl AAP is not a result of interaction with these receptor sites.

The AAP anticonvulsant agents exhibit low to moderate affinities, in the μM range, and high selectivity for the σ_1 site, and no affinity for σ_2 sites. The lack of link to the NMDA receptors may account for the remarkable absence of motor toxicity in these compounds. The anticonvulsant activity of *p*-Cl AAP is possibly by inhibition of glutamate release rather than by the blockade of the NMDA receptor sites.

The AAPs, a new generation of potent, orally active anticonvulsant agents, are far superior to the parent triazolines. The AAPs are highly lipophilic molecules that can cross the blood brain barrier (BBB), and show a high degree of anticonvulsant activity by the oral route with no apparent neurotoxicity and with P.I. values greater than 20.

1.8 Aim and Scope of the Present Study

The evolution of aminoalkylpyridines (AAPs) from 1,2,3-triazolines as a new class of potential anticonvulsants has been published (Deshmukh and Kadaba, 1993). While the toxicology and pharmacological action of these compounds has been extensively studied (Deshmukh and Kadaba, 1992), there is no information available on the metabolic fate of these novel anticonvulsants in mammalian systems. Hence the main aim of the study is to investigate the *in vivo* metabolism of *p*-Cl AAP in rat, a representative AAP with proven anticonvulsant activity with a view to elucidating the mode of action of this novel anticonvulsant.

Specifically, the project involved:

1) physicochemical (preformulation) characterization of five structurally related AAPs (i.e. *p*-F, *p*-Cl, *p*-Br, *p*-CH_3 and *m*-CF_3 AAPs) including determination of partition coefficient, aqueous solubility, and thermal properties;
2) development and validation of sensitive high performance liquid chromatographic methods for detection of *p*-Cl AAP and its metabolites in biological fluids;
3) determination of the pharmacokinetic parameters in the rat following intravenous administration of *p*-Cl AAP; and
4) identification of the urinary metabolic profile following administration of *p*-Cl AAP to rats and investigation of effects of phenobarbitone on the urinary metabolism.

Chapter Two

Experimental

2.1 MATERIALS

All aminoalkylpyridines (AAPs) and *p*-Cl aziridine (AZI-Cl) were synthesized as previously described (Deshmukh, 1993). Heparin (sodium salt) was purchased from B. Braun Melsungen AG (D-34212, Melsungen, Germany) and dissolved in laboratory prepared physiological saline (0.9%, w/v) to a final concentration of 100 I.U./ml. Sodium carbonate (Na_2CO_3), sodium bicarbonate ($NaHCO_3$), citric acid ($C_6H_8O_7.1H_2O$) and disodium phosphate (Na_2HPO_4) (Anala-R grade) were obtained from BDH Laboratory Supplies (England). All water used was freshly distilled, deionized and filtered.

Delory and King's carbonate-bicarbonate buffer, pH 10.0 was prepared by mixing 53.4 ml of 0.1 M sodium carbonate (10.6 g/L) with 46.6 ml of 0.1 M sodium bicarbonate (8.4 g/L).

McIlvaine's citric acid-phosphate buffer was made up by mixing 9.8 ml of 0.1 M citric acid (21.0 g/L) with 91.2 ml of 0.2 M disodium phosphate (28.4 g/L). All pH measurements were taken at 20 °C using a Hanna pH meter model HI 8418 (HANNA Instrument, USA) and all buffers were stored at 4 °C.

Male Sprague-Dawley rats (body weight 250-300 g) were bred at and supplied by the Laboratory Animal Service Centre at The Chinese University of Hong Kong and were housed in a light-, temperature- and humidity-controlled environment. Animals were fed on standard rat food - RM3(E) from Special Diet Services Ltd. (Witham, Essex, U.K.) and allowed access to water *ad libitum*.

Octan-1-ol (GPR grade) was obtained from BDH Laboratory Supplies (England). For the partition coefficient determination, both n-octanol and the citric acid-phosphate buffer (pH 7.4) were pre-saturated with each other before use.

Methanol, acetonitrile and diethylamine were HPLC grade purchased from BDH Laboratory Supplies (England).

β-Glucuronidase (E. Coli K12) and β-glucuronidase/Arylsulfatase (Helix pomatia) were obtained from Boehringer Mannheim (GmBH, Germany). Acetate buffer (pH5.0) was prepared by diluting glacial acetic acid (pro analysis grade) from Merck, (Germany) with water (1.146 ml in 100 ml) and mixing with 35.2 ml of a solution of sodium acetate (pro analysis grade) (1.46 g in 100 ml water) from BDH Laboratory Supplies (England). The pH was adjusted and the volume made up to 100 ml. The buffer was stored at 4 °C. *p*-Cl AAP was freshly prepared by dissolving in 50 % β-cyclodextrin solution. Sodium salt of phenobarbitone was dissolved in laboratory prepared physiological saline.

Ether for anaesthesia was obtained from BDH Laboratory Supplies (Poole, BH15, 1TD, England).

Translucent PE tubings (0.5 mm ID, 1.00 mm OD and 0.86 ID, 1.27 mm OD) were obtained from Portex (England). Needles (23G) and 1 ml syringes were purchased from B. Braun Melsungen AG (D-34212, Melsungen, Germany).

2.2 PREFORMULATION STUDIES ON AMINOALKYLPYRIDINES

2.2.1 *Determination of Partition Coefficients*

Stock solutions of *p*-F, *p*-Cl, *p*-Br, *p*-CH_3 and *m*-CF_3 AAP (16 μg/ml) were prepared in citric acid-phosphate buffer (pH 7.4). 25 ml of the stock solution was mixed with 2.5 ml n-octanol in a separating funnel and shaken for 10 minutes. After allowing the mixture to stand for 2 hours, the aqueous phase was collected and assayed for AAP by UV spectrophotometry (Shimadzu Model UV-160A spectrophotometer) at appropriate λ_{max} (235.0, 250.4, 251.6, 241.4 and 247.6 nm for *p*-F, *p*-Cl, *p*-Br, *p*-CH_3 and *m*-CF_3 AAP respectively). Six replicate determinations were performed for each AAP. Calibration curves covering the concentration range 0 - 15 μg/ml for the various AAPs were constructed. Each concentration was measured four times (n=4).

2.2.2 *Determination of Aqueous Solubilities*

The solubilities of *p*-F, *p*-Cl, *p*-Br, *p*-CH_3 and *m*-CF_3 AAP from 25 °C to 60 °C were determined as follows. Excess amounts of AAPs were placed in the citric acid-phosphate buffer (pH 7.4) in capped micro-centrifuge tubes and equilibrated for one week at a defined temperature in a thermostatic bath to ensure the attainment of equilibrium. The supernatant was pipetted and assayed for AAP by UV spectrophotometry (Shimadzu Model UV-160A spectrophotometer) at appropriate λ_{max} (235.2, 250.0, 251.6, 242.6 and 247.4 nm for *p*-F, *p*-Cl, *p*-Br, *p*-CH_3 and *m*-CF_3 AAP respectively). One week of equilibration time was considered adequate since the solubility did not show any further increase after three more days of equilibration.

Triplicate determinations were made for each AAP. Calibration curves for *p*-F, *p*-Cl, *p*-Br, *p*-CH_3 and *m*-CF_3 AAP covering appropriate concentration ranges in citric acid-phosphate buffer were constructed as described in the previous section.

The solubility data was analyzed by Van't Hoff equation:

$$\ln Cs = \frac{-\Delta H^{solution}}{RT} + K$$

2.2.3 *Determination of Thermal Properties*

The melting point, T_m, and enthalpy of fusion, ΔH^f, of various AAP samples of *p*-F, *p*-Cl, *p*-Br, *p*-CH_3 and *m*-CF_3 AAP (1 - 2 mg) were determined in non-hermetically sealed aluminium pans heated at a rate of 5 °C / min. in a DSC (Perkin Elmer DSC6) (U.S.A.) using nitrogen as the purge gas and indium as the calorimetric standard. The T_m was taken as the temperature at the point of intersection of the leading line of the steepest slope and the baseline. ΔH^f was calculated from the peak area which was determined by means of a DSC6 Software on an IBM computer interfaced with the thermal analyzer. The ΔS^f was calculated from

$$\Delta S^f = \frac{\Delta H^f}{T_m}$$

(Since $\Delta G^f = 0$ during melting).

2.3 DEVELOPMENT OF A HIGH PERFORMANCE LIQUID CHROMATOGRAPHIC ASSAY for *p*-Cl AMINOALKYLPYRIDINE

2.3.1 *HPLC Apparatus and Conditions*

The HPLC system consisted of a gradient programmer (model 2360), a HPLC pump (model 2350), a variable wavelength UV/Vis detector (model V$^{4®}$), and computing integrator hardware and software (ChemResearch 150) (all from ISCO Inc., Lincoln, U.S.A.). The column was a reversed phase Apex ODS 5μ (25 x 0.46 cm) column (Jones Chromatography, Hengoed, U.K.). An ODS guard column (Alltech Associates, Inc., USA) was used to protect the analytical column. Samples were introduced into the system via a Valco injector fitted with a 20 μl loop. Detection of the eluents was by UV absorption at 254 nm. Chromatograms and retention times were recorded, and peak areas were calculated by (computerised) electronic integration. The HPLC analysis was performed at ambient temperature. The mobile phase consisting of methanol : acetonitrile : water (30 : 30 : 40. v/v) and diethylamine (200 μl/L) was eluted at 1 ml/min., and was filtered and degassed prior to use.

2.3.2 *Animal Treatments and Biological Fluid Collection*

Blank rat blood was obtained by cardiac puncture, and heparinised saline (100 I.U., 60 μl per ml of blood) was added to the blank blood. Blank rat urine was obtained from male Sprague-Dawley rats housed in perspex metabolic cages. The control blood and urine were stored at 4 °C.

2.3.3 *Solid Phase Extraction*

C18 cartridges (Waters Corp., U.S.A.) used for solid phase extraction were pre-conditioned with 2 ml of methanol followed by 2 ml of distilled water before use. Following the loading of samples, the cartridge was washed with 2 ml of distilled water and then eluted with 2 ml of methanol. The eluents were evaporated to dryness, and the residues reconstituted with 100 μl of the HPLC mobile phase prior to the chromatographic analysis.

2.3.4 *Construction of Calibration Curves for p-Cl AAP in Rat Blood*

The level of *p*-Cl AAP in blood varied markedly. In order to measure the *p*-Cl AAP levels accurately at both the high and low concentrations, it was necessary to construct two standard curves covering the concentration ranges of 0 to 1.0 μg/ml and 0 to 10.0 μg/ml, respectively.

The calibration curves were constructed by spiking various amounts of *p*-Cl AAP (10 μg/ml or 100 μg/ml in methanol) into control blank rat blood (250 μl). For the low range calibration curve, four concentrations (0.2, 0.4, 0.6 and 1.0 μg/ml) were made and each was measured thrice (n=3). For the high range calibration curve, solutions of four different concentrations (2.0, 4.0, 6.0 and 10.0 μg/ml) were prepared and each solution was measured thrice (n=3). The internal standard, *p*-Cl AZI (100 μl of 10 μg/ml in methanol for low range standard curve, or 100 μl of 100 μg/ml in methanol for the high range standard curve), was added to the blood mixture with the appropriate amounts of the Delory and King's carbonate-bicarbonate buffer (pH 10.0) and made up to a total volume of 1 ml prior to the solid phase extraction as described

in section 2.3.3. HPLC was conducted under the conditions mentioned in section 2.3.1 with UV detection at 254 nm. Peak area ratios of drug / internal standard (*p*-Cl AAP/AZI-Cl) were then plotted against concentrations of *p*-Cl AAP.

2.3.5 *Construction of Calibration Curves for p-Cl AAP in Rat Urine*

Calibration curves for *p*-Cl AAP in urine were constructed in essentially the same way as that for *p*-Cl AAP in blood. Varying amounts of *p*-Cl AAP (100 μg/ml or 1000 μg/ml in methanol) were spiked into control rat urine (0.5 ml) to produce concentrations in the ranges of 0-10 μg/ml and 0-100 μg/ml, together with a fixed amount of the internal standard, *p*-Cl AZI (100 μl of 100 μg/ml in methanol for the low range standard curve, or 100 μl of 1000 μg/ml in methanol for the high range standard curve). For the low range calibration curve, five points of concentration 0.0, 2.0, 4.0, 6.0 and 10.0 μg/ml were made and each point was detected in triplicate (n=3). For the high range calibration curve, the five points of concentration 10.0, 20.0, 40.0, 60.0 and 100.0 μg/ml were made and again each point was detected in triplicate (n=3). Again, the final volume of the urine mixture was adjusted to 1 ml with Delory and King's carbonate-bicarbonate buffer (pH 10.0) and subjected to extraction as described in section 2.3.3.

2.3.6 Accuracy and Precision in the Quantitation of p-Cl AAP in Biological Fluids

Intra- and inter-day assay variability was investigated to determine the accuracy and precision of the developed assay. Known amounts of *p*-Cl AAP were spiked into blank blood (0.25 ml) and urine (0.5 ml) to produce the final

concentrations in the following two ranges for each blank: 0.2 - 0.8 and 2 - 4 μg/ml for blood; 2.0 - 8.0 and 25.0 - 75.0 μg/ml for urine. The internal standard, *p*-Cl AZI was spiked (100 μl of 10 μg/ml and 100 μg/ml for both low and high levels in blood respectively; and 100 μl of 100 μg/ml and 1000 μg/ml for both low and high levels in urine respectively) into the mixtures. The final volume of the mixtures was adjusted with the Delory and King's buffer (pH 10.0) to 1 ml before the solid phase extraction as mentioned in section 2.3.3. The resulting sample mixtures were analyzed on the same day and three separate days respectively for intra- and inter-day variability. The percentage difference between the amount of *p*-Cl AAP determined and the amount spiked was taken as a measure of accuracy and the coefficient of variation (C.V.) as a measure of assay precision.

2.4 PRELIMINARY PHARMACOKINETICS OF *p*-Cl AAP FOLLOWING INTRAVENOUS ADMINISTRATION

2.4.1 *Cannulae Preparation*

A knot was made onto the cannula by introducing the PE tubing with larger diameter onto the smaller diameter PE tubing.

2.4.2 *Dosage*

p-Cl AAP was dissolved into 50% β-cyclodextrin. A single dose of *p*-Cl AAP (20 mg/kg) was administered intravenously.

2.4.3 *Animal Surgery and Sample Collection*

Rats were surgically prepared 24 hours before administration of the *p*-Cl AAP. Cannulae were implanted into the jugular vein under light anaesthesia by ether. For the insertion of the jugular vein cannula, a longitudinal incision (approximately 2 cm) was made on the skin above the vein. The tissues surrounding the vein were cleared to expose approximately 1 cm of the vein itself. The ends of the exposed vein were secured with loose ligatures and a small puncture was made on the wall of the vein by the needle (23 G). The prepared cannula was attached to a 1 ml syringe charged with heparin and inserted into the vein in the direction of the heart to a distance of about 2 cm. The ligatures were then secured tightly in front and at the back of the knot to ensure the cannula remained in place upon recovery of the animal. Heparined saline (200 μl, 100 I.U./ml) was administered through the cannula to prevent the blocking of the tube by the coagulation of the blood. The syringe was disconnected from the cannula and replaced with a 1 cm light stainless steel pin and the cannula exteriorised on the back of the neck in the intracapsular region. The surgical incisions were then closed using cotton sutures and the wound swabbed with ethanol-dipped cotton wool.

The carotid artery was cannulated in a similar manner, with a ventral mid cervical incision made to expose the carotid artery. The carotid artery is found in a much deeper position than the jugular vein and in close proximity to the vagus nerve. The other important difference to vein cannulation is that the upper ligature on the artery was made secure before making an incision to stop blood from being pumped out under the great pressure that exists in the artery. Again the cannula was exteriorised and the incision site on the animal front closed with sutures. The operation lasted approximately 30 minutes.

Cannulated rats were allowed to recover overnight before administration of *p*-Cl AAP. Drug (20 mg/kg) were administered *via* the jugular cannulae and serial blood samples were collected at appropriate time intervals (pre-dosed, and 5, 15, 30 and 45 min., 1, 2, 3, 4 and 5 hours post-dosed). The pH of the blood sample taken (250 µl) were immediately raised by the addition of Delory and King's carbonate-bicarbonate buffer (pH 10.0) to prevent any possible *ex vivo* alterations in drug concentration. Samples were stored at 4 °C before solid phase extraction as previously described and analysis by HPLC (section 2.3).

2.4.4 *Pharmacokinetic Calculations*

Pharmacokinetic parameters were determined by noncompartmental pharmacokinetic data analysis, using the PK Solutions 2.0 software (Summit Research Services, Ashland, U.S.A.). The equations used were shown below:

Elimination rate constant (k_e) = -2.303 x slope

Half-life = 0.693 / k_e

Area Under Curve (AUC) = $AUC_{(0-t)}$ + [last drug concentration] / k_e

Volume of distribution (Vd) = Dose administered / (k_e x AUC)

Clearance (CL) = Dose administered / AUC

2.5 URINARY METABOLIC STUDIES OF *p*-Cl AAP

2.5.1 *Animal Treatment and Urine Collection*

Male Sprague-Dawley rats (200 - 250 g) were divided into three groups with five rats for each group. Rats in the first group were pretreated with phenobarbitone (80 mg/kg/day, intra-peritoneal) for three consecutive days prior to the administration of *p*-Cl AAP. The rats in the first phenobarbitone pretreated group and the second groups without phenobarbitone pretreatment were administered *p*-Cl AAP intra-peritoneally with a single bolus dose (100 mg/kg). Rats in the third group (control group) were administered with the vehicle, 50 % β-cyclodextrin, alone. All the rats in these three groups were placed in individual perspex metabolic cages with free access to food and water. Urine free of faeces was collected for 0-24 hr and 24-48 hr respectively. In order to avoid possible degradation of excreted parent drug and metabolites, the urine was immediately frozen by collecting into tubes immersed in liquid nitrogen. The collected urine sample was stored at -20 °C until analysis.

2.5.2 *Deconjugation Assay*

The urine samples collected were subjected to deconjugation using β-glucuronidase and β-glucuronidase / arylsulphatase enzymes, separately. These enzymes hydrolyze glucuronide and/or sulphate conjugates into corresponding phase I metabolites respectively.

Three 1 ml aliquots of each urine sample were taken. To the first aliquot was added β-glucuronidase (1000 units) in acetate buffer (pH 5.0; 1 ml); to the second, β-glucuronidase / Arylsulphatase (1000 units each) in acetate buffer (pH 5.0; 1 ml); and

to the third, buffer alone (pH 5.0; 1 ml). All sample mixtures were then incubated overnight in a water bath at 37 °C. The samples were subjected to solid phase extraction and then analyzed by HPLC as mentioned in section 2.3.3 and below.

2.5.3 *Non-deconjugated Urine Sample Treatment*

5 ml of urine sample was taken and extracted by solid phase extraction and analyzed by HPLC as mentioned in section 2.3.

2.5.4 *Separation of Metabolites by HPLC*

The samples were dried and subjected to HPLC analysis after reconstitution with the mobile phase as mentioned in section 2.3. Metabolites (indicated by characteristic peaks in the chromatogram) were collected as different fractions after passage through an Alltima C18 100A 5U (250 x 10 mm) column (Alltech Associates, Inc., USA). An ODS guard column (Alltech Associates, Inc., USA) was used to protect the preparative column. The apparatus and conditions were similar to those mentioned in section 2.3.1 except the flow rate was increased to 4 ml/min. The fractions were dried and stored at -80 °C until analysis.

2.5.5 *Identification of Metabolites by LC/MS*

The metabolite in each fraction was analyzed by liquid chromatography/mass spectrometry (LC/MS). The LC analysis employed a HP 1090 Liquid Chromatograph (Hewlett Packard Company, U.S.A.) and similar HPLC conditions to those in section 2.3. For the MS analysis, a triple-stage quadrupole mass spectrometer (Finnigan MAT TSQ 7000 System, Germany) with atmospheric pressure chemical ionization (APCI)

method were employed for a direct probe MS analysis, a quadrupole ion trap mass spectrometer (Finnigan MAT GCQ DPC System, Germany) with chemical ionization (CI) and electron impact ionization (E.I.) were performed. In APCI mode, the ionization current used was 5 μA and the ion polarity selected were both positive and negative. The capillary and vaporizer temperature was 150 and 400 °C, respectively. Nitrogen was used as the sheath gas and the pressure was 40 psi. The electron multiplier voltage was 1200 V. The range of mass scanned was 110 to 500 a.m.u. and the scan time was 1 second. For the MS/MS experiment, the range of mass scanned was 0 to 400 a.m.u. The scan time was 0.5 second. The collision gas used was argon and the gas pressure and energy was 0.2 Pa and 5-40 eV, respectively. In EI mode, the ionization voltage was -20 eV and the ion source temperature was 190 °C. The electron multiplier voltage was 1200 V. The scanned mass range was 10 - 500 a.m.u. and the scan time was 0.5 second. For CI-MS was employed in the MS/MS analysis and the mass range scanned was 0 - 400 a.m.u. and the scan time was 0.5 second. The collision gas was helium. The gas pressure and energy were 0.1 Pa and 30 eV, respectively.

2.5.6 Quantitative Analysis

Prior to solid phase extraction, the urine samples were spiked with 10 μg and 100 μg of internal standard, *p*-Cl AZI for the deconjugation and non-deconjugation treatment of samples respectively. The extracts from solid phase extraction (section 2.3.3) were analyzed by HPLC as described in section 2.3.

The peak area ratio of the *p*-Cl AAP to the internal standard was recorded, and the amount of the *p*-Cl AAP in urine extracts was determined by using the calibration curves constructed as mentioned in section 2.3.

Since there are no authentic samples for the construction of calibration curves of the respective metabolites, relative amount of the metabolites was stated in the whole study. The peak area ratio obtained for the metabolite to the internal standard, *p*-Cl AZI, was recorded and the peak area ratio to those metabolites appeared as phase I metabolites was considered to be 100 %. The amounts of the glucuronide and sulphate conjugates of the metabolites were determined as the percentage of their respective phase I metabolites, i.e., the ratio of the peak area ratio of the glucuronide or sulphate conjugates to the peak area ratio of their phase I metabolite.

For those metabolites which did not appear as phase I metabolites, those peak area ratios of the glucuronide conjugate (to the peak area of the internal standard) were considered as 100 %. For those sulphate-conjugated metabolites, the relative amounts were determined as the percentage of its respective glucuronide conjugates, as mentioned previously.

The amounts of the glucuronide conjugates of the metabolites were calculated by subtracting the amount of phase I metabolite from those of the amount found after β-glucuronidase deconjugation. The relative amounts of the sulphate conjugates of the metabolites were calculated by subtracting the amounts of phase I metabolite and glucuronide conjugate of the metabolite from those of the amount found after β-glucuronidase / arylsulphatase deconjugation.

When comparing the effect on the relative amount of each metabolite between the phenobarbitone and non-phenobarbitone pretreatment, those amounts of the

metabolites from non-phenobarbitone pretreated rats were considered as 100 %. The amounts of those metabolites excreted from phenobarbitone pretreated rats were taken as the percentage of the amounts of those from the non-phenobarbitone pretreated rats.

2.5.7 *Preparation of the authentic β-amino alcohol*

50 mg of ADD17014 was dissolved in 2.4 ml water. Then, 40 µl hydrochloric acid (1 M) was added in dropwise. The reaction mixture was stood at room temperature with continued stirring for 7 hours. The reaction was stopped by addition of 650 µl sodium hydroxide (1 M). The β-amino alcohol was extracted by diethyl ether and any residual water was removed by anhydrous magnesium sulphate. The β-amino alcohol was purified by HPLC using Alltima C18 100A 5U (250 x 10 mm) column (Alltech Associates, Inc., USA) with the mobile phase consisting of the mixture of methanol, acetonitrile and water in the ratio of 25 : 25 : 50 (together with 20 µl of diethylamine per 100 ml of mobile phase). The identity of obtained β-amino alcohol was confirmed by HPLC/MS/MS.

2.6 STATISTICAL ANALYSIS

All results were expressed as means ± standard deviations. Analysis of variance (ANOVA, single factor) was used to compare results between different groups. A probability (p) of less than 0.05 was considered statistically significant.

Chapter Three

Results and Discussion

3.1 PREFORMULATION STUDIES ON AMINOALKYLPYRIDINES

3.1.1 PARTITION COEFFICIENT (K°_{w})

The calibration curves for the determination of partition coefficients of the various AAPs were constructed and Table 3.1.1 shows the equations computed for the calibration plots. For all calibration curves there was excellent linearity (linear correlation coefficient > 0.999; n = 5; $P<0.05$). Each data point was determined four times.

Table 3.1.1 Linear equations computed for the calibration plots for the partition coefficient determination of various aminoalkylpyridines.

AAP	Equation	R^2
p-F	y = 0.0316 x + 0.0024	0.9999
p-Cl	y = 0.0495 x - 0.0019	0.9998
p-Br	y = 0.0481 x + 1E-05	1
p-CH_3	y = 0.0478 x + 0.0006	1
m-CF_3	y = 0.024 x - 0.0028	0.9998

The partition coefficients obtained for the aminoalkylpyridines are shown in Table 3.1.2. While the *p*-F, *p*-Cl, *p*-Br, and *p*-CH_3 AAPs showed no statistically significant differences in their K°_{w}, the *m*-CF_3 AAP exhibited a much lower K°_{w} (37.23 ± 1.2). It may be explained by increased ionization of the *m*-CF_3 substituted

aniline resulting in a greater fraction of the compound being partitioned into the aqueous phase.

Table 3.1.2 Preformulation parameters of aminoalkylpyridines.

AAP	Partition Coefficient	ΔH^s (kJ/mol)	Melting Temp. (°C)	Temperature Range (°C)	ΔH^f (kJ/mol)	ΔS^f (J/mol/K)
***p*-F**	71.96 ± 7.2	25.06 ± 1.4	84.05 ± 0.7	82.4 ~ 87.8	19.0 ± 0.6	53.6 ± 1.6
***p*-Cl**	75.61 ± 1.8	23.88 ± 2.4	105.1 ± 0.6	103.4 ~ 108.3	21.5 ± 0.9	57.0 ± 2.4
***p*-Br**	82.29 ± 6.0	25.02 ± 1.4	107.5 ± 0.3	107.9 ~ 110.5	21.7 ± 0.7	57.1 ± 1.8
***p*-CH_3**	73.72 ± 4.5	20.24 ± 1.1	94.0 ± 0.2	94.4 ~ 97.0	23.4 ± 1.7	63.7 ± 4.6
***m*-CF_3**	37.23 ± 1.2	34.76 ± 1.8	150.8 ± 0.3	151.0 ~ 153.3	33.8 ± 1.9	79.8 ± 4.5

3.1.2 AQUEOUS SOLUBILITY

The calibration curves used for the determination of aqueous solubility of the various AAPs were constructed and Table 3.1.3 shows the equation computed for the calibration plots of them. For all calibration curves there was excellent linearity ($r > 0.999$; $P < 0.05$; $n = 4$) (each data point was measured four times).

Table 3.1.3 Linear equations computed for the calibration plots for the aqueous solubility determination of various aminoalkylpyridines.

AAP	Equation	R^2
p-F	y = 0.0341 x - 0.0022	0.9998
p-Cl	y = 0.0623 x - 0.0042	0.9999
p-Br	y = 0.0561 x + 0.0018	0.9998
p-CH_3	y = 0.049 x - 2 x 10^{-16}	0.9997
m-CF_3	y = 0.0162 x - 0.0014	0.9991

The solubilities of various AAPs in water increased with an increase in temperature (Table 3.1.4 and Figure 3.1.1). In addition, the solubilities depended on the substitutent on the benzene ring of the AAPs, and decreased in the following order: *p*-F AAP > *p*-CH_3 AAP > *p*-Cl AAP > *p*-Br AAP > *m*-CF_3 AAP.

Table 3.1.4 Aqueous solubilities of various aminoalkylpyridines at different temperatures.

Temp. (°C)	Types of AAP				
	p-F	*p*-Cl	*p*-Br	*p*-CH_3	*m*-CF_3
	Concentration (M), x 10^{-5}				
25	204.4 ± 2.4	33.8 ± 1.2	12.4 ± 0.1	86.7 ± 2.2	5.83 ± 0.4
30	221.8 ± 1.8	34.9 ± 0.7	13.1 ± 0.1	87.7 ± 1.3	6.06 ± 0.2
37	282.6 ± 5.4	55.2 ± 5.9	18.3 ± 0.3	112.8 ± 2.2	8.91 ± 0.5
45	330.9 ± 5.1	57.6 ± 3.8	22.4 ± 0.3	135.3 ± 1.0	12.7 ± 0.6
50	428.7 ± 2.7	66.2 ± 6.4	24.5 ± 0.7	153.5 ± 4.9	16.2 ± 0.6
55	506.1 ± 4.2	75.6 ± 4.5	31.5 ± 0.6	178.7 ± 6.8	18.4 ± 1.2
60	569.2 ± 9.2	96.7 ± 8.7	34.4 ± 1.2	192.0 ± 16.6	24.1 ± 0.4

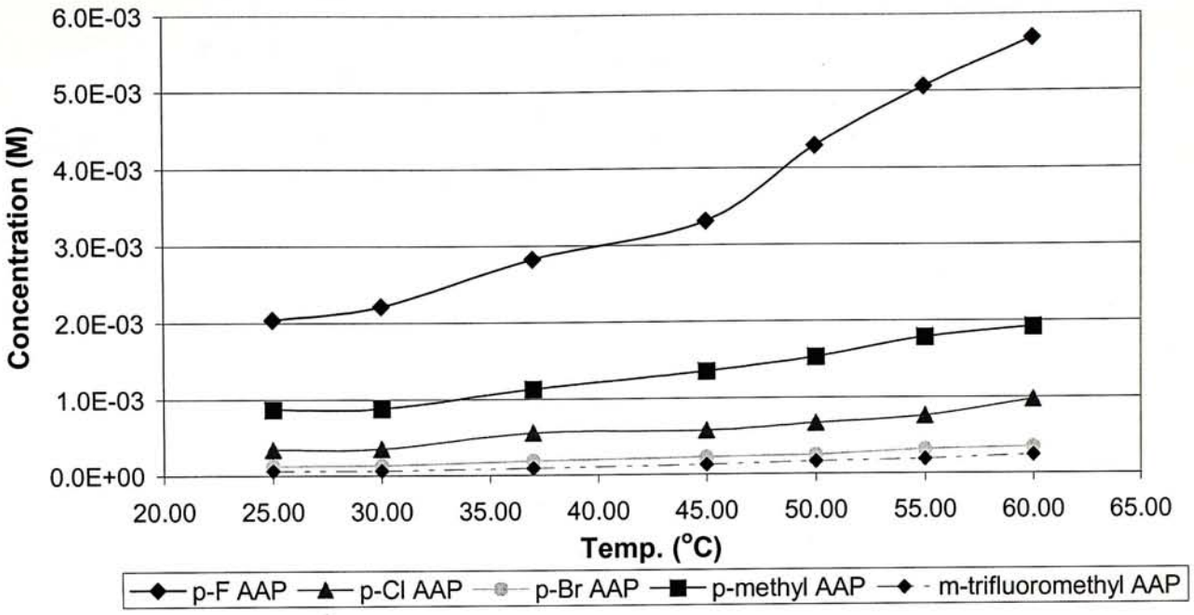

Figure 3.1.1 Plot of aqueous solubilities of AAPs against temperature (°C).

The solubility data were analyzed using the van't Hoff equation, and the associated plots and regression equations are shown in Figure 3.1.2.

The van't Hoff plots for the various AAPs displayed good linearity ($r = 0.95$ - 0.99; $n = 7$; $p < 0.05$), showing that the van't Hoff equation was obeyed by all the AAPs. The apparent molar enthalpy of solution, ΔH^s, of each AAP was determined from the slope of the plot, and the values are presented in Table 3.1.2. There were no statistically significant differences in ΔH^s among the three halogen substituted AAPs. The *p*-CH_3 AAP had a lower ΔH^s (20.24 ± 1.1 kJ/mol) while the ΔH^s of the *m*-CF_3 AAP (34.76 ± 1.8 kJ/mol) was the highest of all the five AAPs. As can be seen later, the change in the enthalpy of fusion, ΔH^f, of these AAPs parallel closely that of the ΔH^s.

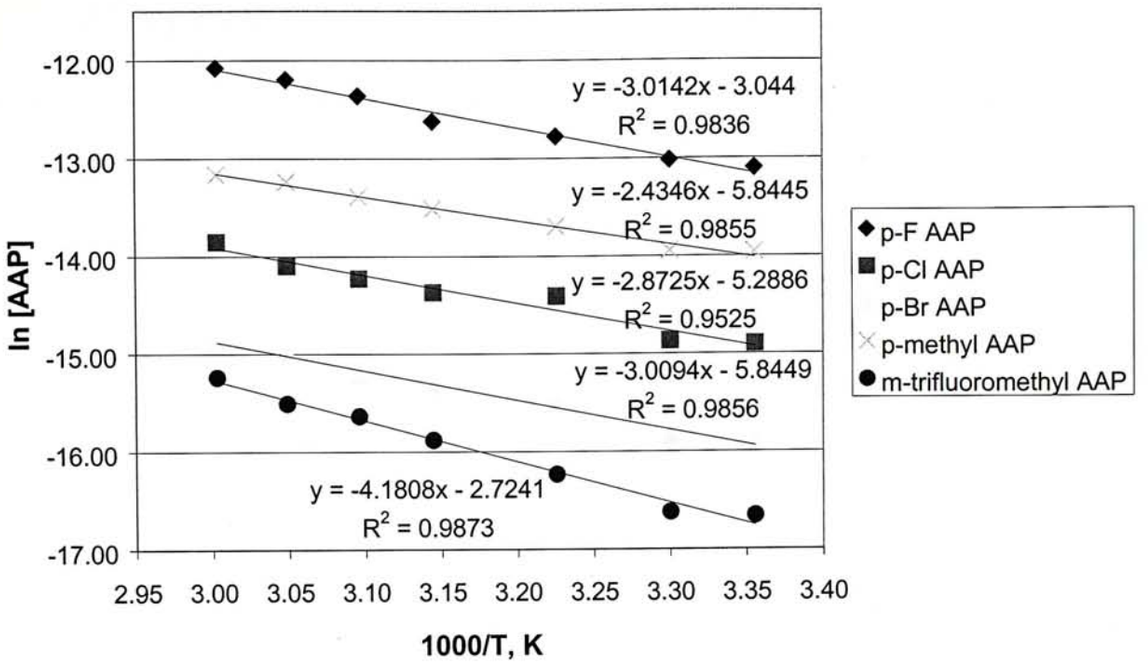

Figure 3.1.2 Van't Hoff plots on the saturated aqueous concentration of AAPs.

The ΔH^f values are similar in magnitude to the ΔH^s (being lower by 1 - 6 kJ/mol), suggesting that the aqueous solubilities of the AAPs are governed predominantly by solute-solute interaction in the solid state. This argument is based on the following thermodynamic considerations.

The dissolution of a solid in a solvent can be viewed as being equivalent to the melting of the solid (break down of solute-solute interaction) followed by mixing of the resulting liquid solute with the solvent (establishment of solute-solvent interaction). The enthalpy of solution, ΔH^s ,of the solid is therefore given by

$$\Delta H^s{}_T = \Delta H^f{}_T + \Delta H_{mix}$$

where $\Delta H^f{}_T$ is the enthalpy of fusion at the absolute temperature T of the solution, which is invariably below the normal melting point T_m of the solid, and ΔH_{mix} is the enthalpy of liquid-liquid mixing.

ΔH^f is positive (i.e. endothermic transition) since energy is required to break down the solute-solute interaction to effect melting while ΔH_{mix} is generally negative (i.e. exothermic transition) if there exists an affinity between the solute and the solvent.

In present study, the ΔH^f measured was that at the melting point. Since the quantitative effect of temperature on ΔH^f is not known, it is not possible to estimate ΔH^f at the absolute temperature T of the solution. However, if it is assumed that the effect of temperature on ΔH^f for the five AAPs is closely similar, the contribution of ΔH^f (i.e. solute-solute interaction) to the ΔH^s term would still be predominant compared with that of the ΔH_{mix} (solute-solvent interaction). The dominant effect of the solute-solute interaction (i.e. crystal structure) on solubility has been further substantiated by the good correlation between the aqueous solubilities and melting points of the AAPs (see later discussion).

3.1.3 THERMAL ANALYSIS

The thermograms of the DSC studies on AAPs (Figure 3.1.3 - 3.1.7) displayed single sharp endotherms corresponding to melting with flat baseline at temperature above melting, suggesting that (a) the AAPs do not contain any solvent of crystallization, and (b) the AAPs are thermostable. However, the predecessor anticonvulsants, triazolines, exhibited decomposition (data not shown) as the temperature was raised to about 155 °C.

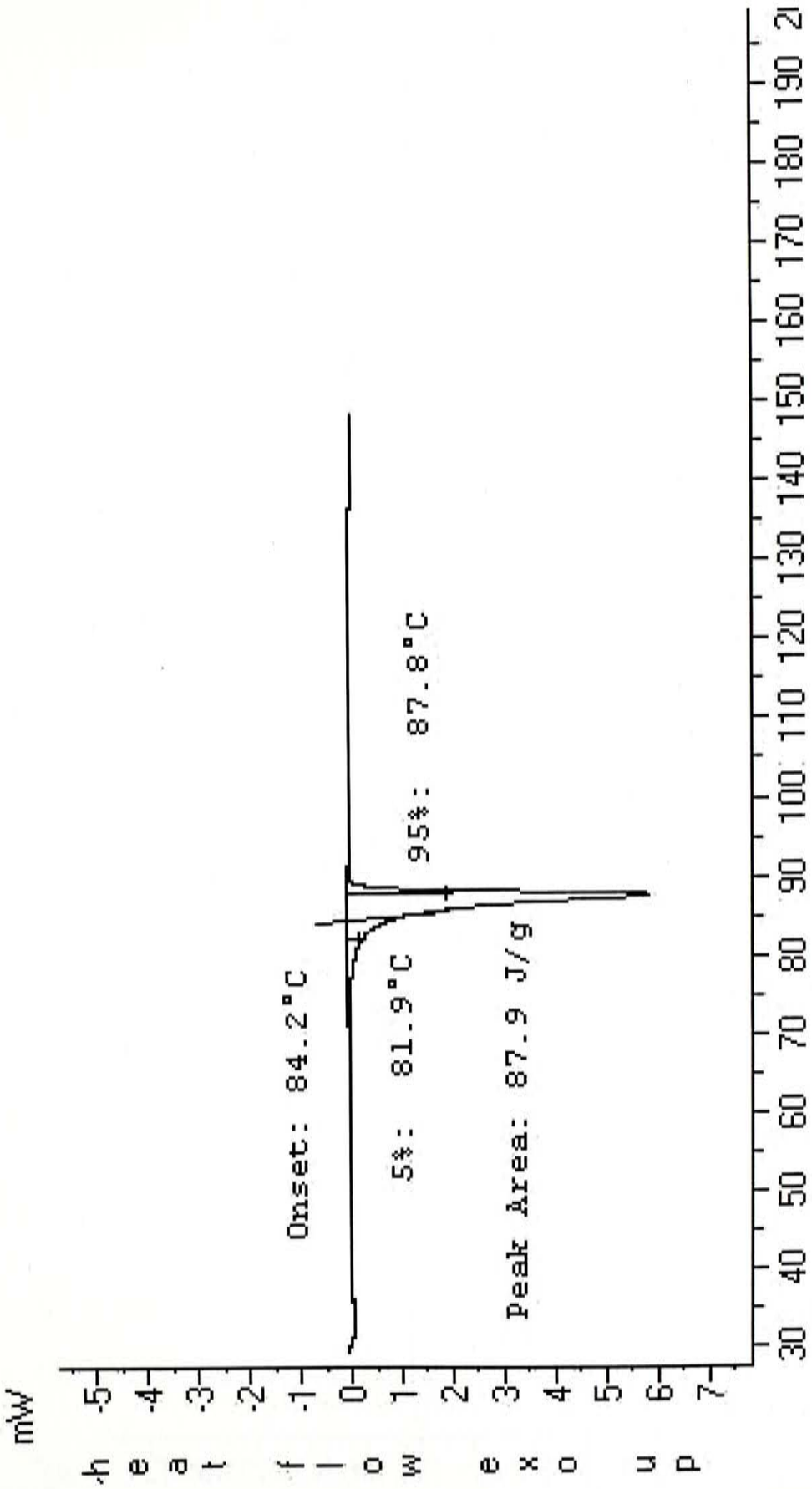

Figure 3.1.3 DSC thermogram of *p*-F AAP.

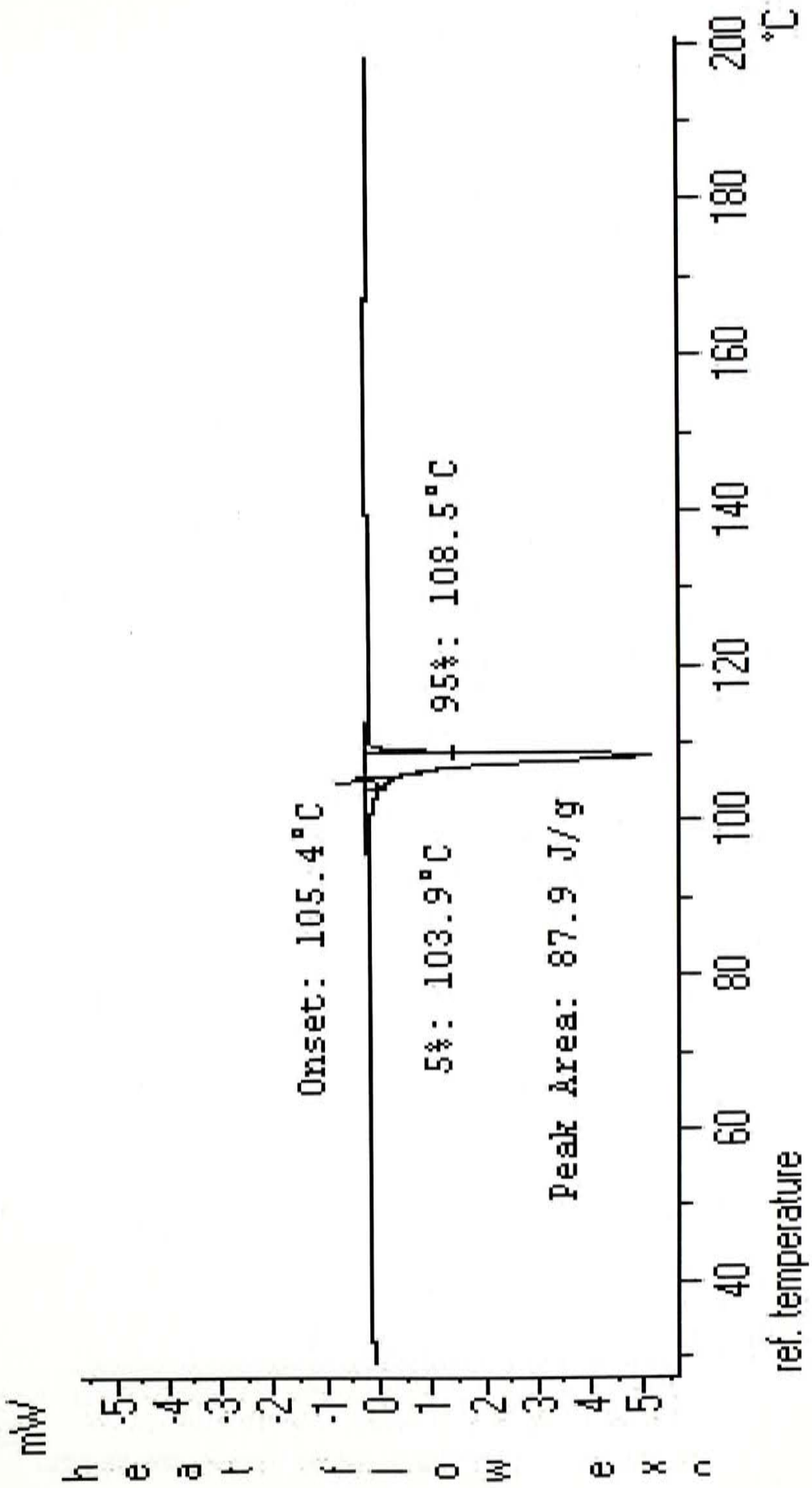

Figure 3.1.4 DSC thermogram of *p*-Cl AAP.

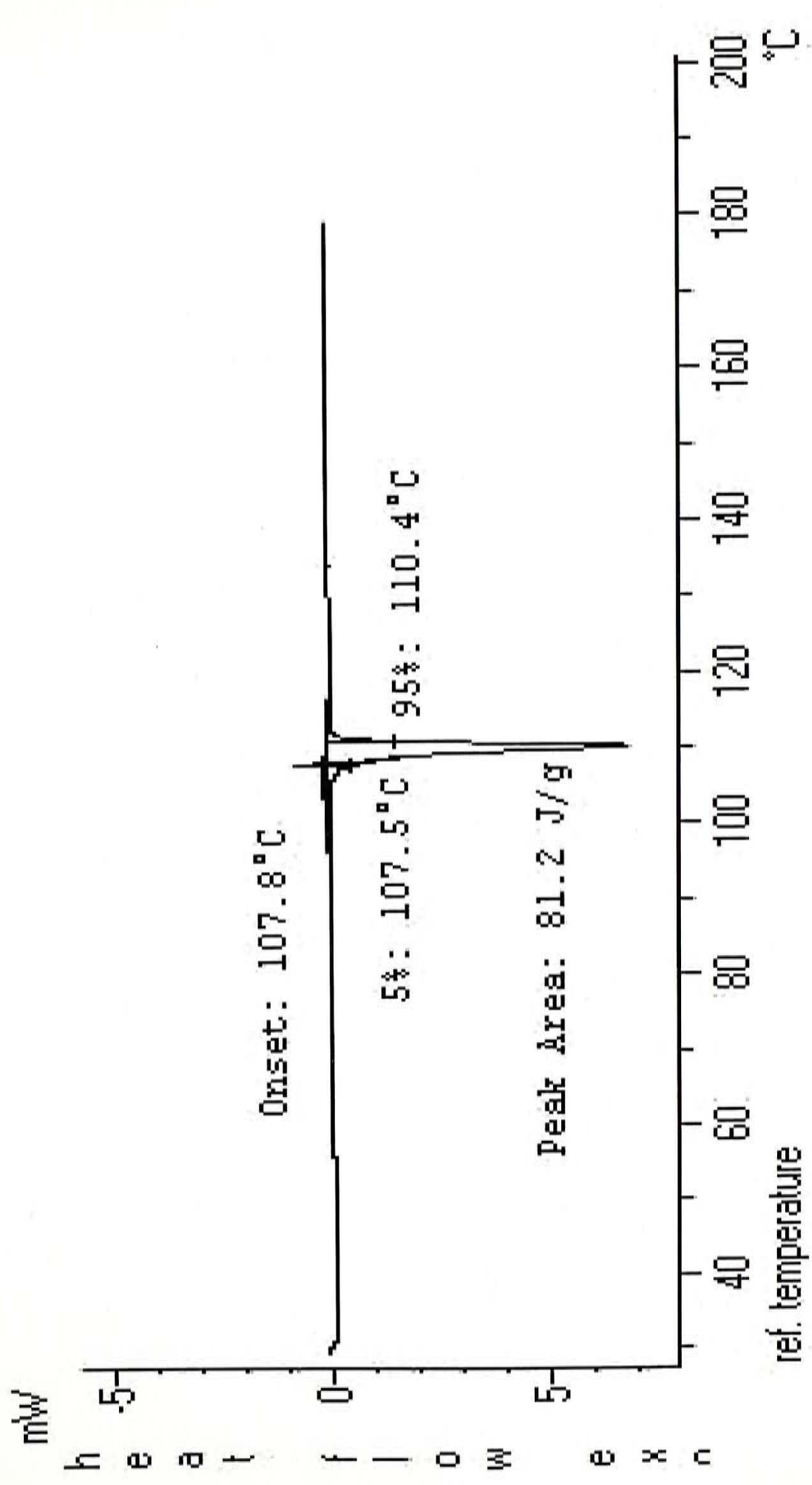

Figure 3.1.5 DSC thermogram of *p*-Br AAP.

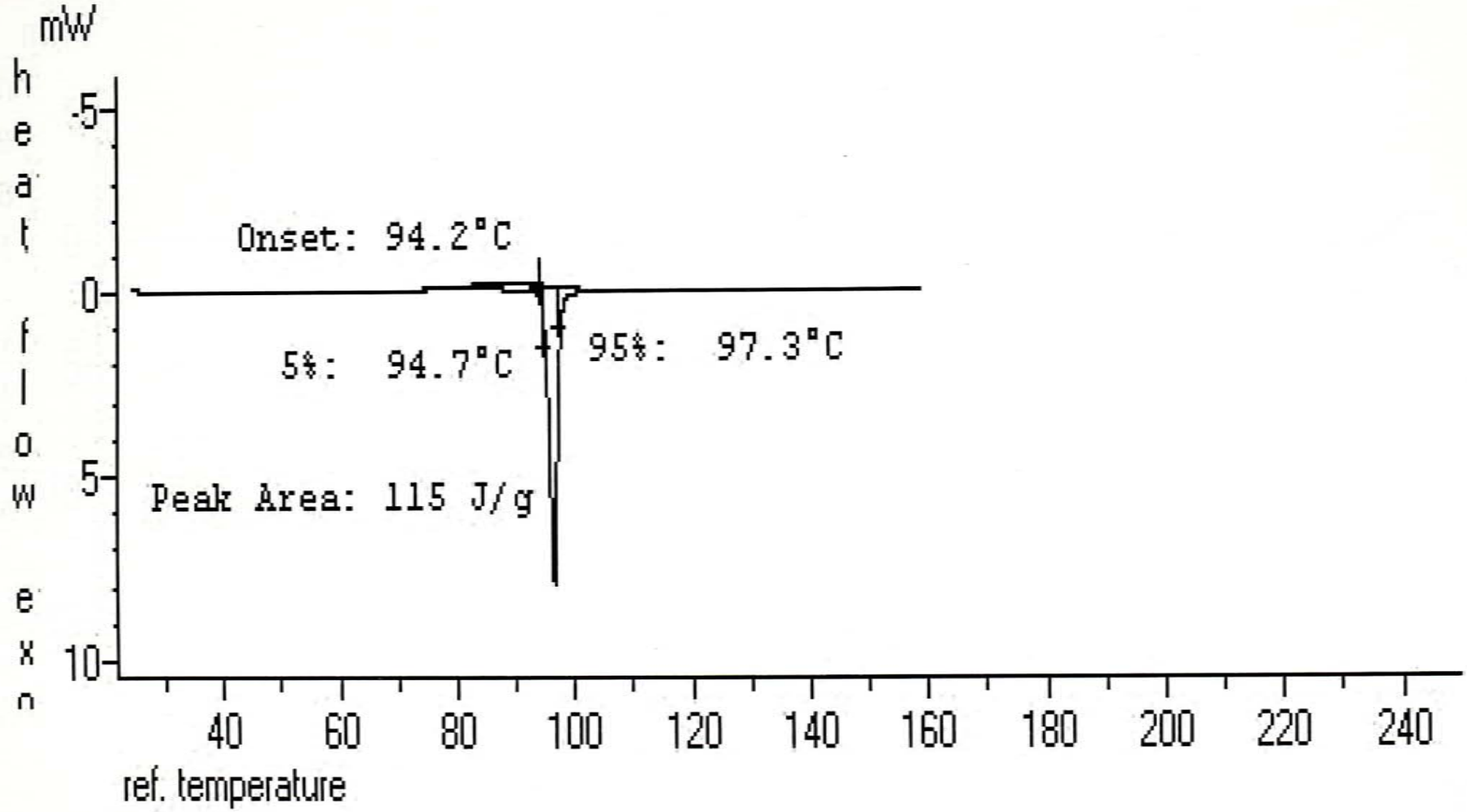

Figure 3.1.6 DSC thermogram of *p*-CH_3 AAP.

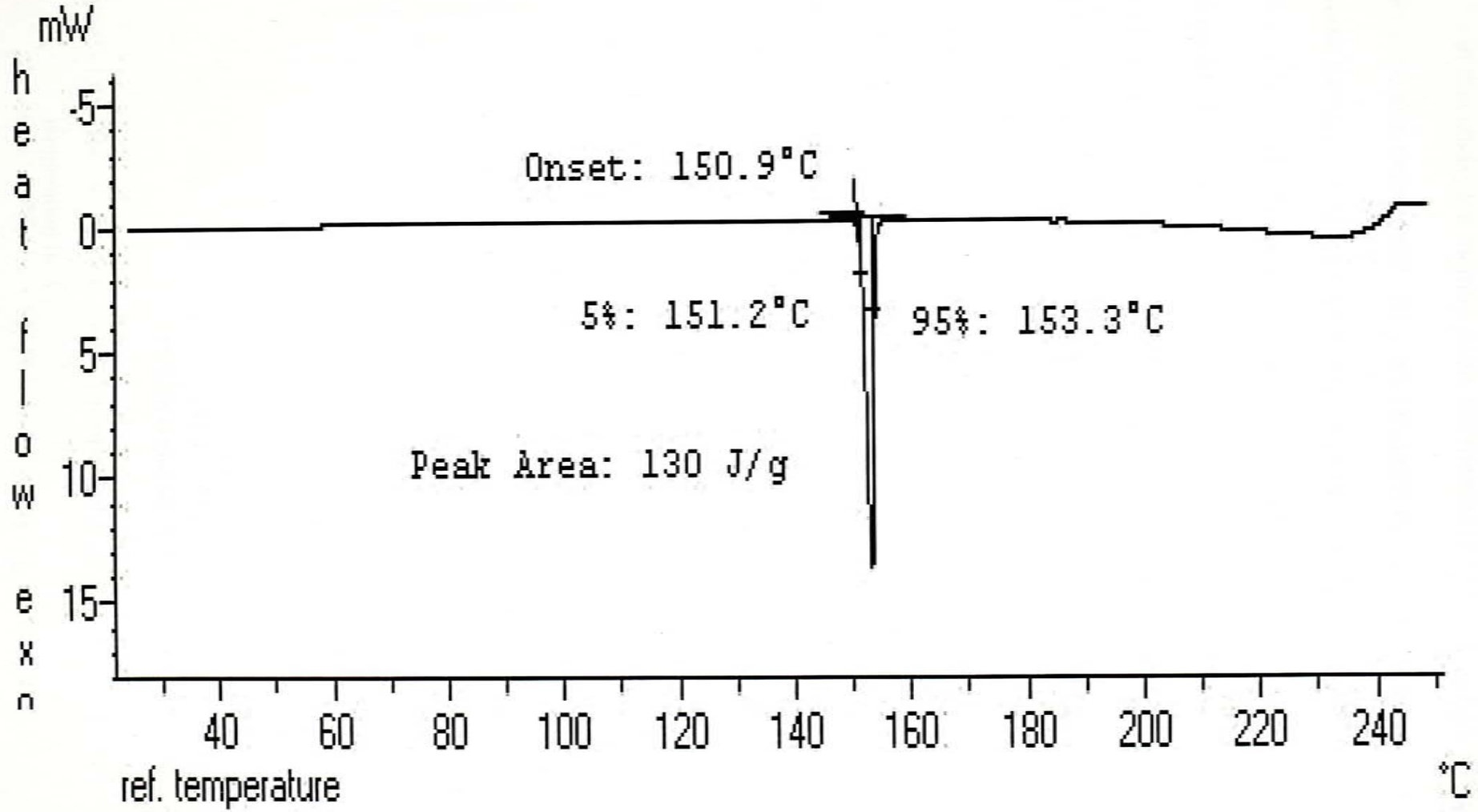

Figure 3.1.7 DSC thermogram of *m*-CF_3 AAP.

In this study, the melting point, the melting temperature range, ΔH^f and ΔS^f of AAPs were also determined. They are tabulated in Table 3.1.2. The melting point of the three halogen-substituted AAPs increased in the following order: *p*-F AAP < *p*-Cl AAP < *p*-Br AAP. Interestingly, there were only small (statistically insignificant) differences of the ΔH^f and ΔS^f among these three AAPs. The aqueous solubilities of the AAPs were found to be related to their melting points; the higher the melting point of the AAPs, the lower was the solubility. By plotting the aqueous solubilities of the AAPs (on logarithm scale) against the melting temperature (Yamaoka, 1983) in Figure 3.1.8, a significant linear correlation ($r^2 = 0.8008$; $r = 0.895$; $n = 5$; $p < 0.05$) was obtained. This suggested that the solubilities of AAPs was governed by the solute-solute interaction in the crystal structure, as alluded to earlier.

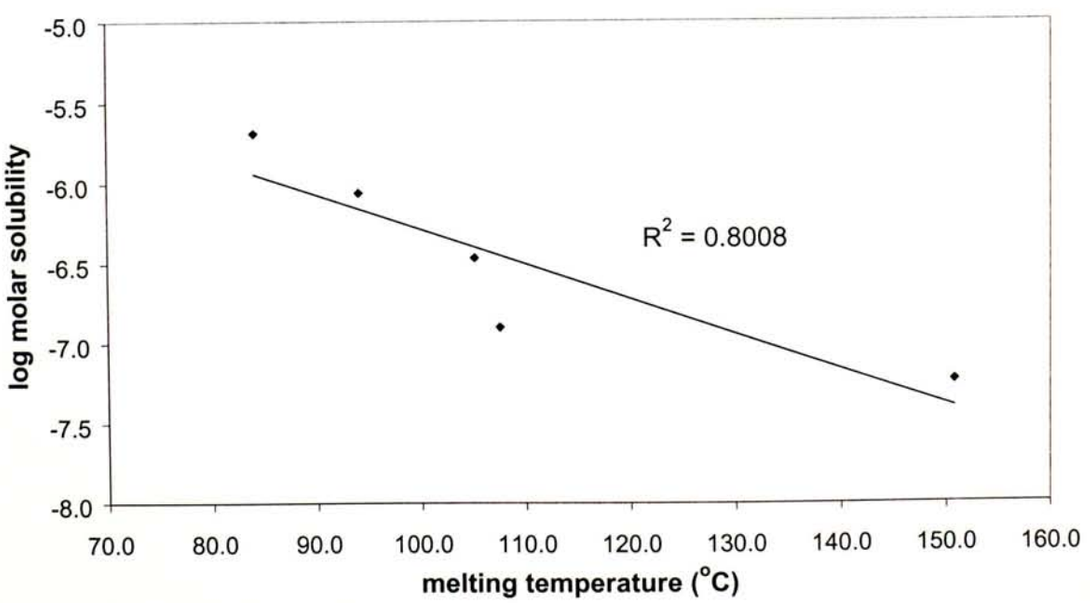

Figure 3.1.8 Plot of the log molar aqueous solubility of AAPs against the melting temperature in °C.

From the plot, the data point for the *m*-CF_3 member appears to deviate from the linear trend of those of the *para*-substituted members, suggesting that the former may be an atypical observation (i.e. outlier). This is perhaps not unexpected since the CF_3 member is *meta*-substituted while the rest of the AAPs are *para*-substituted. Exclusion of the *m*-CF_3 AAP from the plot afforded an $r^2 = 0.93$ ($r = 0.96$; $n = 4$; $p < 0.05$), an improvement of 13 % in terms of predictability.

In general, all the physical properties of AAPs were shown to depend on the chemical structure of the compounds.

3.2 DEVELOPMENT OF A HIGH PERFORMANCE LIQUID CHROMATOGRAPHIC ASSAY FOR *p*-Cl AMINOALKYLPYRIDINE

3.2.1 SOLID PHASE EXTRACTION

The solid phase extraction technique allowed separation of the parent drug and its putative metabolites from endogenous interfering substances. The HPLC chromatograms of the extracts of blank blood and urine containing, *p*-Cl AAP (parent drug), *p*-Cl AZI (internal standard) and the putative metabolite of *p*-Cl AAP, β-amino alcohol (β-AA, putative metabolite) are shown in Figure 3.2.1. From the chromatograms, retention times for the *p*-Cl AAP, β-AA and *p*-Cl AZI peaks, were found to be 7.8, 4.7 and 9.3 minutes, respectively. A good separation of these compounds with baseline separation was obtained. Very few interfering peaks at the retention times of the drug and the internal standard were observed, indicating that the solid phase extraction procedure is effective for removing endogenous compounds in the blood and urine samples.

3.2.2 CONSTRUCTION OF CALIBRATION CURVES FOR *p*-Cl AAP IN THE RAT BLOOD

Table 3.2.1 shows the peak area ratios of *p*-Cl AAP to *p*-Cl AZI, an internal standard, for both lower and higher concentration ranges in rat blood, and the corresponding calibration plots are shown in Figure 3.2.2 and 3.2.3. For both ranges there was excellent linearity ($r > 0.998$; $n = 4$; $p < 0.05$) (Each point was measured in triplicate).

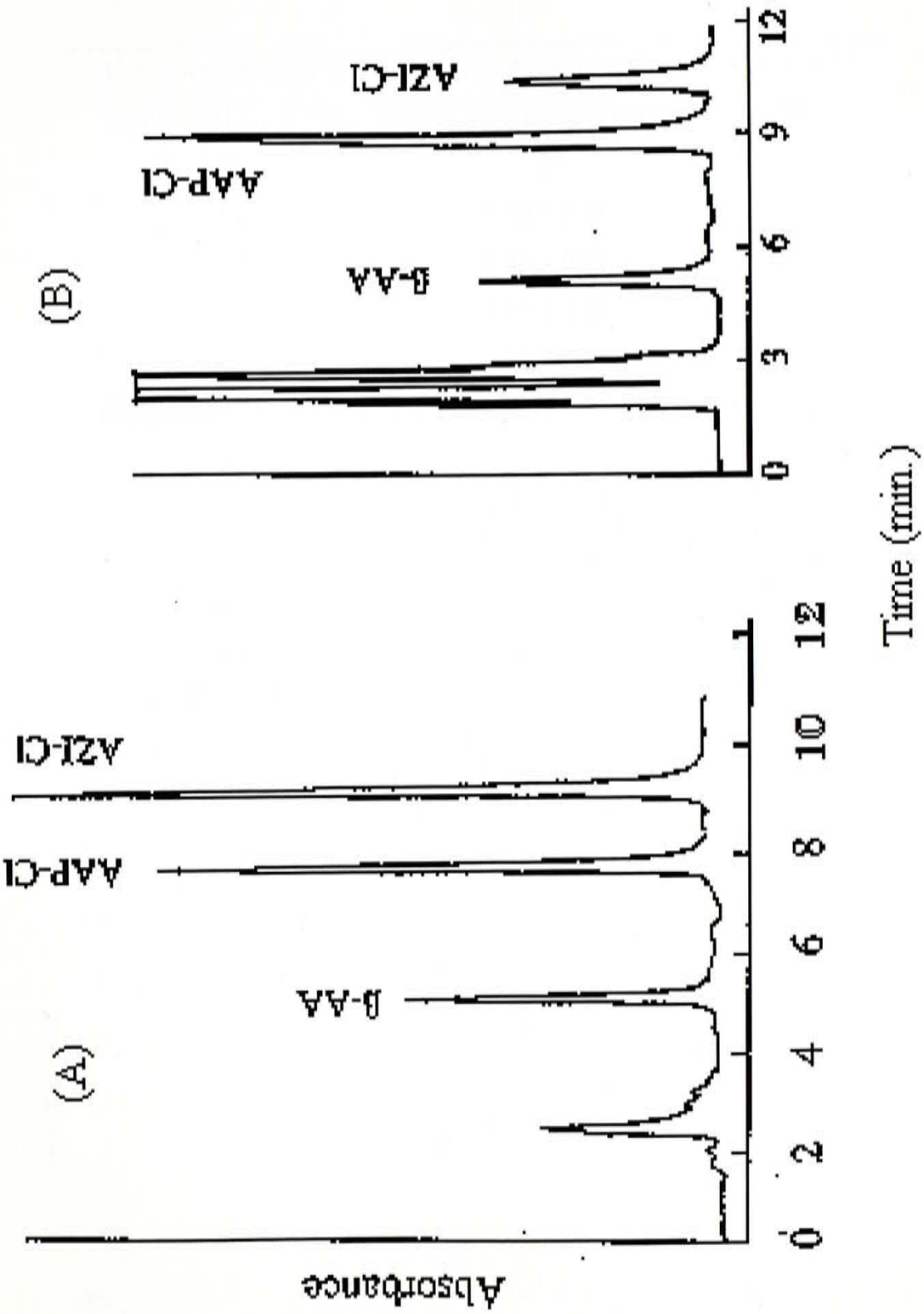

Figure 3.2.1 HPLC chromatograms of the extracts of (A) blank blood and (B) blank urine with addition of the standards.

Table 3.2.1 Peak area ratios found in the construction of calibration curves for *p*-Cl AAP in rat blood.

Concentration (μg/ml)	Peak Area Ratio *	C.V. (%) **
Low range ($y = 2.191x - 0.1568$, $R^2 = 0.9991$, mean C.V. = 5.58 %)		
0	0	-
0.2	0.30 ± 0.01	3.3
0.4	0.72 ± 0.03	4.2
0.6	1.13 ± 0.03	2.6
1.0	2.05 ± 0.25	12.2
High range ($y = 0.1672x - 0.0355$, $R^2 = 0.9973$, mean C.V. = 3.65 %)		
0	0	-
2.0	0.28 ± 0.01	3.6
4.0	0.62 ± 0.01	1.6
6.0	1.01 ± 0.02	2.0
10.0	1.62 ± 0.12	7.4

* Mean ± s.d. (n = 3)

** C.V. (%) = (s.d. / mean value) x 100 %

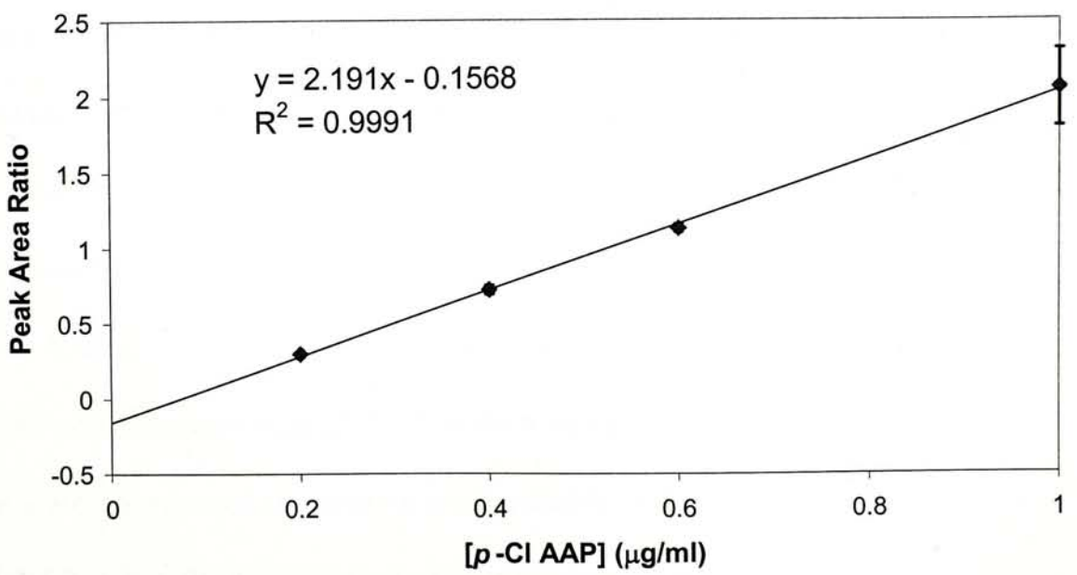

Figure 3.2.2 Calibration curve in the range 0-1.0 μg/ml for *p*-Cl AAP in rat blood.

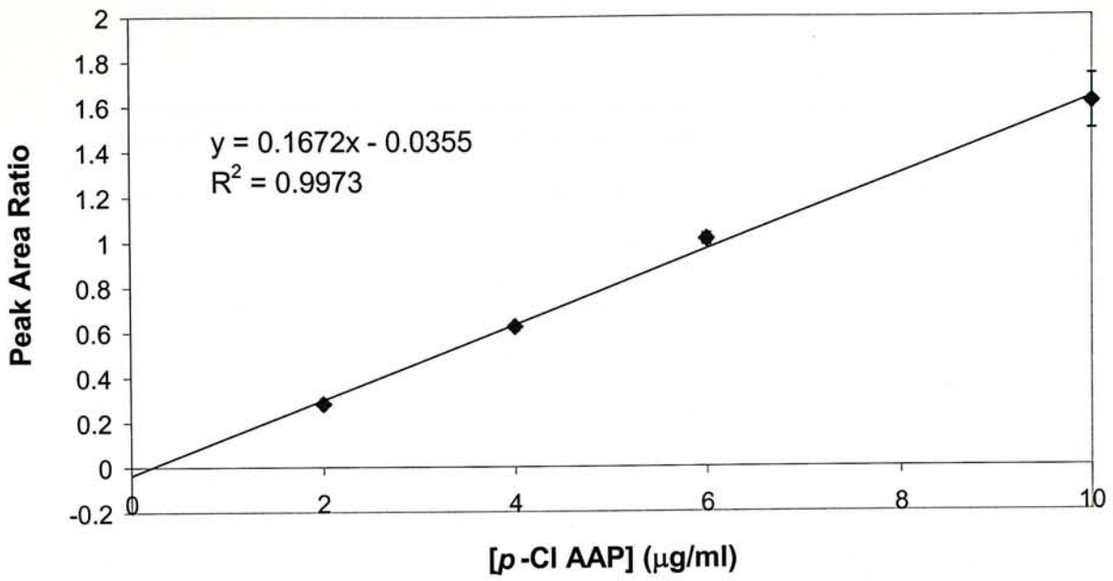

Figure 3.2.3 Calibration curve in the range 0-10.0 µg/ml for *p*-Cl AAP in rat blood

3.2.3 CONSTRUCTION OF CALIBRATION CURVES FOR *p*-Cl AAP IN THE RAT URINE

The peak area ratios of *p*-Cl AAP to *p*-Cl AZI for both lower and higher concentration ranges in rat urine are shown in Table 3.2.2, and the associated calibration curves are shown in Figure 3.2.4 and 3.2.5. The plot was linear over the high and low concentration ranges ($r > 0.98$; $n = 4$; $p < 0.05$) (each point was measured in triplicate).

A large deviation might result at two extremities of the calibration curve. High and low concentration ranges of calibration curves for *p*-Cl AAP in both rat blood and urine were constructed to ensure a more reliable and accurate quantitative analysis of *p*-Cl AAP in bio-fluid within these concentration ranges.

Table 3.2.2 Peak area ratios found in the construction of calibration curves for *p*-Cl AAP in rat urine.

Concentration (μg/ml)	Peak Area Ratio *	C.V. (%) **
Low range ($y = 0.1864x - 0.1081$, $R^2 = 0.9995$, mean C.V. = 2.1 %)		
0	0	-
2.0	0.28 ± 0.01	3.6
4.0	0.62 ± 0.02	3.2
6.0	1.01 ± 0.01	1.0
10.0	1.76 ± 0.01	0.6
High range ($y = 0.0128x + 0.0547$, $R^2 = 0.9745$, mean C.V. = 8.08 %)		
0	0	-
2.0	0.26 ± 0.01	3.8
4.0	0.57 ± 0.01	1.8
6.0	0.92 ± 0.03	3.3
10.0	1.28 ± 0.3	23.4

* Mean ± s.d. (n = 3)

** C.V. (%) = (s.d. / mean value) x 100 %

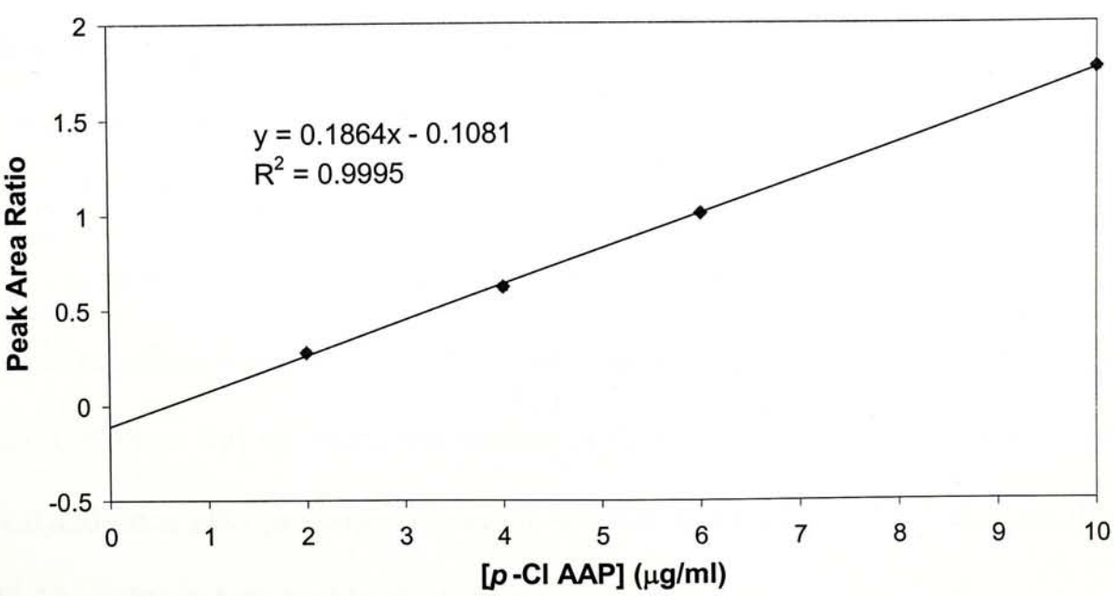

Figure 3.2.4 Calibration curve in the range 0-10 μg/ml for *p*-Cl AAP in rat urine.

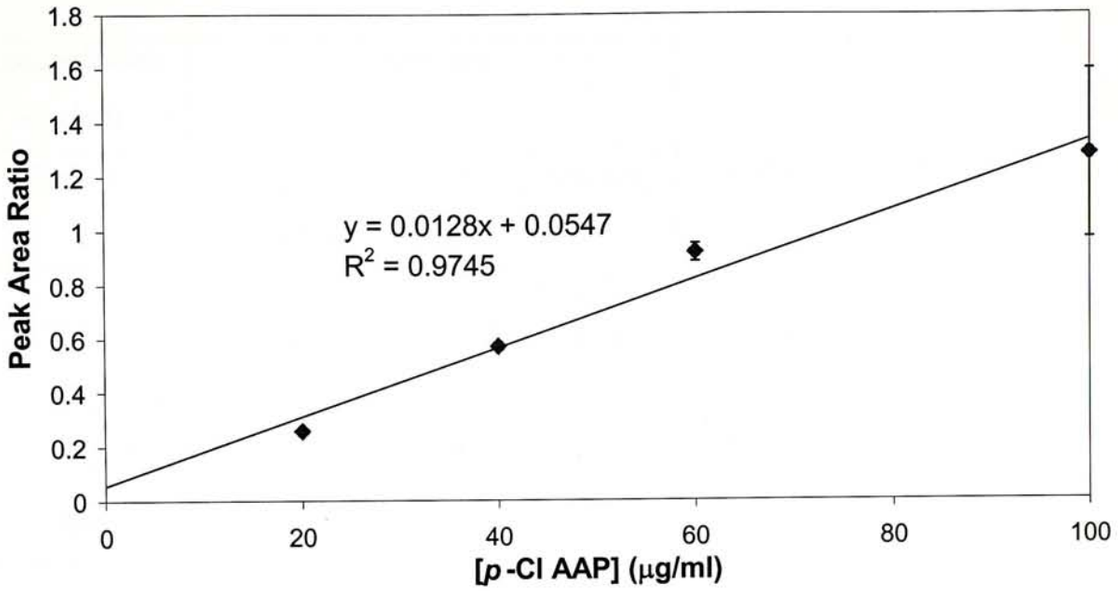

Figure 3.2.5 Calibration curve in the range 0-100 μg/ml for *p*-Cl AAP in rat urine

3.2.4 ACCURACY AND PRECISION IN THE QUANTITATION OF *p*-Cl AAP IN THE BIOLOGICAL SAMPLES

The developed assay was reproducible at both low and high concentrations with overall intra- and inter-day variations of less than 12.5% and 17.5%, respectively (as shown in Table 3.2.3). The accuracy of the assay was within a range of 83 to 98% for blood and 86 to 99% for urine samples.

In addition, the stability of *p*-Cl AAP in rat blood and urine, its recovery and limit of detection were determined by our research group (Lin, *et al.* 1998). It was found that there was no significant change in the concentration of *p*-Cl AAP in both blood and urine after prolonged storage at 4°C for at least 3 months, indicating that it is highly stable in both rat blood and urine.

Table 3.2.3 Intra- and inter-day variability for the assay of *p*-Cl AAP spiked in rat blood and urine.

Concentration (μg/ml)	Intra-day			Inter-day		
Spiked	Found (μg/ml)	C.V. (%)	Accuracy (%)	Found (μg/ml)	C.V. (%)	Accuracy (%)
Blood (n=3)						
0.2	0.18 ± 0.01	3.3	10.0	0.23 ± 0.04	17.4	15.0
0.8	0.67 ± 0.03	3.7	16.2	0.87 ± 0.09	10.6	8.8
2.0	1.73 ± 0.17	9.8	13.5	2.22 ± 0.35	15.8	11.0
4.0	3.92 ± 0.48	12.2	2.0	4.34 ± 0.56	12.9	8.5
Urine (n=3)						
2.0	2.10 ± 0.03	1.7	5.0	2.28 ± 0.32	14.0	14.0
8.0	7.74 ± 0.14	1.8	3.2	8.10 ± 0.56	6.9	1.3
25.0	22.6 ± 1.19	5.3	9.8	24.2 ± 1.78	7.4	3.2
75.0	81.2 ± 4.44	5.5	8.2	75.3 ± 1.64	2.2	0.4

C.V. (%) = (standard deviation/mean) x 100%

Accuracy (%) = [(mean measured conc. - spiked conc.) / spiked conc.] x 100%

The extraction recovery of *p*-Cl AAP from both blood and urine samples was 92 ± 3.0% and the limit of detection for this drug was 100 ng/ml in both urine and blood, respectively. A simple, sensitive and specific HPLC assay has been developed for the analysis of this novel aminoalkylpyridine anticonvulsant, *p*-Cl AAP, in rat biofluids which has been fully validated. This HPLC method allows the quantitative analysis of

p-Cl AAP in rat bio-fluids, and is useful for studying the metabolic and pharmacokinetic profiles of this novel anticonvulsant.

Since the preliminary metabolic studies in rats failed to show the presence of β-AA (the postulated active metabolite of *p*-Cl AAP), HPLC quantitation of this putative metabolite was not necessary and thus not reported here.

HPLC has many advantages over gas chromatography quantitatively and qualitatively. In gas chromatography, the solute must be volatile and thermally stable, whereas in liquid chromatography, high molecular weight compounds and those that are thermally labile, polar or non-volatile can be analyzed.

Since our *p*-Cl AAP is not volatile and only heat stable up to 250 °C as was described in the previous section, the detection of this novel anticonvulsant by HPLC is preferable.

3.3 PRELIMINARY PHARMACOKINETICS OF *p*-Cl AAP FOLLOWING INTRAVENOUS ADMINISTRATION

The concentrations of *p*-Cl AAP in blood as a function of time after single intravenous (i.v.) bolus administration of 20 mg/kg is shown in Table 3.3.1. The blood concentration-time curve is presented in Figures 3.3.1. The pharmacokinetic parameters are given in Table 3.3.2.

Table 3.3.1 Concentration of *p*-Cl AAP in blood after intravenous administration of 20 mg/kg.

Time	Concentration (μg/ml) *
5 min.	4.04 ± 0.74
15 min.	2.45 ± 0.46
30 min.	1.91 ± 0.33
45 min.	1.62 ± 0.22
1 hr.	1.47 ± 0.20
2 hr.	1.19 ± 0.09
3 hr.	1.03 ± 0.11
4 hr.	0.85 ± 0.11
5 hr.	0.74 ± 0.11

* Mean ± s.d. (n=5)

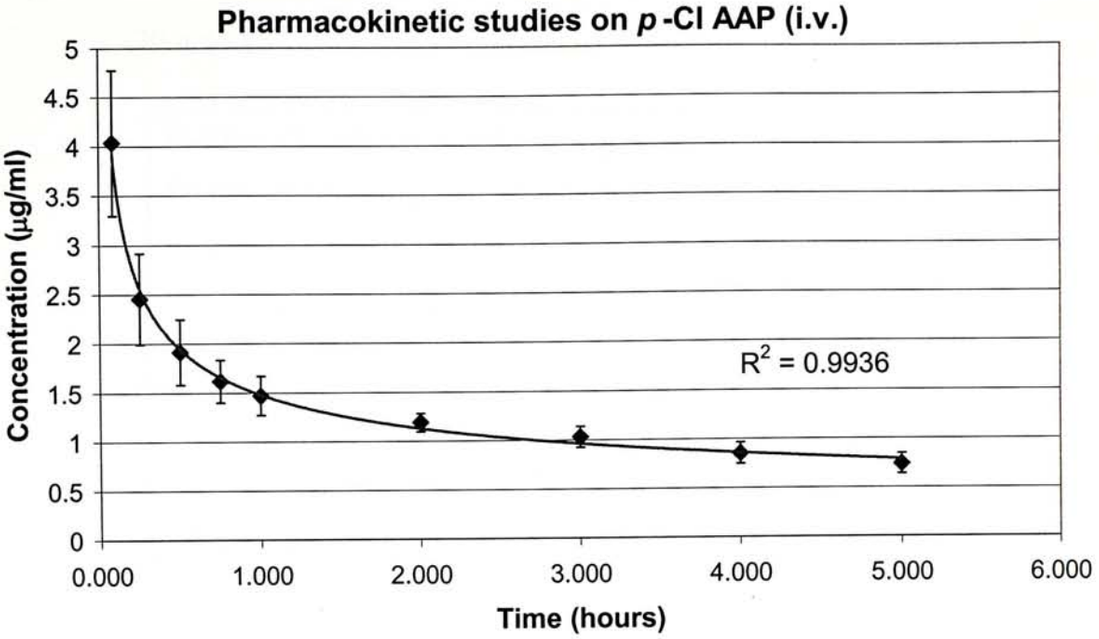

Figure 3.3.1 Blood concentration-time profiles of *p*-Cl AAP after single i.v. bolus administration to male Sprague-Dawley rats (20 mg/kg) (n = 5).

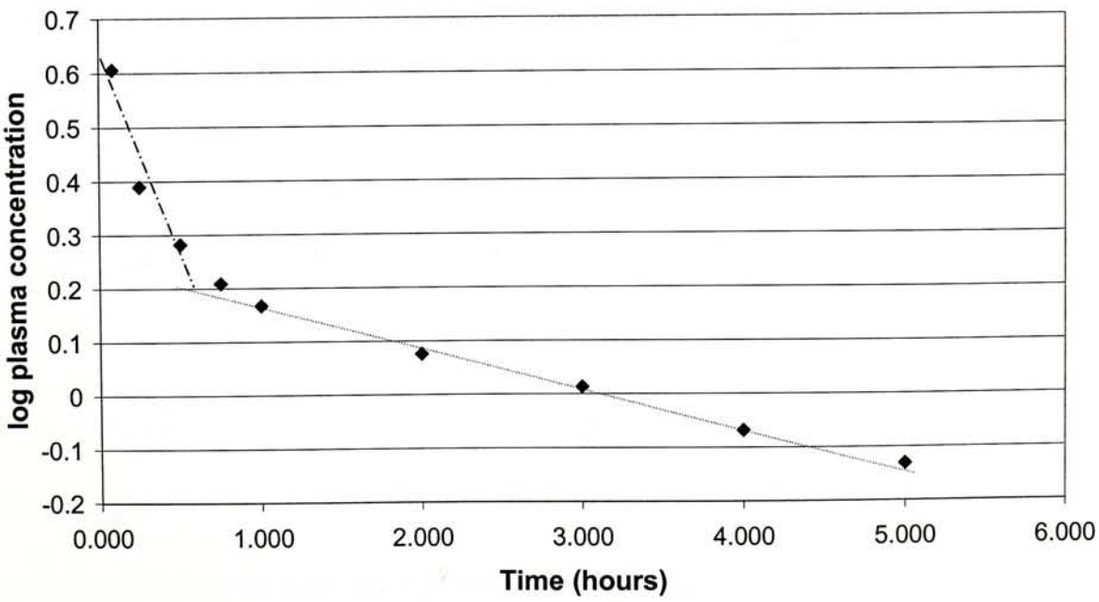

Figure 3.3.2 Log concentration of *p*-Cl AAP against time.

Table 3.3.2 Pharmacokinetic parameters of *p*-Cl AAP after intravenous administration (20 mg/kg).

Pharmacokinetic parameters	
Elimination rate (hr^{-1})	0.14 ± 0.04
Elimination half life (hr)	5.0 ± 0.9
Distribution rate (hr^{-1})	0.49 ± 0.2
Distribution half life (hr)	2.34 ± 1.0
Area Under Curve (AUC) (μg/ml•hr)	11.84 ± 1.7
Volume of distribution (Vd) (L/kg)	12.71 ± 4.6
Clearance (CL) (ml/hr)	1779.4 ± 315

The pharmacokinetic data for the intravenous single bolus administration showed a bi-exponential decline in the blood concentration of *p*-Cl AAP, characteristic of a two-compartmental model (Figure 3.3.2). The area under curve (AUC) was 11.84 ± 1.7 μg/ml•hr. The volume of distribution (Vd) was 12.71 ± 4.6 L, indicating extensive extravascular distribution. The clearance (CL) was 1779.4 ± 315 ml/hr. The elimination rate and half life of *p*-Cl AAP were 0.14 ± 0.04/hr and 5.0 ± 0.9 hrs, respectively. The distribution rate and half-life were 0.49 ± 0.2/hr and 2.34 ± 1.0 hrs, respectively.

β-cyclodextrin was used as a vehicle for the administration of *p*-Cl AAP to rats. It is enzymatically modified starches consisting of glucopyranose units in a ring system. It is crystalline, non-hygroscopic and feature a cylinder shaped, macro-ring structure with an internal axial cavity. The outer surface of cyclodextrin is hydrophilic

whilst the internal cavity is apolar. These properties make cyclodextrin a useful material for solubilizing lipophilic molecules. β-cyclodextrin is the most frequently used vehicle because of its favourable cavity size for pharmaceutical compounds. In addition, no covalent binding is involved in solubilizing *p*-Cl AAP or other lipophilic compounds. As *p*-Cl AAP is a very lipophilic compound, β-cyclodextrin is a good vehicle for the administration of this novel anticonvulsant.

3.4 URINARY METABOLIC STUDIES OF *p*-Cl AAP

3.4.1 QUALITATIVE STUDIES : IDENTIFICATION OF METABOLITES

Typical HPLC chromatograms obtained from analysis of urinary extracts pre- and post-dose of *p*-Cl AAP are shown in Figure 3.4.1. Three major peaks are clearly shown in the post-dose sample which were absent in the pre-dose (control) urine sample. Figure 3.4.2 shows the HPLC chromatograms of the urine sample after β-glucuronidase and aryl sulphatase / β-glucuronidase deconjugation. After β-glucuronidase deconjugation (Figure 3.4.2 (A)) of the urine sample, three more peaks were found from the chromatograms. These additional peaks represented the glucuronide conjugates of the metabolites. These metabolites were formed due to the deconjugation by β-glucuronidase. After aryl-sulphatase / β-glucuronidase deconjugation (Figure 3.4.2 (B)) of the urine sample, another four peaks were observed from the chromatograms when compared with non-deconjugated urinary extract. These additional peaks represented either glucuronide and/or sulphate conjugates which were deconjugated by β-glucuronidase and/or aryl sulphatase / β-glucuronidase, respectively. When compared with the samples deconjugated by β-glucuronidase only, only one more peak was obtained (peak 7, Figure 3.4.2 (B)), indicating that only sulphate conjugate of this metabolite was excreted from rat urine.

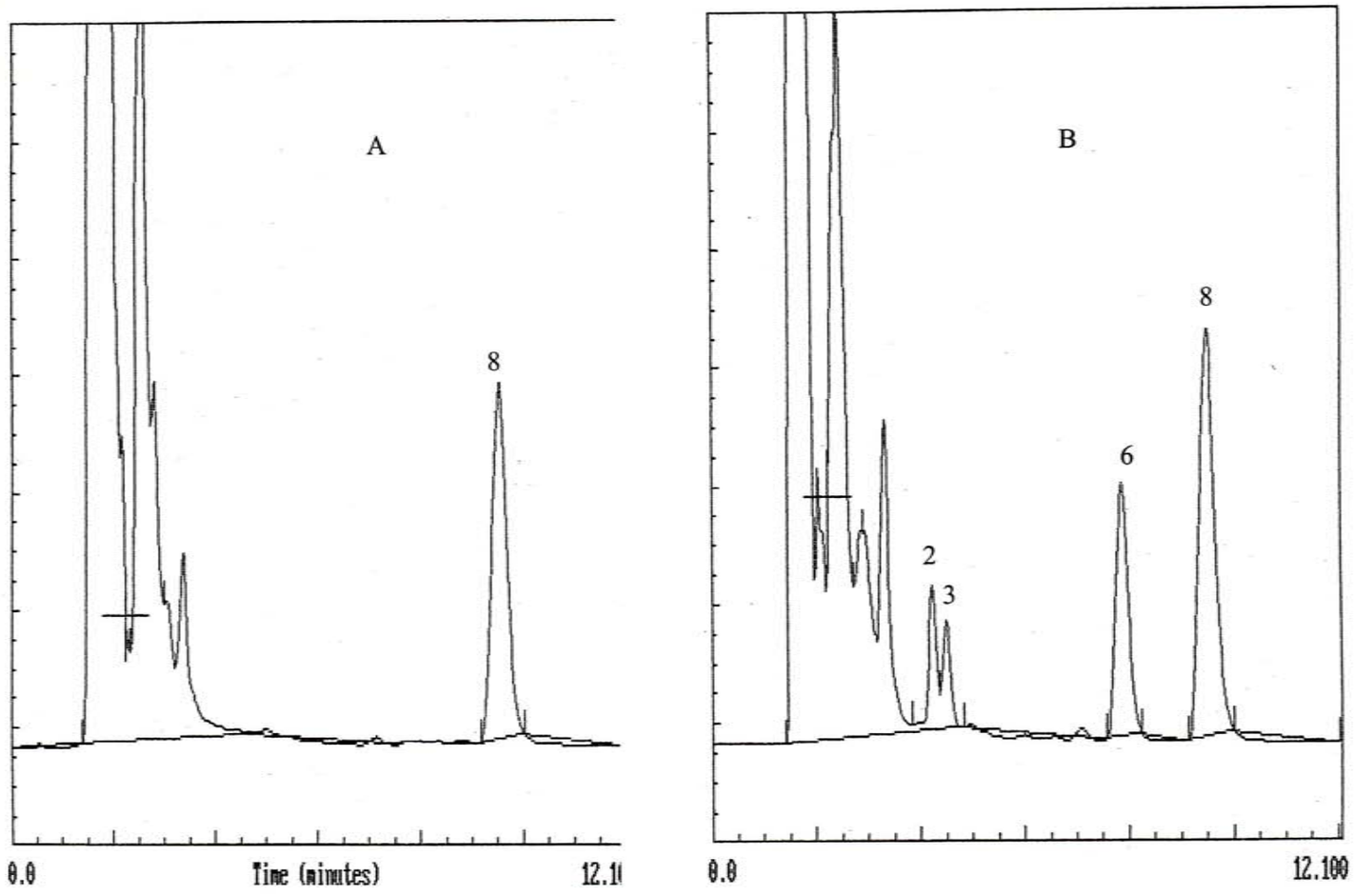

Figure 3.4.1 A) HPLC chromatogram of control rat urine spiked with the internal standard, B) HPLC chromatogram of rat urine following *p*-Cl AAP administration.
(2 = metabolite-2, 3 = metabolite-3, 6 = *p*-Cl AAP, 8 = internal standard)

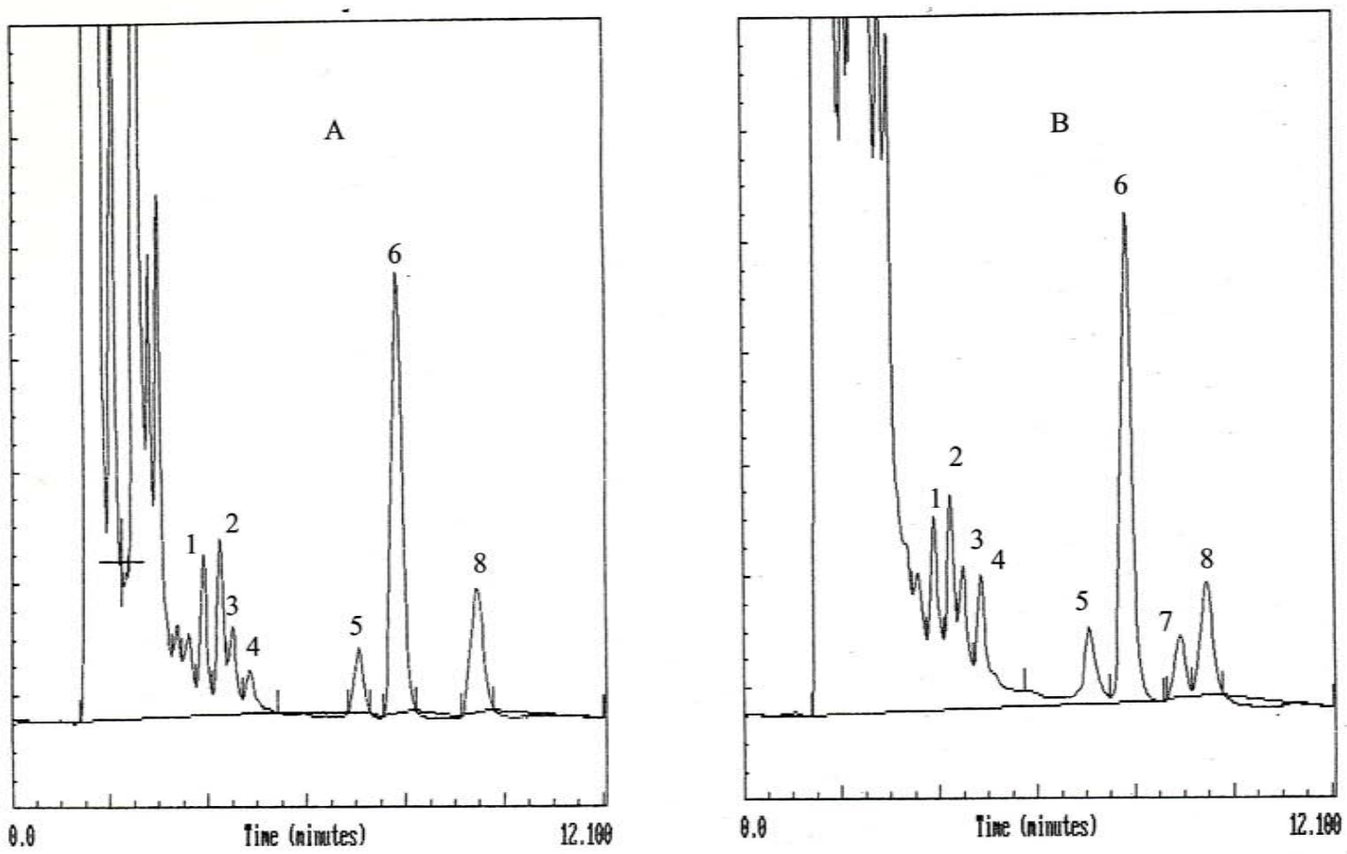

Figure 3.4.2 HPLC chromatogram of rat urine following *p*-Cl AAP administration A) β-glucuronidase and B) Aryl-sulphatase/β-glucuronidase deconjugation.
(1 = metabolite-1, 2 = metabolite-2, 3 = metabolite-3, 4 = metabolite-4, 5 = metabolite-5, 6 = *p*-Cl AAP, 7 = metabolite-6, 8 = internal standard)

Based on the HPLC data (retention time) shown in Table 3.4.1, peaks 6 and 8 were *p*-Cl AAP and the internal standard, *p*-Cl AZI respectively. However, β-amino alcohol was not formed as a urinary metabolite of *p*-Cl AAP by comparison of the HPLC prospects of the authentic standard (Table 3.4.1)

Table 3.4.1 Retention times of *p*-Cl AAP, internal standard (*p*-Cl AZI) and unknowns / putative metabolites. (n = 5)

Compound		Retention Time * (min.)
Authentic samples		
β-amino alcohol (β-AA)		4.67
p-Cl AAP		7.96
p-Cl AZI		9.60
Metabolites in urine of rats administrated with *p*-Cl AAP		
Peak 1	(metabolite-1)	3.91
Peak 2	(metabolite-2)	4.25
Peak 3	(metabolite-3)	4.50
Peak 4	(metabolite-4)	4.87
Peak 5	(metabolite-5)	7.13
Peak 6	(*p*-Cl AAP)	7.88
Peak 7	(metabolite-6)	8.95
Peak 8	(*p*-Cl AZI)	9.49

* HPLC conditions as outlined in section 2.3.1.

In order to identify the chemical structures of the suspected metabolites, crude urinary extracts were analyzed by on-line HPLC/MS. However, since the utilized HPLC conditions failed to separate all analytes from various interfering compounds

present in the crude extract, the resulting mass spectra were not suitable for structural elucidation. Therefore, the crude extract after enzymatic deconjugation was further separated into four fractions by a preparative HPLC. The purified fractions were then analyzed by HPLC/MS/MS with atmospheric pressure chemical ionization (APCI) interface at both positive and negative ion modes.

Figure 3.4.3 show the negative ion mass spectrum of the parent drug, *p*-Cl AAP. An intense peak at *m/z* 291 (Figure 3.4.3 (A)) and corresponding Cl-isotope peak at *m/z* 293 with about 30 % intensity. This confirmed that analyte contains Cl atom. As demonstrated in the corresponding MS/MS spectrum (Figure 3.4.3 (B)), the ion at *m/z* 291 degraded readily to form a daughter ion at *m/z* 231, which represented the quasi-molecular ion of *p*-Cl AAP. The different of 60 mass units is due to the loss of acetic acid, which present in the mobile phase form adduct with the parent drug. Selecting ion of *m/z* 231 for further MS/MS study (Figure 3.4.3 (C)), no characteristic fragmentations can be found. This indicated that the molecule of *p*-Cl AAP is very stable under the utilized conditions for APCI-MS and MS/MS analysis.

As mentioned in the previous paragraph, chloride isotope peak with 2 mass units apart aids the identification of the chlorine-containing compounds. In the following, the elucidation of structure of the metabolites of *p*-Cl AAP assisted by the characteristic mass spectrum of chloride related compounds. However, in the MS/MS spectrum, the daughter ions degraded from the selected mother ions will not exhibit the Cl isotope peak, because only the single ion containing the most abundant ^{35}Cl will be selected for collision-induced dissociation (CID).

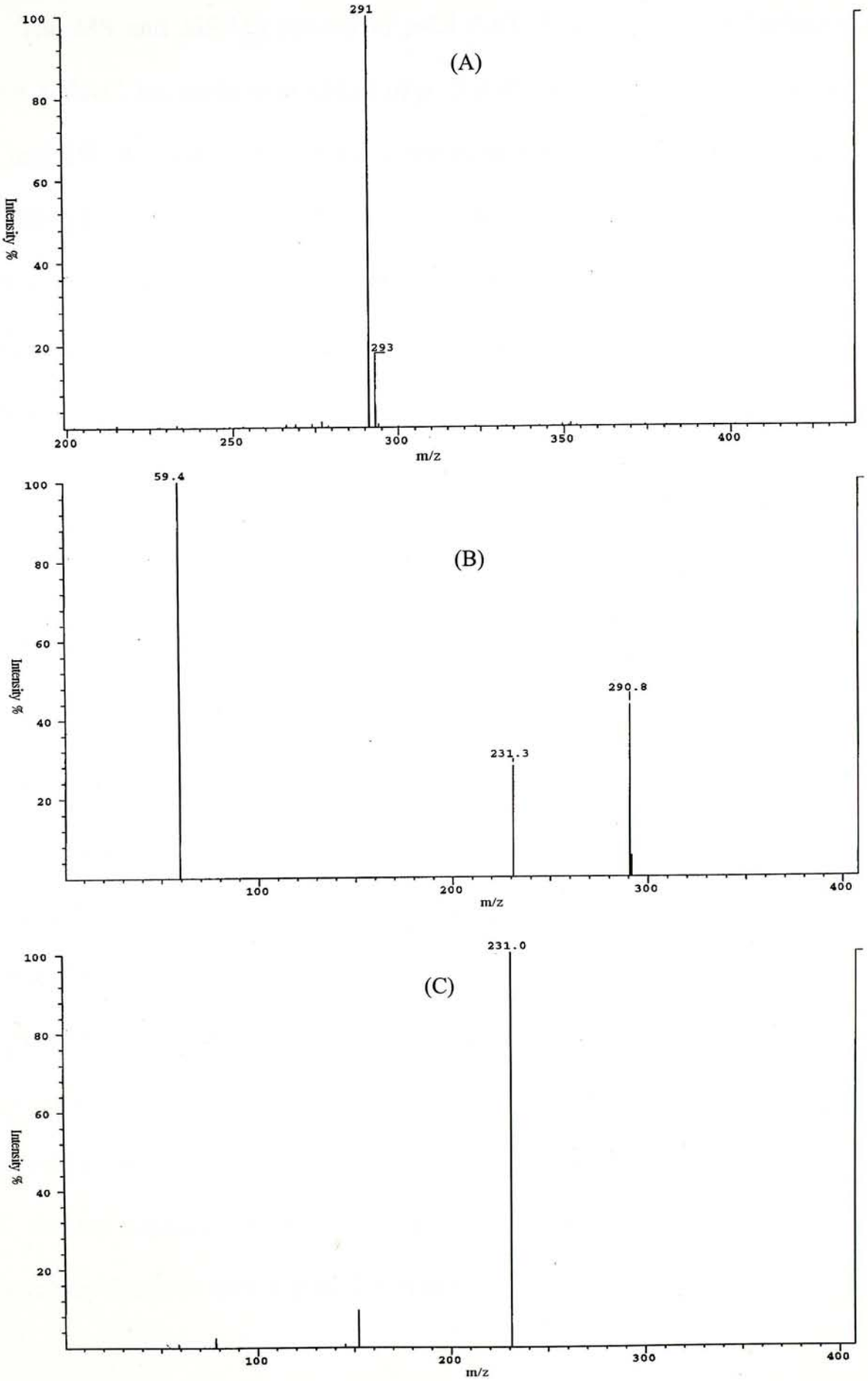

Figure 3.4.3 Negative-ion mass spectra of *p*-Cl AAP, A) MS spectrum, B) MS/MS spectrum (select ion at *m/z* 291), C) MS/MS spectrum (select ion at *m/z* 231).

The MS and MS/MS spectra of *p*-Cl AAP demonstrated the formation of "solvent adduct", i.e. acetic acid adduct of *p*-Cl AAP. For the soft ionization, such as APCI and ESI, it is very common that compounds with a small molecule present in the mobile phase can interact with the analytes to form the "solvent adduct". As this adduct is not covalently bound compound, only small amount of energy can cause its dissociation. Therefore, a quasi-molecular ion can be easily yielded in the MS/MS spectrum with a suitable CID energy (Williams and Fleming, 1987).

As shown in Figure 3.4.4, the total ion chromatogram obtained from HPLC/MS/MS analysis of fraction 1 exhibited two peaks, which were defined to be metabolite-1 and metabolite-2, respectively, by comparison of their retention times with those obtained in the HPLC-UV analysis as discussed in the section 2.3. For metabolite-1, the negative ion mass spectrum showed a quasi-molecular ion at *m/z* 279 $[M-1]^-$, together with a Cl isotope peak at *m/z* 281, indicating that it is a drug related metabolite (Figure 3.4.5 (A)), and its corresponding reconstructed ion chromatogram obtained by using selective ion monitoring (SIM) programmer also confirmed that only one metabolite contained such a molecular ion (Figure 3.4.4). Therefore, the molecular weight of metabolite-1 was determined to be 280 Da, indicating addition of three oxygen atoms in the parent *p*-Cl AAP. The MS result suggested that this analyte is an oxidized metabolite. Furthermore, using a CID energy of 30 eV, the negative-ion MS/MS spectrum of this metabolite did not show any characteristic fragment ions (Figure 3.4.5 (B)).

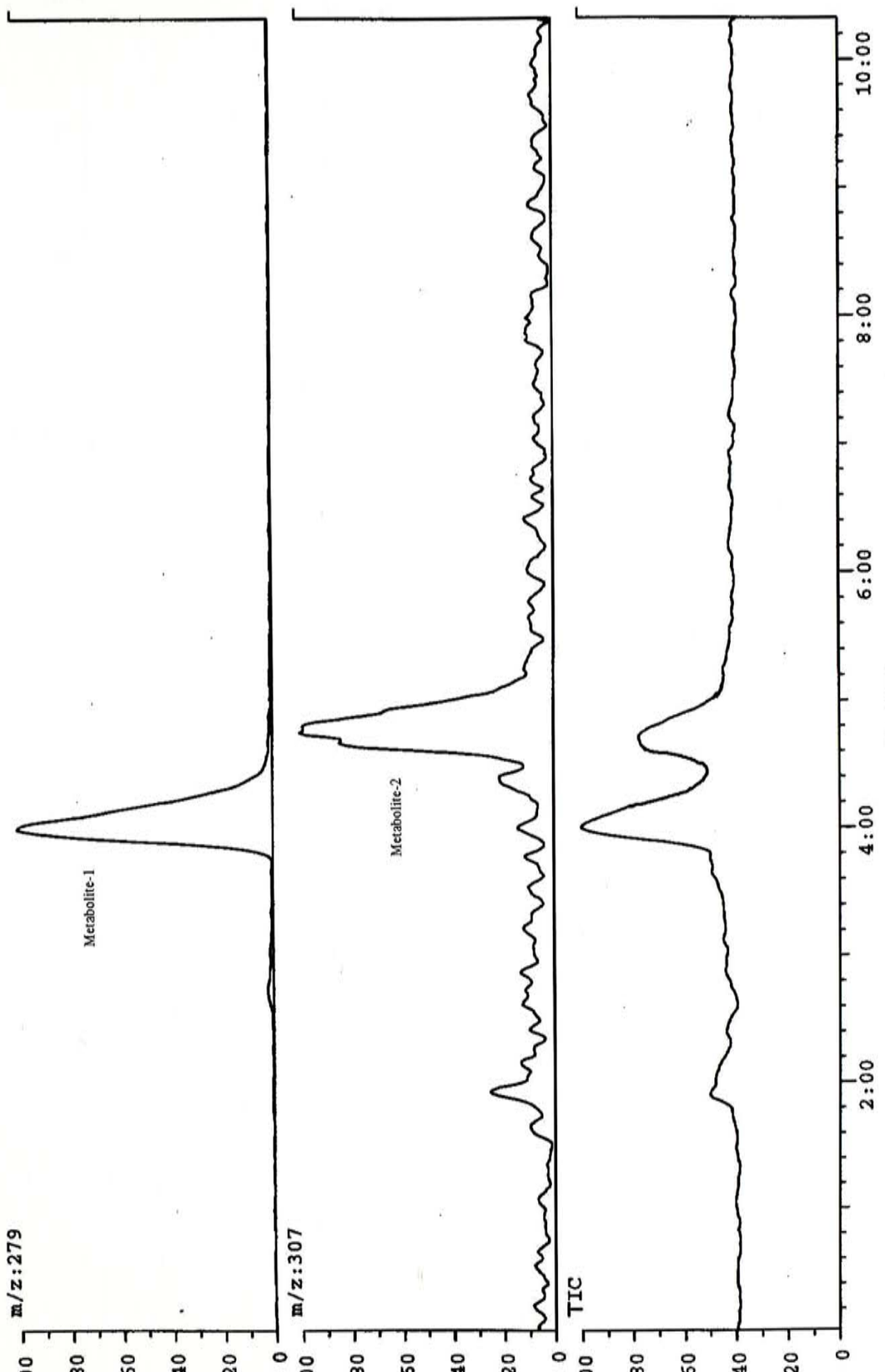

Figure 3.4.4 Total ion and reconstructed ion chromatograms obtained from HPLC/MS analysis of fraction 1. TIC, total ion current.

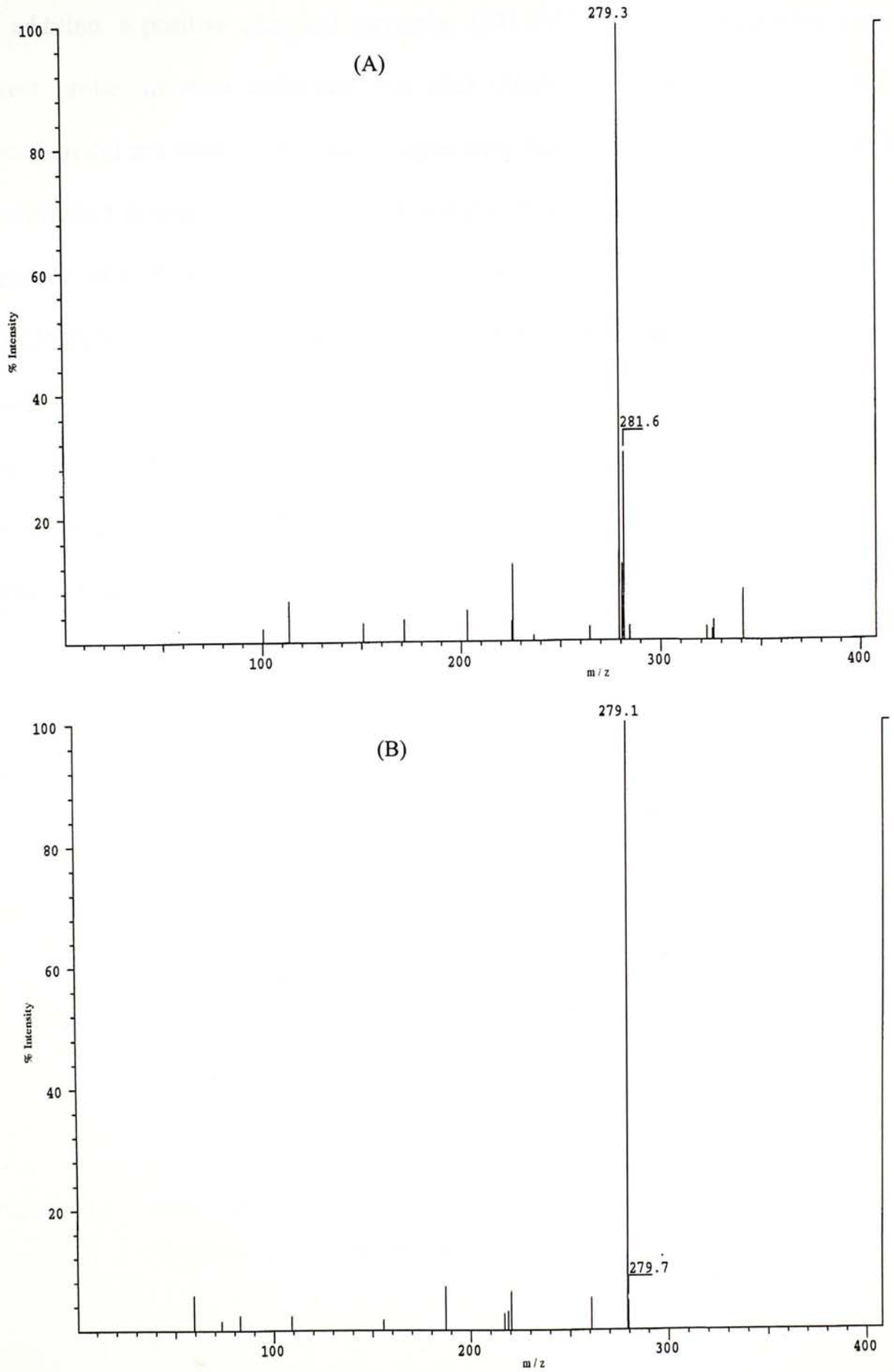

Figure 3.4.5 Negative-ion mass spectra of metabolite-1 from respective chromatograms of Figure 3.4.4. A) MS spectrum, B) MS/MS spectrum of metabolite-1.

In addition, a positive chemical ionization (CI) MS/MS of this metabolite using a direct probe insertion technique was also conducted. The resultant CI-MS/MS spectrum did not show fragmentation again (not shown). These results suggested that metabolite-1 is relatively stable to CID, and thus this compound should have a general structure of C_5H_4N-$CH(CH_3)$-NH-C_6H_5, similar to that of the parent *p*-Cl AAP. In APCI-MS/MS, phenolic groups are difficult to be dissociated (Herbert *et al.*, 1967), while hydroxyl groups generally generate fragment ions with a loss of water, a 18 mass units. Furthermore, in the case of *N*-oxide, a loss of 16 mass units corresponding to an oxygen atom is commonly observed (Herbert *et al.*, 1967). Therefore, the oxidative sites are likely in the aromatic rings, i.e. three hydroxyl functional groups substituted in the aromatic rings. Thus, the structure of metabolite-1 has been tentatively identified as trihydroxylated *p*-Cl AAP, *N*-[4-(2-hydroxychlorophenyl)]-1-[4-(2,6-dihydroxypyridyl)]ethylamine (Figure 3.4.6).

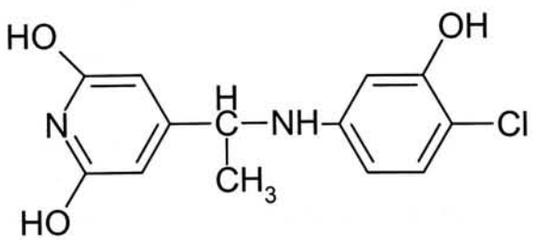

Figure 3.4.6 Structure of metabolite-1, *N*-[4-(2-hydroxychlorophenyl)]-1-[4-(2,6-dihydroxypyridyl)]ethylamine.

The positions of three hydroxyl groups could not be assigned in the present study. However, it is likely that two hydroxyls are situated at 3 and 5 positions in the pyridine ring and the third is at the 3 position in the benzene ring.

Metabolite-1 was only found after glucuronidase and/or aryl-sulphatase deconjugation. Therefore, the identified urinary metabolite-1 is mainly in its *O*-glucuronide and *O*-sulphate conjugates. However, whether or not all hydroxyl groups or only one of them were conjugated could not be determined in this study. In addition, arylamine sulphate might also form. Further studies involving the use of Nuclear Magnetic Resonance (NMR) and Infrared (IR) analysis are required for a definitive identification of this metabolite.

The negative ion APCI-MS spectrum obtained from HPLC/MS/MS analysis of the second analyte, metabolite-2, in fraction 1 showed the highest mass ion at *m/z* 307 with Cl isotope peak at *m/z* 309 (Figure 3.4.7 (A)). As demonstrated in the corresponding MS/MS spectrum (Figure 3.4.7 (B)), the ion at *m/z* 307 easily degraded to form a daughter ion at *m/z* 247, which represented the quasi-molecular ion of metabolite-2. Therefore, molecular weight of metabolite-2 was determined to be 248 Da, and the ion at *m/z* 307 ($[M + AcOH-1]^-$) was an acetic acid adduct of metabolite-2. Compared with molecular weight of the parent *p*-Cl AAP (232 Da), metabolite-2 has one more oxygen atom in the structure and should be the oxidized metabolite of *p*-Cl AAP. However, this metabolite is not the β-amino alcohol as its retention time does not match that of the authentic standard.

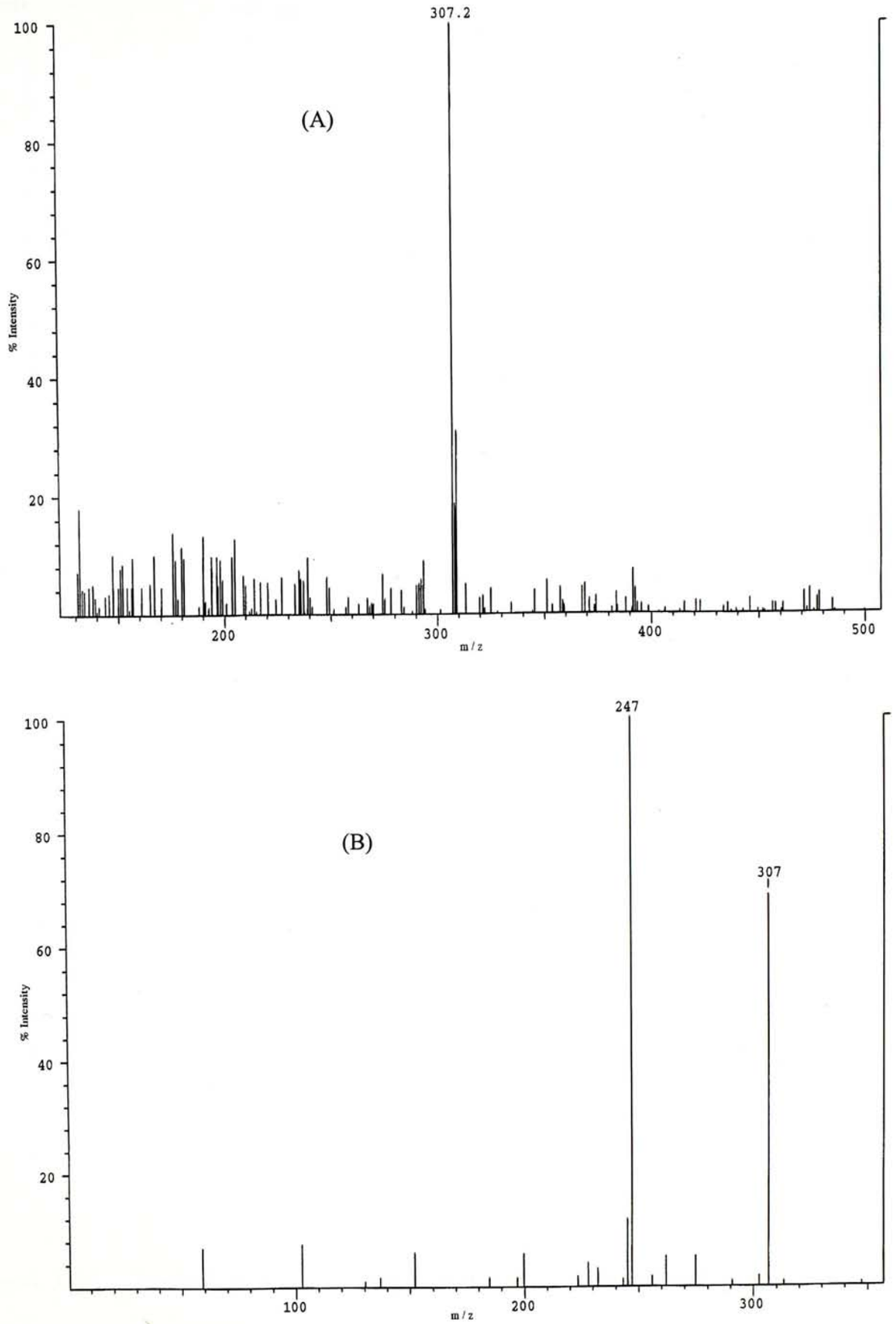

Figure 3.4.7 Negative-ion mass spectra of metabolite-2 from respective chromatograms of Figure 3.4.4. A) mass spectrum, B) MS/MS spectrum of metabolite-2.

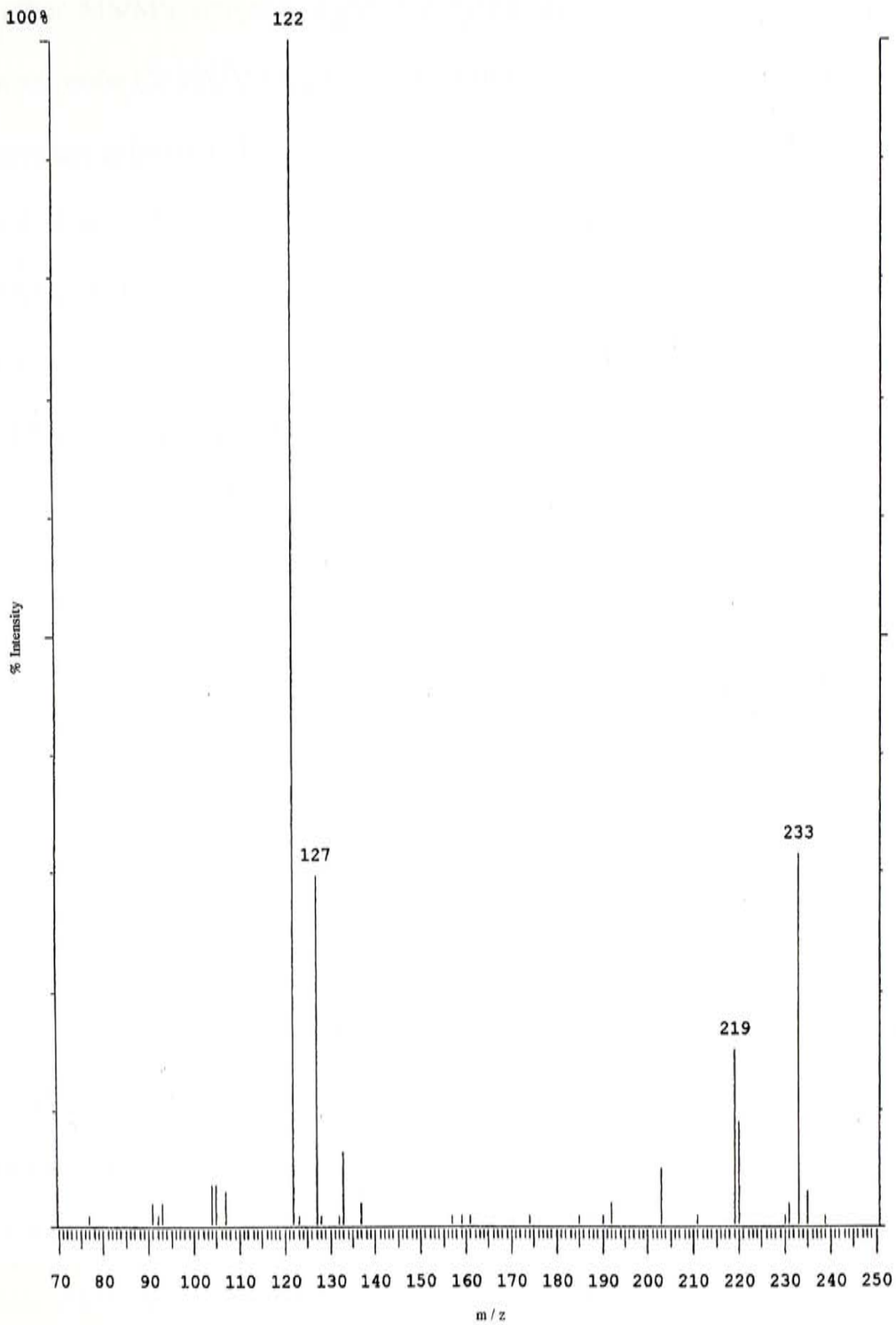

Figure 3.4.8 Positive-ion CI-MS/MS spectrum of metabolite-2.

Further MS/MS analysis of this metabolite did not produce other fragment ions, a direct probe CI-MS/MS analysis with a positive ion mode was performed. CI-MS/MS spectrum exhibited characteristic ions at *m/z* 122, the base peak, and other fragment ions at *m/z* 233, 219 and 127, respectively (Figure 3.4.8). Based on the fragment pattern, metabolite-2 was tentatively identified as *N*-[4-(chorophenyl)]-1-hydroxyl-1-[4-(pyridyl)]ethylamine. The proposed structure of metabolite-2 is shown in Figure 3.4.9 and mass fragment pathway in Figure 3.4.10.

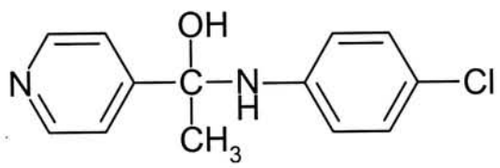

Figure 3.4.9 Structure of metabolite-2, *N*-[4-(chlorophenyl)]-1-hydroxy-1-[4-(pyridyl)]ethylamine.

As shown in Figure 3.4.10, the fragment ion at *m/z* 122 was generated *via* a loss of a neutral molecular [HN-C_6H_4Cl + OH], which is favourable for carbinolamine moiety and could not be observed in the MS spectrum of the parent *p*-Cl AAP. The CI-MS/MS spectrum also suggested that this oxidized metabolite should not be the aromatic ring hydroxylated *p*-Cl AAP, since phenolic metabolites could not be fragmented as demonstrated in MS spectrum of the parent *p*-Cl AAP (Herbert *et al.*, 1967). Therefore, the hydroxyl group is most likely located at the α carbon atom, and the assigned structure was derived (Figure 3.4.9).

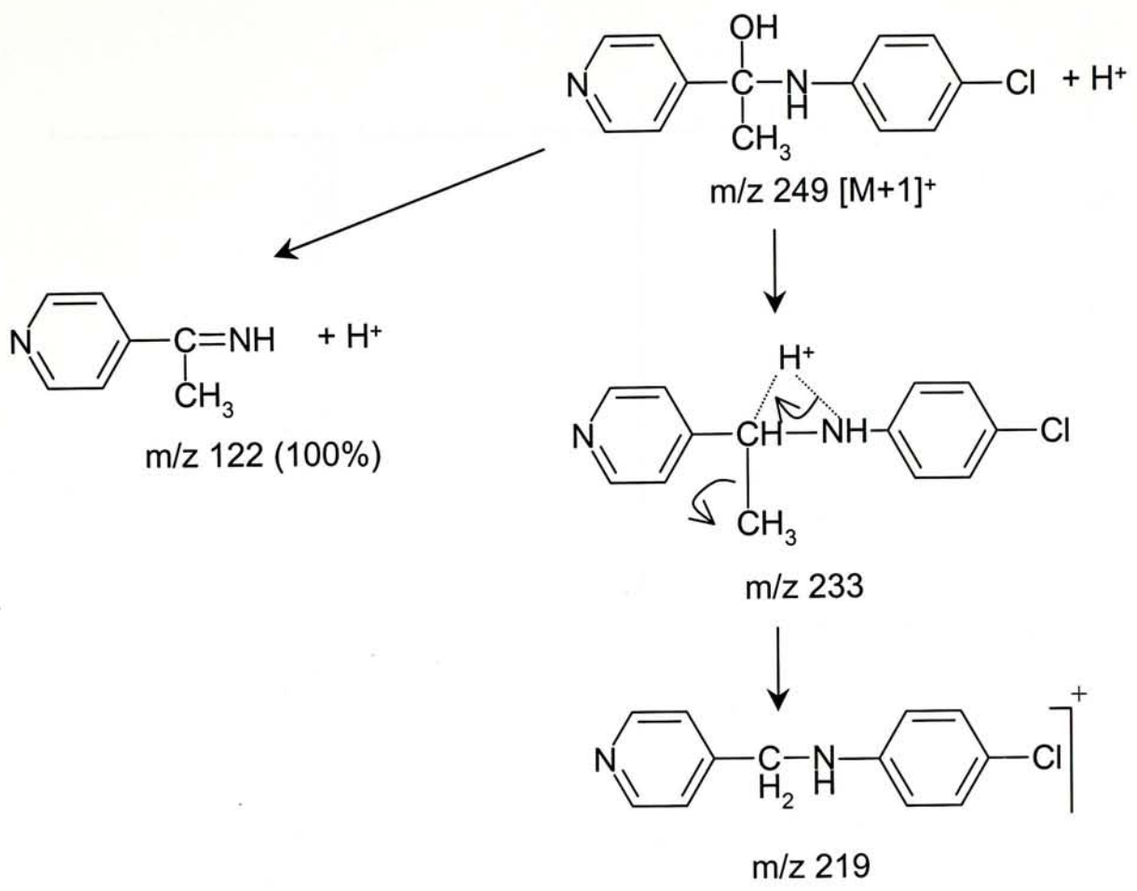

Figure 3.4.10 Possible fragment pattern of metabolite-2 in positive ion CI-MS.

Both phase I and phase II of this metabolite were found in the rat urine. For the phase II metabolite, the glucuronide and sulphate conjugates were all identified. The hydroxyl functional group should be a main site for *O*-glucuronidation. Whilst, arylamine sulphation is most likely for sulphate conjugate.

The total ion and reconstructed ion chromatograms obtained from HPLC/MS/MS analysis of fraction 2 are shown in Figure 3.4.11. Two peaks corresponding to metabolite-3 and metabolite-4 were observed.

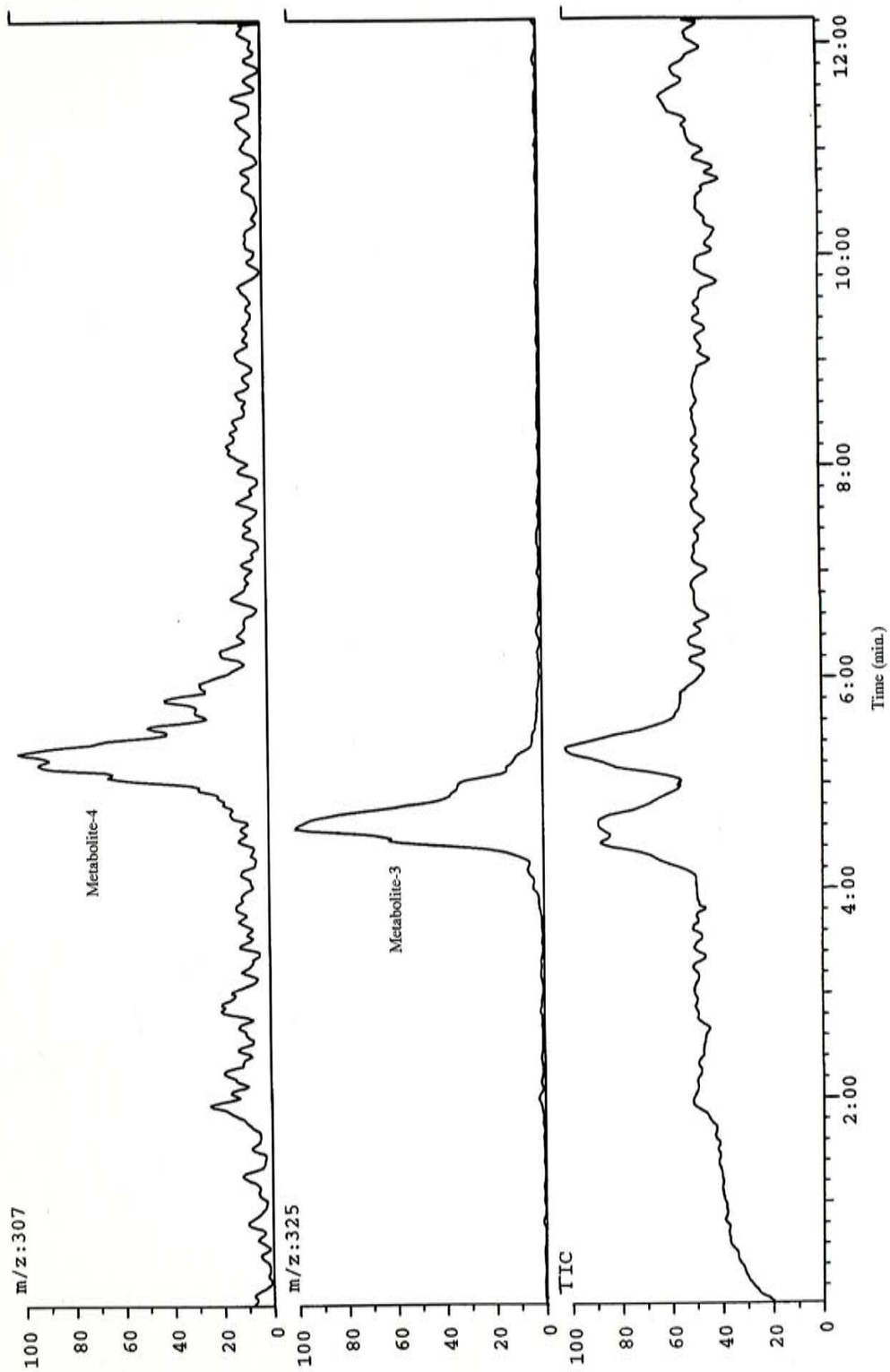

Figure 3.4.11 Total ion and reconstructed ion chromatograms obtained from HPLC/MS analysis of fraction 2. TIC, total ion current

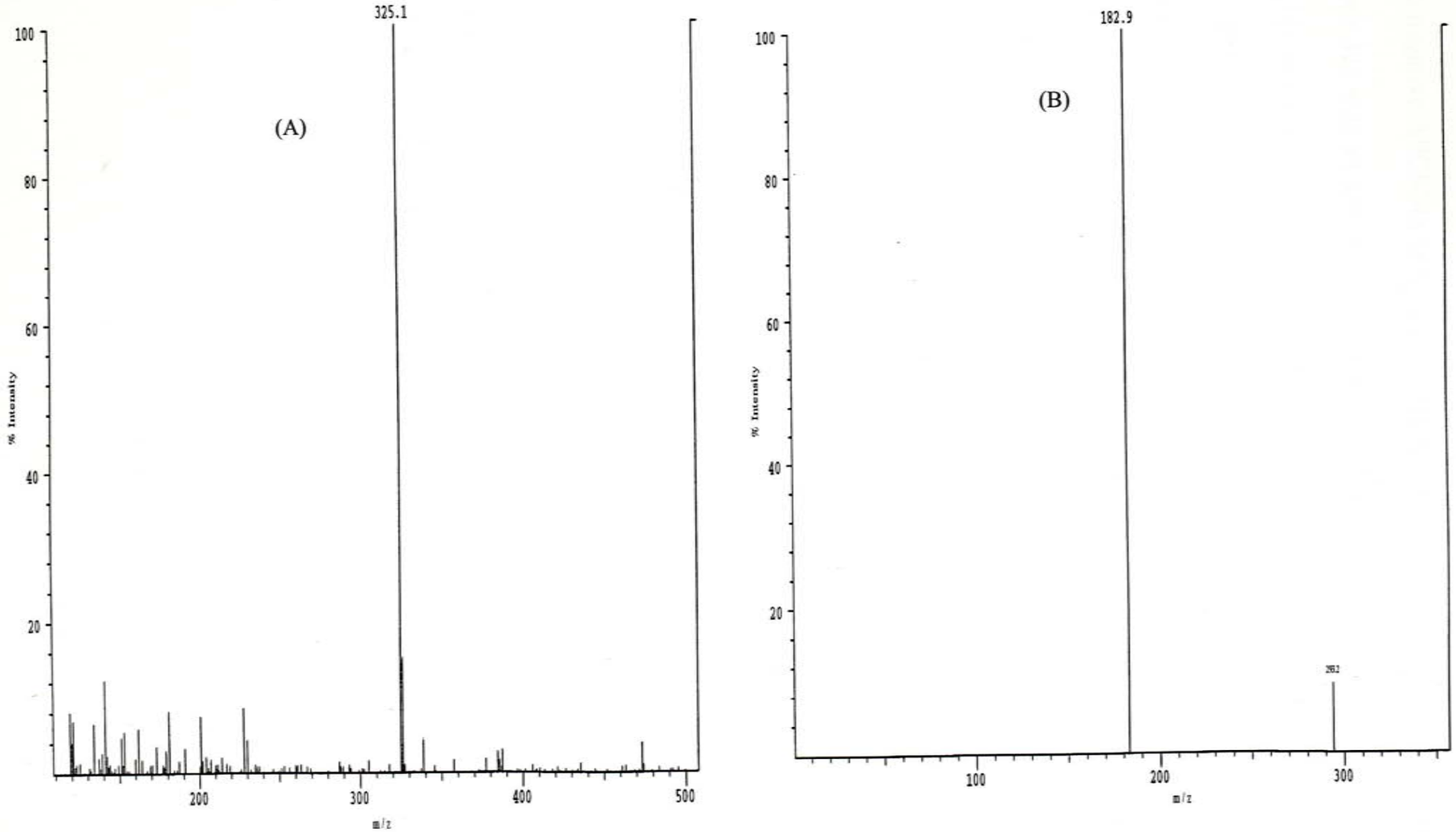

Figure 3.4.12 Negative-ion mass spectra of metabolite-3 from respective chromatograms of Figure 3.4.11. A) MS spectrum, B) MS/MS spectrum of metabolite-3.

The negative APCI-MS spectrum of metabolite-3 showed an ion of the highest mass at *m/z* 325 with an appropriate intensity of Cl isotope peak (Figure 3.4.12 (A)), which readily lost a 32 mass unit corresponding to a methanol molecule, to give an ion at *m/z* 293 as shown in the MS/MS spectrum (Figure 3.4.12 (B)). Therefore, the molecular weight of metabolite-3 was determined to be 294 Da, and the ion at *m/z* 325 corresponded to the methanol adduct of metabolite-3. Compared with the molecular weight of metabolite-1, metabolite-3 had a 14 mass unit more, and this suggested that two hydroxyl and one carboxylic acid groups were introduced into the parent *p*-Cl AAP (Figure 3.4.13).

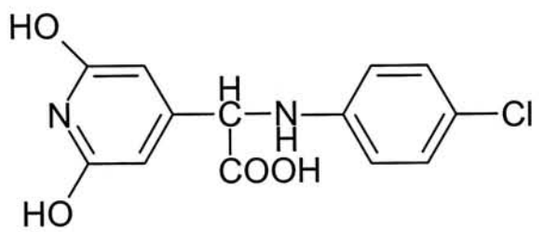

Figure 3.4.13 Structure of metabolite-3, 2-[(4-chlorophenyl)]amino-2-[4-(2,6-dihydroxypyridyl)]ethanoic acid.

Substitution of the two hydroxyl groups were assigned at 3 and 5 position in the pyridine ring, which was demonstrated by the most intensive peak at *m/z* 183 in the MS/MS spectrum (Figures 3.4.12 (B) and 3.4.14). Therefore, the structure of metabolite-3 was identified as 2-[(4-chlorophenyl)]amino-2-[4-(2,6-dihydroxypyridyl)]ethanoic acid.

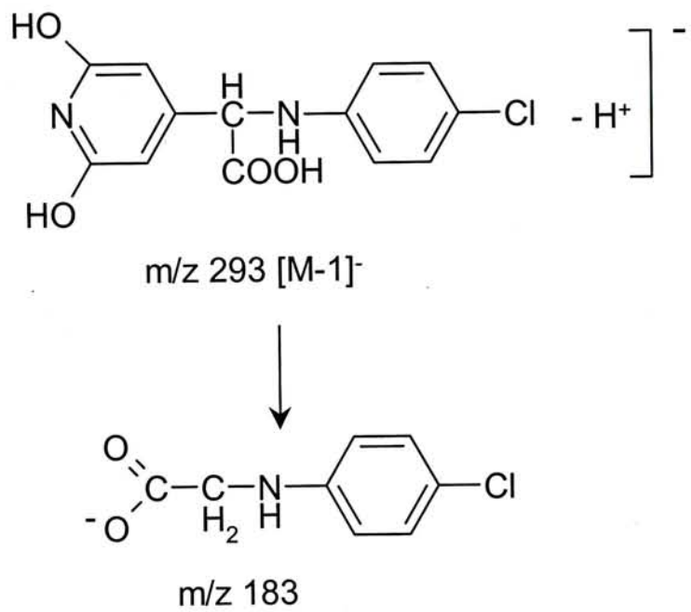

Figure 3.3.14 Possible fragment pattern of metabolite-3 in negative ion APCI MS/MS.

The fragment ion of *m/z* 183 indicates the hydroxyl group can only present in the pyridine ring since hydroxyl group in benzene ring is difficult to remove (Herbert *et al.*, 1967). On the other hand, if hydroxyl group in the carbon next to the amine, a loss of 18 mass unit represent the water molecule should be observed in the MS/MS spectrum. However, no such fragment pattern can be found. Again, hydroxylamine is unstable in that its formation is thermodynamically not favorable.

Both phase I and phase II forms, including glucuronide and sulphate conjugates, of metabolite-3 were found in the urine of rats dosed with *p*-Cl AAP. *O*-glucuronidation and *O*-sulphation can occur on both phenol and carboxylic acid functional groups, however, the site(s) for these conjugations could not be determined in the present study.

For metabolite-4, the HPLC/MS/MS analysis for fraction 2 showed the ion with 100 % intensity at *m/z* 247 corresponding to the quasi-molecular ion in the negative ion APCI MS/MS spectrum (Figure 3.4.15 (B)), and the highest mass ion at *m/z* 307 (observed in the MS spectrum) resembling its acetic acid adduct, and its corresponding Cl isotope ion indicating drug-related metabolite (Figure 3.4.15 (A)). Therefore, the molecular weight of this metabolite was determined as 248 Da, which has one more oxygen atom than that of the parent *p*-Cl AAP (molecular weight of 232 Da). Furthermore, a direct probe positive electron impact (EI) MS analysis was carried out for elucidation of the structure of metabolite-4. In the EI-MS spectrum (Figure 3.4.16 (A)), molecular ion at *m/z* 248, and other two diagnostic fragment ions at *m/z* 232 and 217 were observed. The mass fragment pattern in Figure 3.4.16 suggests that this metabolite is *N*-oxide of *p*-Cl AAP. A similar mass spectrometric data obtained from a positive ion CI-MS/MS analysis using a direct probe technique further confirmed the identity of metabolite-4 (Figure 3.4.16 (B)). The oxygen in the *N*-oxide dissociates easily in MS/MS analysis, and a loss of oxygen atom from *N*-oxide compounds is a common fragmentation (Herbert *et al.*, 1967). Therefore, metabolite-4 was definitively identified as *N*-oxide of *p*-Cl AAP, and its structure is shown in Figure 3.4.18.

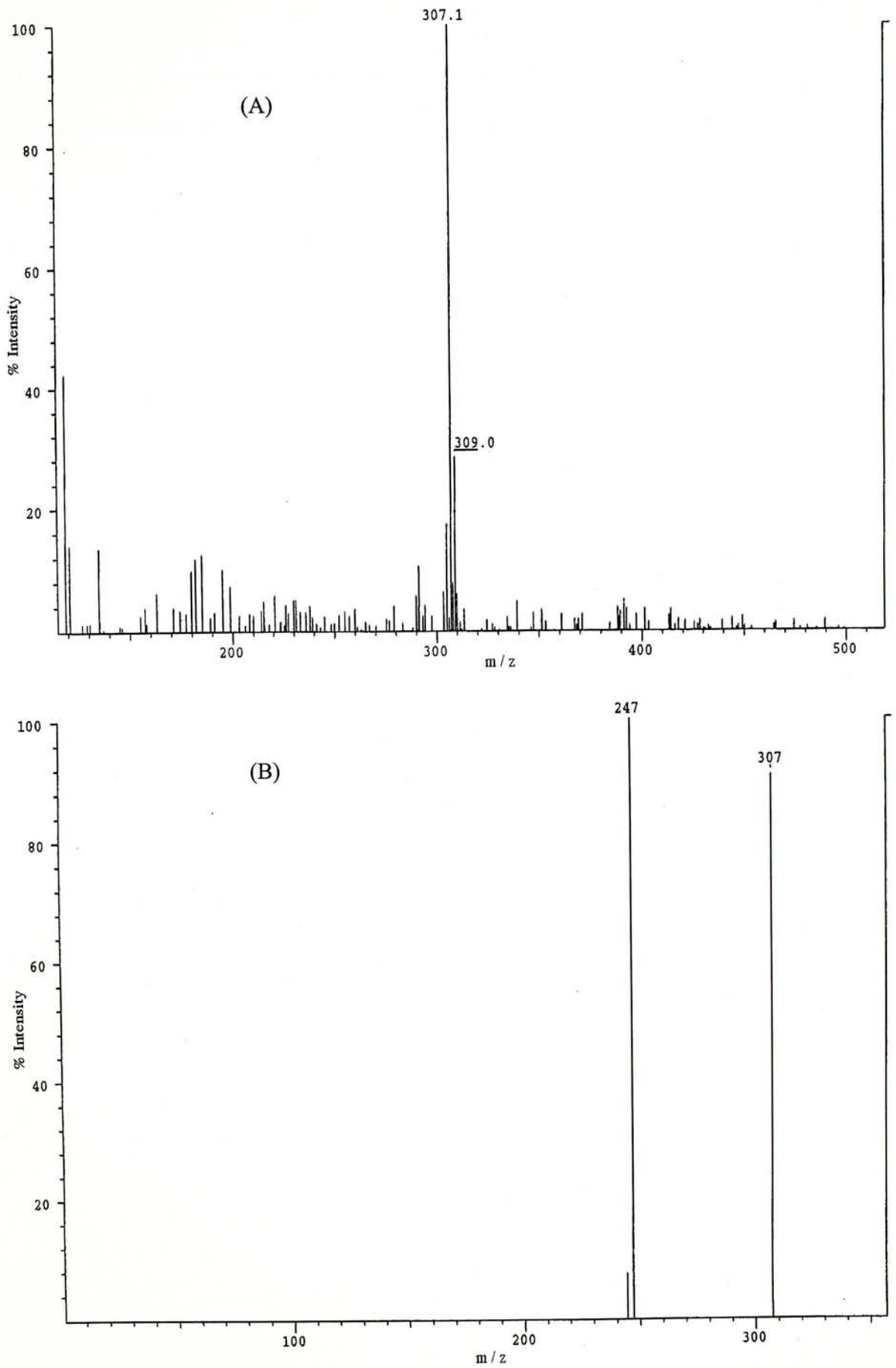

Figure 3.4.15 Negative-ion mass spectra of metabolite-4 from respective chromatograms of Figure 3.4.11. A) MS spectrum, B) MS/MS spectrum of metabolite-4.

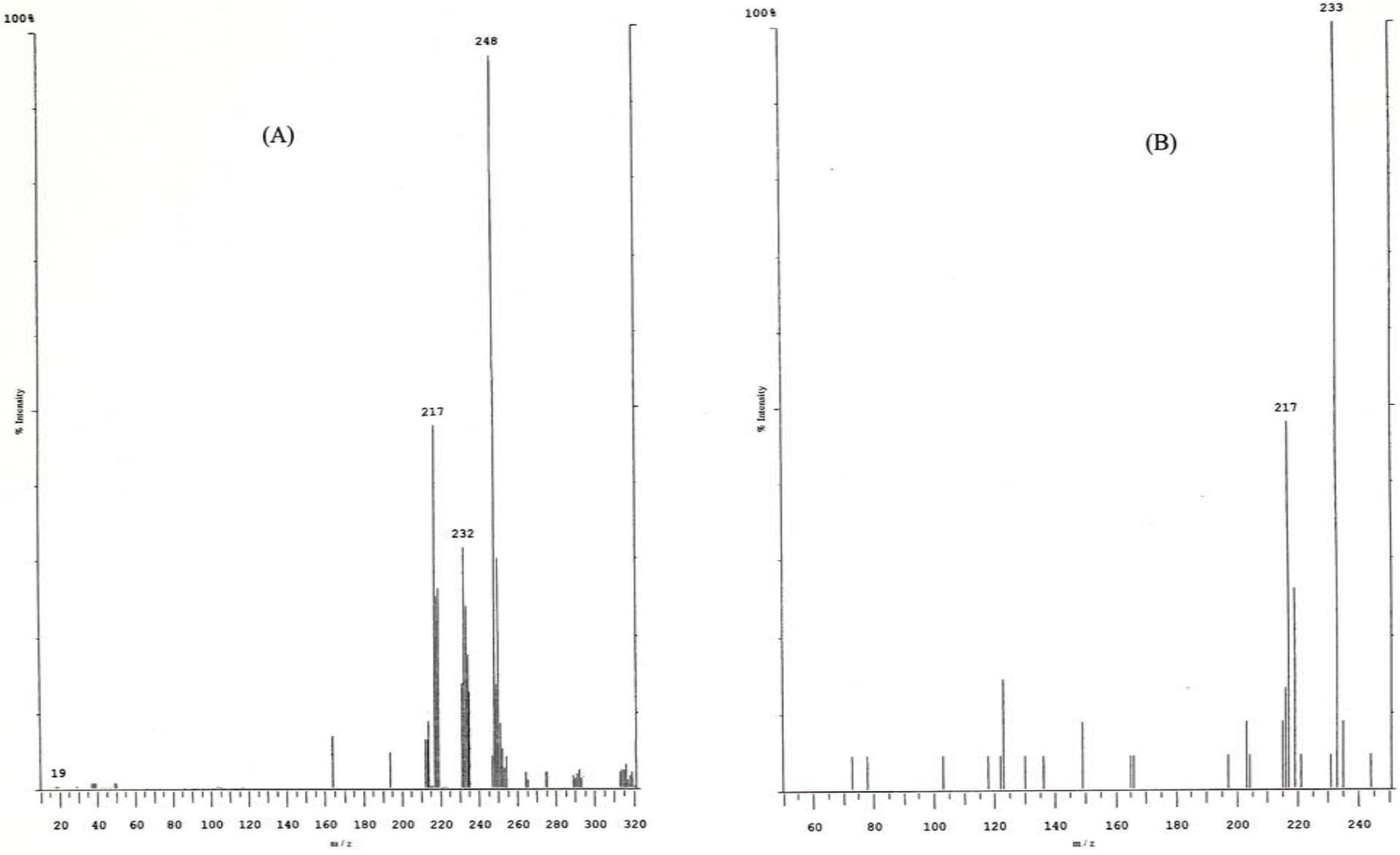

Figure 3.4.16 A) EI-MS spectrum, and B) Positive-ion CI-MS/MS spectrum of mtabolite-4.

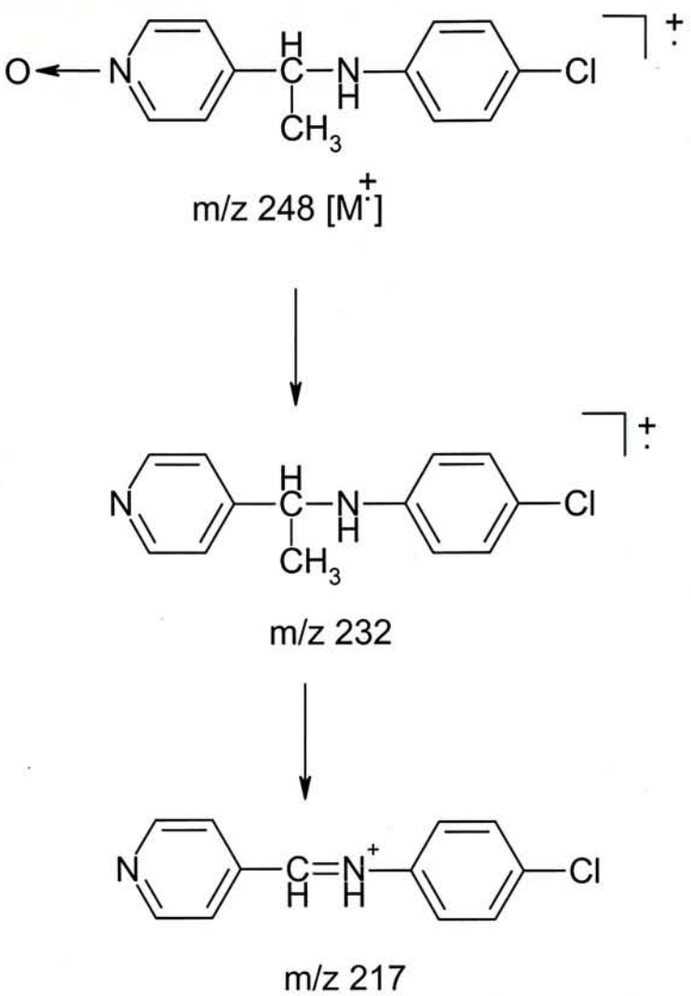

Figure 3.4.17 Possible fragment pattern of metabolite-4 in positive ion EI-MS.

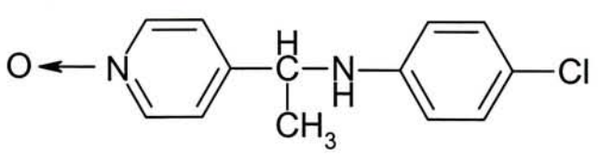

Figure 3.4.18 Structure of metabolite-4, *N*-[4-(chlorophenyl)]-1-[4-(pyridyl *N*-oxide)]ethylamine.

Only phase II metabolites of *N*-oxide of *p*-Cl AAP (metabolite-4), including glucuronide and sulphate conjugates, were found in the rat urine. The possible site for conjugation is nitrogen atom in the arylamine moiety. *N*-glucuronides and *N*-sulphates formed from arylamine have been reported for a wide range of drugs and xenobiotics (Gibson and Skett, 1994). It is interesting to note that, as discussed in next section, the relative amounts of glucuronide and sulphate of *N*-oxide of *p*-Cl AAP found in rat urine were 1 : 2. This observation suggested that arylamine sulphation is more favourable than arylamine glucuronidation. This metabolic preference is also reported for other drugs, for example, only arylamine sulphate conjugate of paracetamol was found (Gibson and Skett, 1994).

Fraction 3 only contained one compound, corresponding to metabolite-5, as demonstrated in the chromatograms of HPLC/MS/MS analysis (Figure 3.4.19). The negative ion APCI-MS spectrum (Figure 3.4.20 (A)) exhibited a highest mass ion at *m/z* 367, whilst the corresponding MS/MS spectrum (Figure 3.4.20 (B)) confirmed the quasi-molecular ion at *m/z* 247 and the ion at *m/z* 367 represented an acetic acid adduct of metabolite-5. Therefore, the molecular weight of metabolite-5 is 248 Da, which is 16 mass unit more than that of the parent *p*-Cl AAP. The positive ion HPLC/MS/MS analysis (not shown) provided similar results, and no further fragment ions were observed. Therefore, based on the HPLC/MS/MS results, metabolite-5 was tentatively assigned as 3-hydroxylated *p*-Cl AAP, namely *N*-[4-(chlorophenyl)]-1-[4-(2-hydroxypyridyl)]ethylamine (Figure 3.4.21).

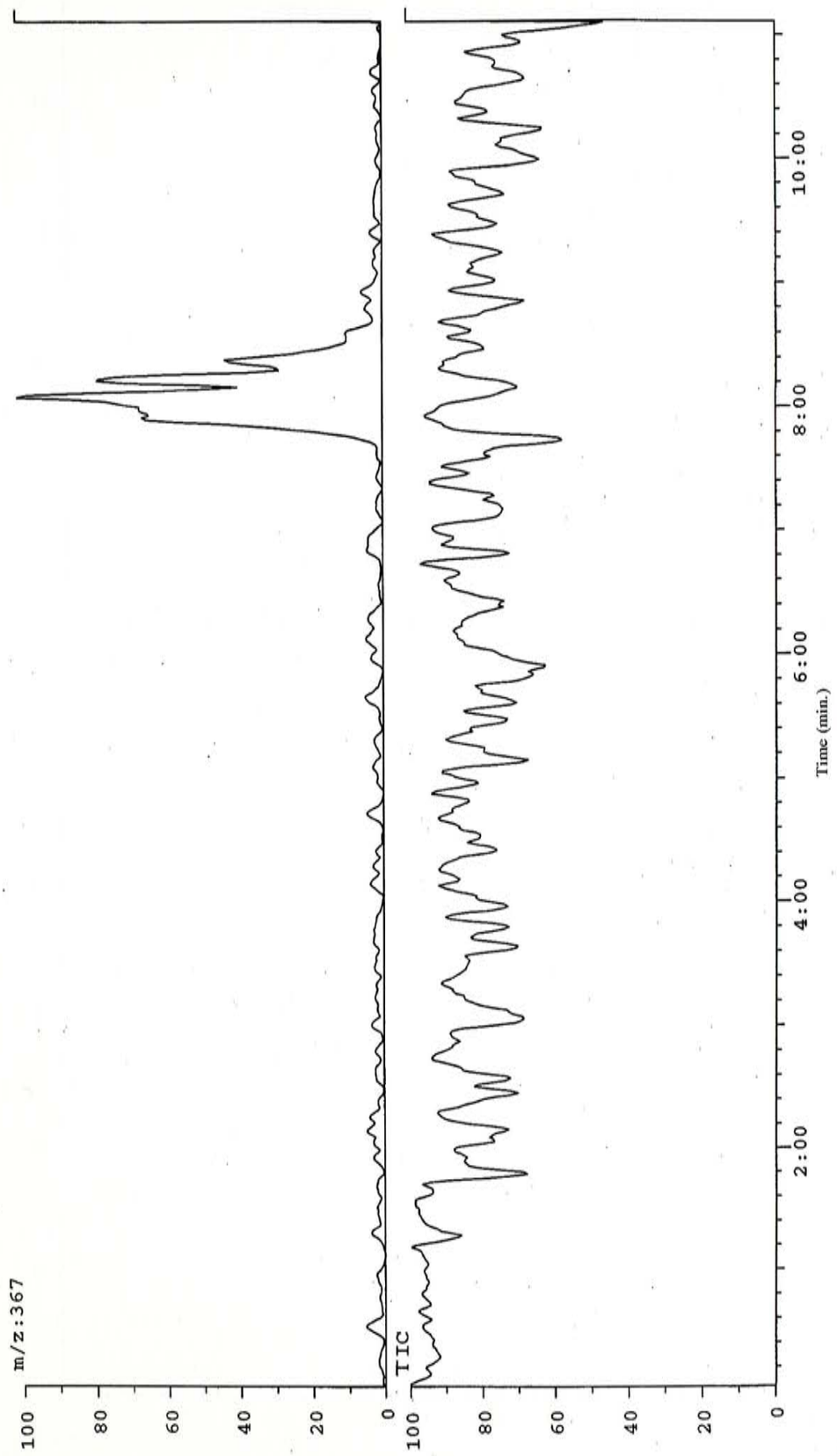

Figure 3.4.19 Total ion and reconstructed ion chromatograms obtained from HPLC/MS analysis of fraction 3. TIC, total ion current.

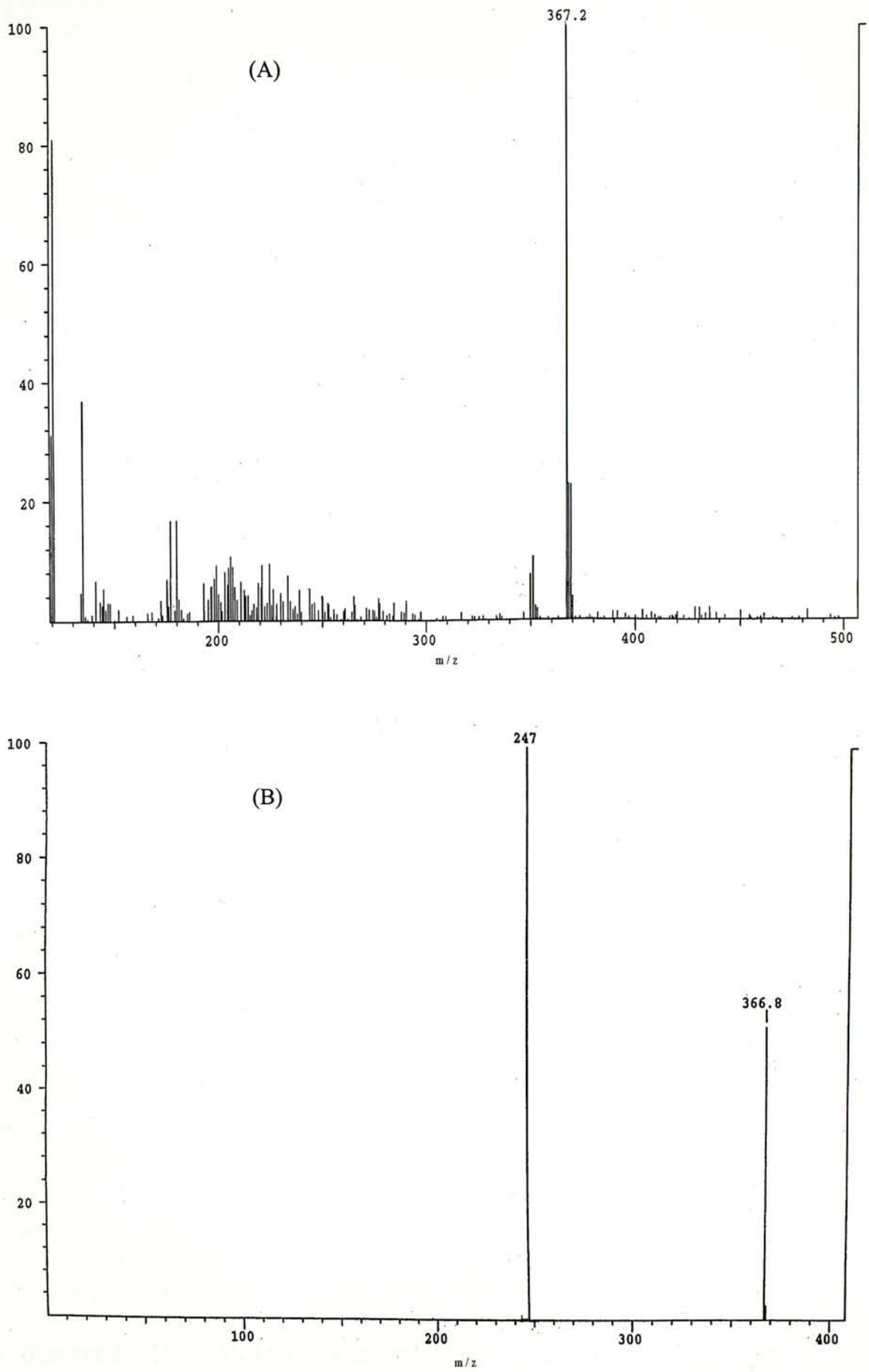

Figure 3.4.20 Negative-ion mass spectra of metabolite-5 from respective chromatograms of Figure 3.4.19. A) MS spectrum, B) MS/MS spectrum of metabolite-5.

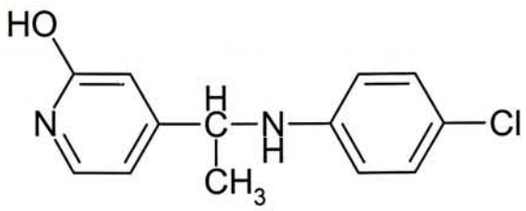

Figure 3.4.21 Structure of metabolite-5, *N*-[4-(chlorophenyl)]-1-[4-(2-hydroxypyridyl)]ethylamine.

As mentioned in previous metabolites, the hydroxyl group in metabolite-5 is most possibly in either pyridine or benzene ring. However, as the substituted chloride deactivates benzene ring via electron withdrawing, the hydroxylation at pyridine ring is much thermodynamically favourable.

For this metabolite, only phase II metabolites, including glucuronide and sulphate conjugates were identified in the urine of rats administered with *p*-Cl AAP, and their amounts were determined to be 1 : 1. For both conjugates, *O*-glucuronidation and *O*-sulphation may predominate.

HPLC/MS/MS analysis of fraction 4 demonstrated that this fraction only contained one compound, metabolite-6 (Figure 3.4.22). Since negative ion MS did not show any signal for this compound, a positive ion (HPLC/MS/MS analysis with APCI interface was conducted. In the positive ion APCI-MS spectrum (Figure 3.4.23 (A)), an ion at *m/z* 247 and 249 (Cl isotope peak) corresponding to the quasi-molecular ion was observed. The MS/MS spectrum of this quasi-molecular ion exhibited a characteristic ion at *m/z* 219, corresponding to a loss of CO molecule (Figure 3.4.23 (B)).

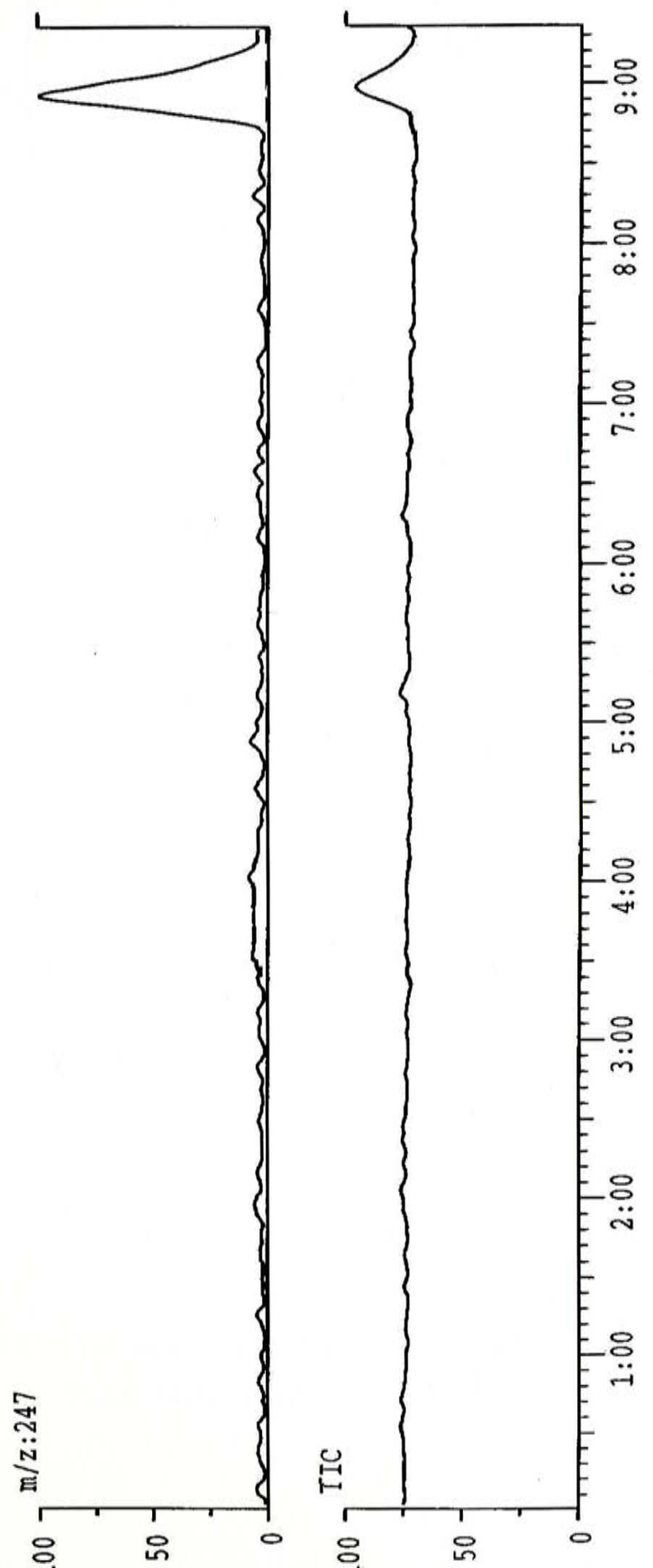

Figure 3.4.22 Total ion and reconstructed ion chromatograms obtained from HPLC/MS analysis of fraction 4. TIC, total ion current

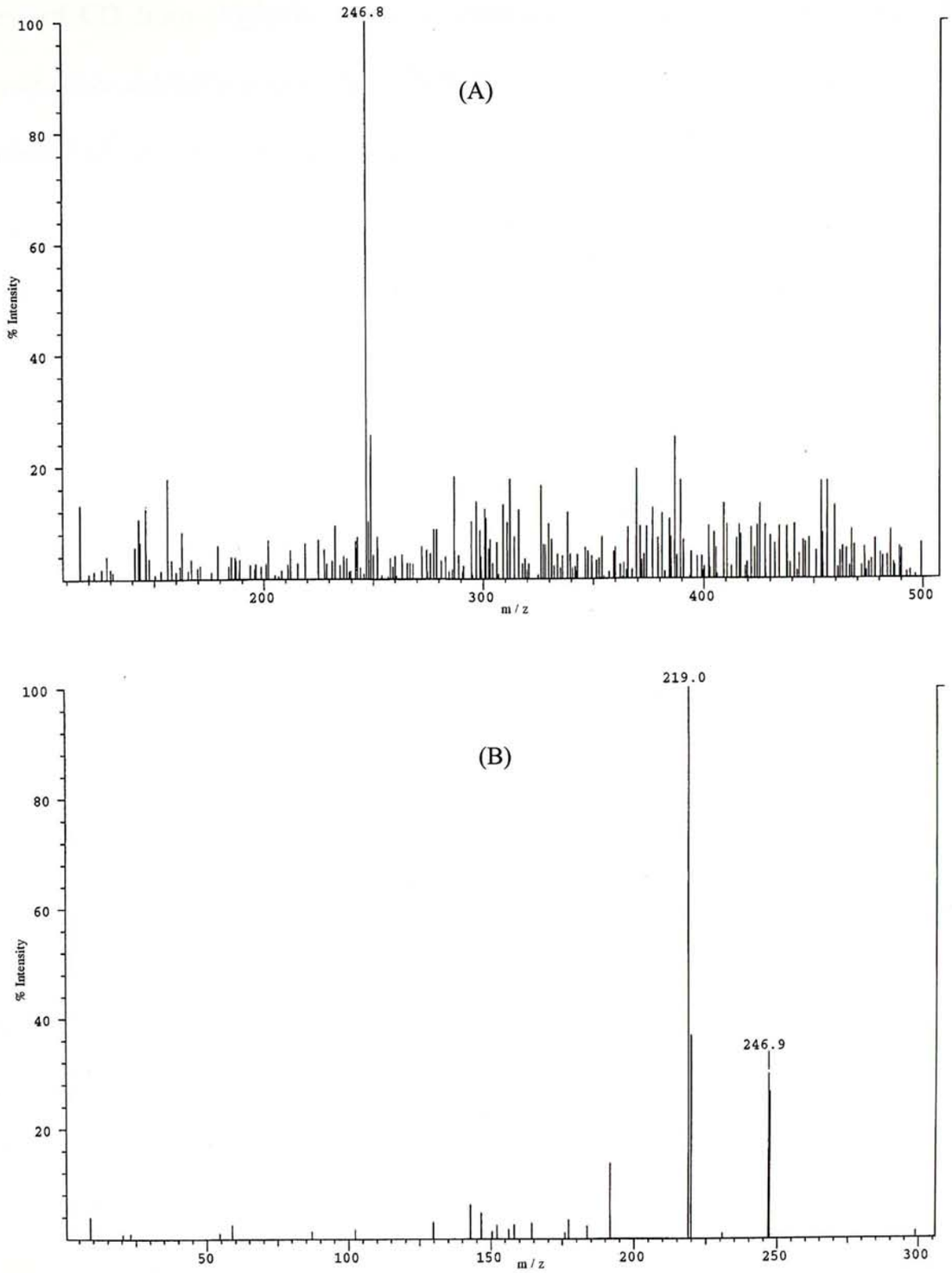

Figure 3.4.23 Positive-ion mass spectra of metababolite-6 from respective chromatograms of Figure 3.4.22. A) MS spectrum, B) MS/MS spectrum of metabolite-6.

The loss of CO from aldehyde in MS is common and often observed in the MS spectra of other aldehyde compounds (Herbert *et al.*, 1967). Therefore, metabolite-6 was identified as *p*-amino aldehyde of the parent drug, named as 2-[4-(chlorophenyl)]amino-2-[4-(pyridyl)]ethanal. The structure of metabolite-6 is shown in Figure 3.4.24, and its mass fragmentation in Figure 3.4.25.

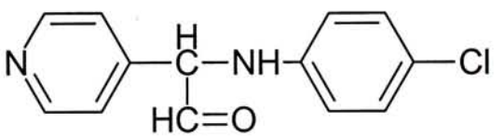

Figure 3.4.24 Structure of metabolite-6, 2-[4-(chlorophenyl)]amino-2-[4-(pyridyl)]ethanal.

Only the sulphate conjugate of metabolite-6 was found as the urinary metabolite of *p*-Cl AAP. Similar to metabolite-4, conjugation can only occur at arylamine nitrogen, thus sulphation predominated.

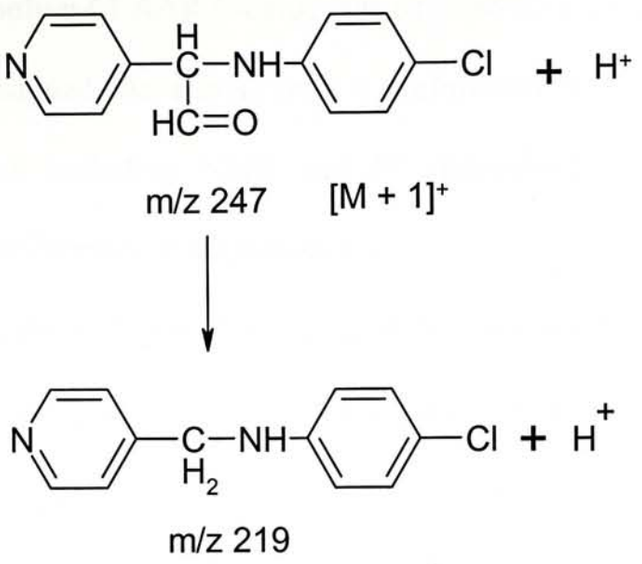

Figure 3.4.25 Possible fragment pattern of metabolite-6 in positive ion APCI-MS/MS.

In the present study, five novel metabolites of *p*-Cl AAP, in the forms of glucuronides and sulphates, were found in the urine of rats dosed with *p*-Cl AAP. These metabolites were tentatively identified as *N*-[4-(2-hydroxychlorophenyl)]-1-[4-(2,6-dihydroxypyridyl)]ethylamine (metabolite-1), *N*-[4-(chlorophenyl)]-1-hydroxy-1-[4-(pyridyl)]ethylamine (metabolite-2), 2-[4-(chlorophenyl)]amino-2-[4-(2,6-dihydroxypyridyl)]ethanoic acid (metabolite-3), *N*-[4-(chlorophenyl)]-1-[4-(pyridyl *N*-oxide)]ethylamine (metabolite-4) and *N*-[4-(chlorophenyl)]-1-[4-(2-hydroxypyridyl)]ethylamine (metabolite-5). The phase I metabolites of *N*-[4-(chlorophenyl)]-1-hydroxy-1-[4-(pyridyl)]ethylamine (metabolite-2) and 2-[4-(chlorophenyl)]amino-2-[4-(2,6-dihydroxypyridyl)]ethanoic acid (metabolite-3) were also isolated from the rat urine. In addition, another novel metabolite, 2-[4-(chlorophenyl)]amino-2-[4-(pyridyl)]ethanal (metabolite-6), was identified as its arylamine sulphate conjugate only. With regard to the structures of the identified

metabolites, only *p*-Cl AAP *N*-oxide was definitively characterized, while others were tentatively assigned. As this is only a preliminary metabolic study on *p*-Cl AAP, further studies including NMR and IR spectrometric analysis are required for definitive identification of the metabolites.

As shown in Figure 3.4.26, the urinary metabolic pathway of *p*-Cl AAP was proposed. Although β-amino alochol, the proposed pharmacologically active metabolite of *p*-Cl AAP was not observed, two metabolites, namely 2-[4-(chlorophenyl)]amino-2-[4-(pyridyl)]ethanal (metabolite-6) and 2-[4-(chlorophenyl)]amino-2-[4-(2,6-dihydroxypyridyl)]ethanoic acid (metabolite-3), were found. As indicated in Figure 3.4.26, during the formation of these two metabolites, a precursor, β-amino alcohol, should be generated in the body first. The present results indicated that the major metabolic pathways for *p*-Cl AAP include phenyl, α- and β-carbon hydroxylation, *N*-oxidation, glucuronidation and sulphation. For the conjugates, *O*-glucuronidation and arylamine sulphation are the major pathways.

As 2-[4-(chlorophenyl)]amino-2-[4-(pyridyl)]ethanal (metabolite-6) was identified as a metabolite of *p*-Cl AAP, the possibility exists that it is further oxidized to form an α-amino acid inside the body. Then two metabolites together with the substituted α-amino acid metabolite, 2-[4-(chlorophenyl)]amino-2-[4-(2,6-dihydroxypyridyl)]ethanoic acid (metabolite-3) identified, might act as the analogues of GABA or other excitatory amino acids to produce the antiepileptic effect of *p*-Cl AAP. Further studies on the pharmacological effects of these metabolites are necessary to verify this inference.

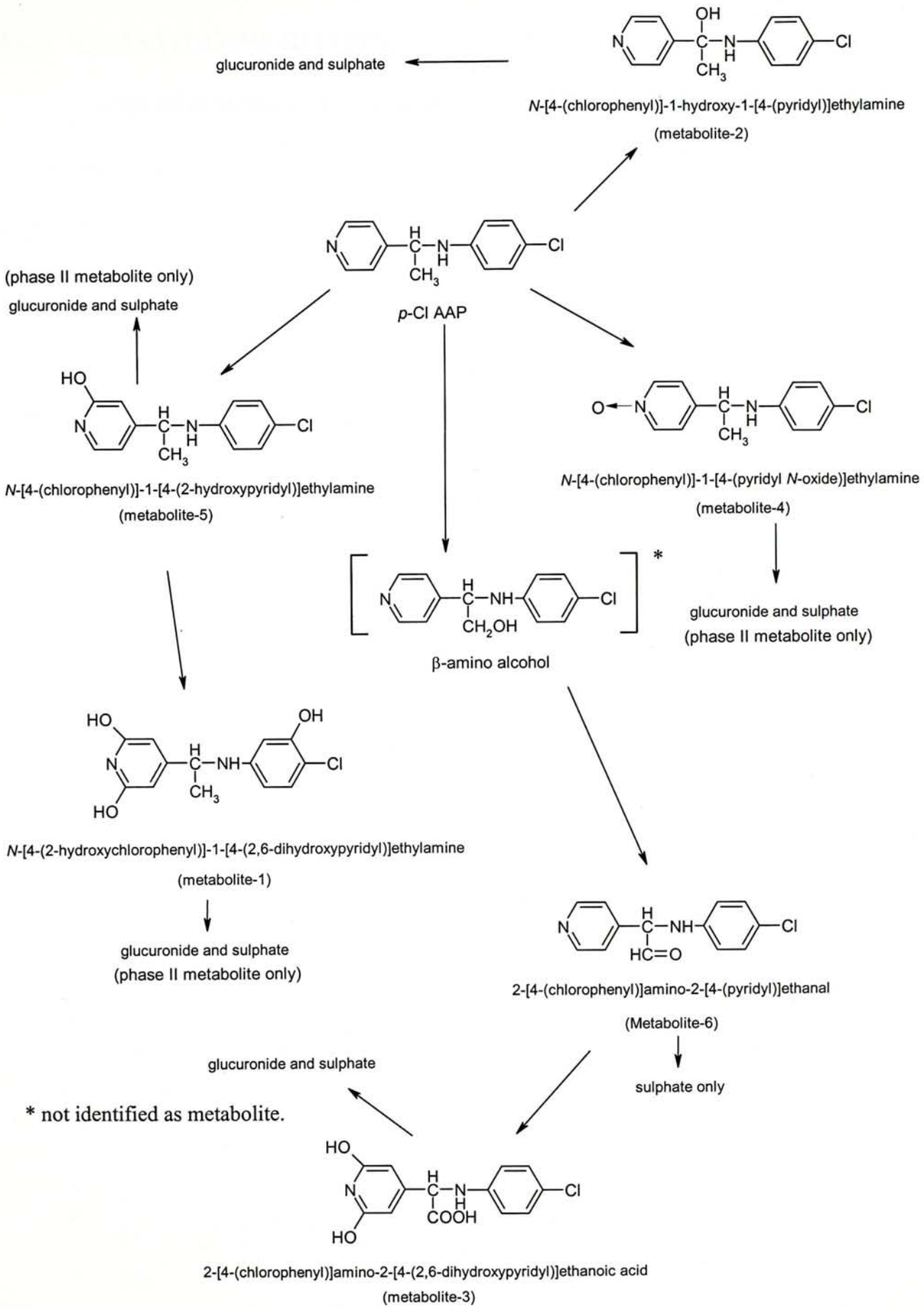

Figure 3.4.26 Possible urinary metabolic pathway of *p*-Cl AAP.

3.4.2 QUANTITATIVE STUDIES

As the calibration curves for the *p*-Cl AAP in bio-fluids have been constructed as mentioned in Chapter 2, the urinary excretion of *p*-Cl AAP in rats was determined and the data are presented in Table 3.4.2 and Figure 3.4.27.

Table 3.4.2 Urinary excretion of *p*-Cl AAP in rats.

	Amount of *p*-Cl AAP* (%)**	
Pretreatment	0 - 24 hour	24-48 hour
Phenobarbitone	0.28 ± 0.07	0.04 ± 0.002
Non-phenobarbitone	0.18 ± 0.01	0.014 ± 0.0008

* Mean ± s.d. (n = 5)

** The amount of the *p*-Cl AAP in urine was expressed as percentage of the amount dosed in rats.

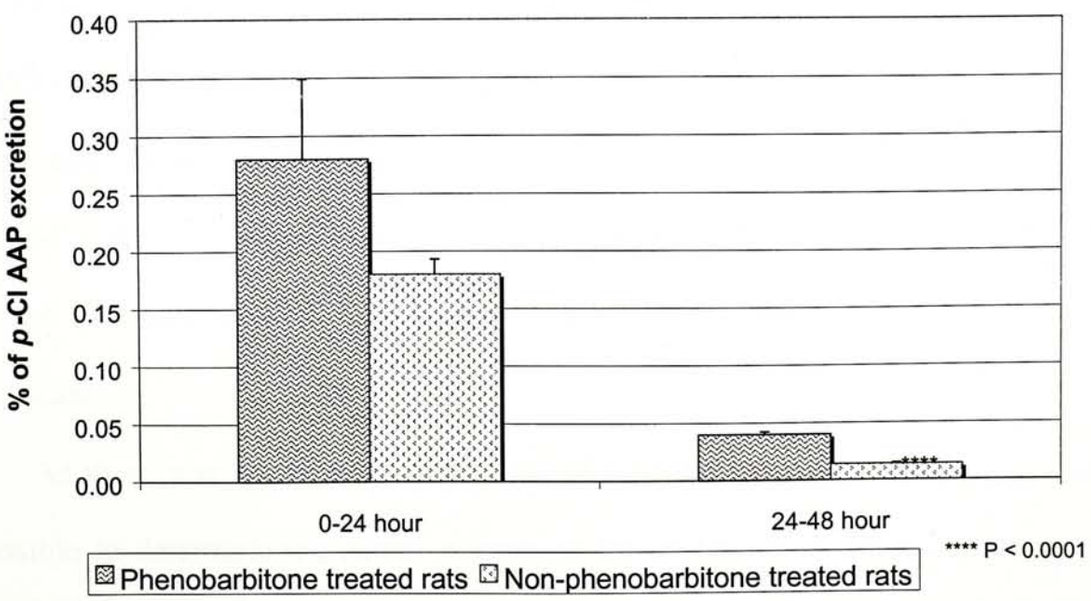

Figure 3.4.27 Urinary excretion of *p*-Cl AAP in rats. (n = 5)

For the phenobarbitone pretreated rats, after 24 and 48 hours, the percentage of *p*-Cl AAP found in urine sample was 0.28 ± 0.07% and 0.04 ± 0.002% with respect to the amount of *p*-Cl AAP administered in the rats, respectively. For the non-phenobarbitone pretreated rats, the corresponding values were 0.18 ± 0.01% and 0.014 ± 0.0008%, respectively. Only trace amounts of the intact parent drug were found in the urine samples. This suggests that the novel anticonvulsant was either highly metabolized or retained inside the body. Trace amounts of *p*-Cl AAP in the urine and almost no metabolite was found in urinary samples after 48 hours. For the metabolic studies, only those samples collected in the 0 - 24 hour period were analyzed.

It is interesting to note that the amount of p-Cl AAP excreted was 55 % higher in phenobarbitone pretreated rats than in the non-phenobarbitone pretreated rats, for both the 0 - 24 hours (the difference here was not statistically significant, $P > 0.05$) and 24 - 48 hours samples ($P < 0.0001$). Phenobarbitone pretreatment on rats has been reported to stimulate the renal excretion of *p*-aminohippuric acid (Storch, 1975, 1976 and 1977) and ioglycamic acid (IGA) (Fleck, 1991). Hence, our results may also suggest that phenobarbitone pretreatment may enhance the renal excretion of the intact *p*-Cl AAP. Further experiments are necessary to determine whether the increased excretion of *p*-Cl AAP is due to the stimulation of the glomerulus or by other means.

As there was a lack of authentic samples of the putative metabolites, it was impossible to determine the actual amount of the metabolites excreted from urine. However, the relative amounts of different urinary metabolites from different pretreated rats could be determined as described in section 2.5.6. The relative amounts

of metabolite-2 and metabolite-3 in phenobarbitone and non-phenobarbitone pretreated rats are tabulated in Tables 3.4.3 and 3.4.4, and shown graphically in Figures 3.4.28 and 3.4.29, respectively. Unless otherwise stated, all reference values for comparison of the amount of each metabolite were set at 100 %.

Table 3.4.3 Metabolite-2 and metabolite-3 excreted from 0-24 hour urine of the phenobarbitone pretreated rats administered with *p*-Cl AAP (80 mg/kg, i.p.). (n = 5)

Treatment on urine sample	Metabolite-2	Metabolite-3
Phase I	100 ± 5.7 %	100 ± 0.3 %
β-glucuronidase deconjugation	209.3 ± 9.9 %	147.6 ± 20.3 %
β-glucuronidase / sulphatase deconjugation	270.3 ± 29.8 %	259.7 ± 30.0 %

Table 3.4.4 Metabolite-2 and metabolite-3 excreted from 0-24 hour urine of the non-phenobarbitone pretreated rats administered with *p*-Cl AAP (80 mg/kg, i.p.). (n = 5)

Treatment on urine sample	Metabolite-2	Metabolite-3
Phase I	100 ± 5.8 %	100 ± 10.1 %
β-glucuronidase deconjugation	146.8 ± 9.6 %	141.5 ± 6.7 %
β-glucuronidase / sulphatase deconjugation	183.3 ± 13.9 %	233.5 ± 8.7 %

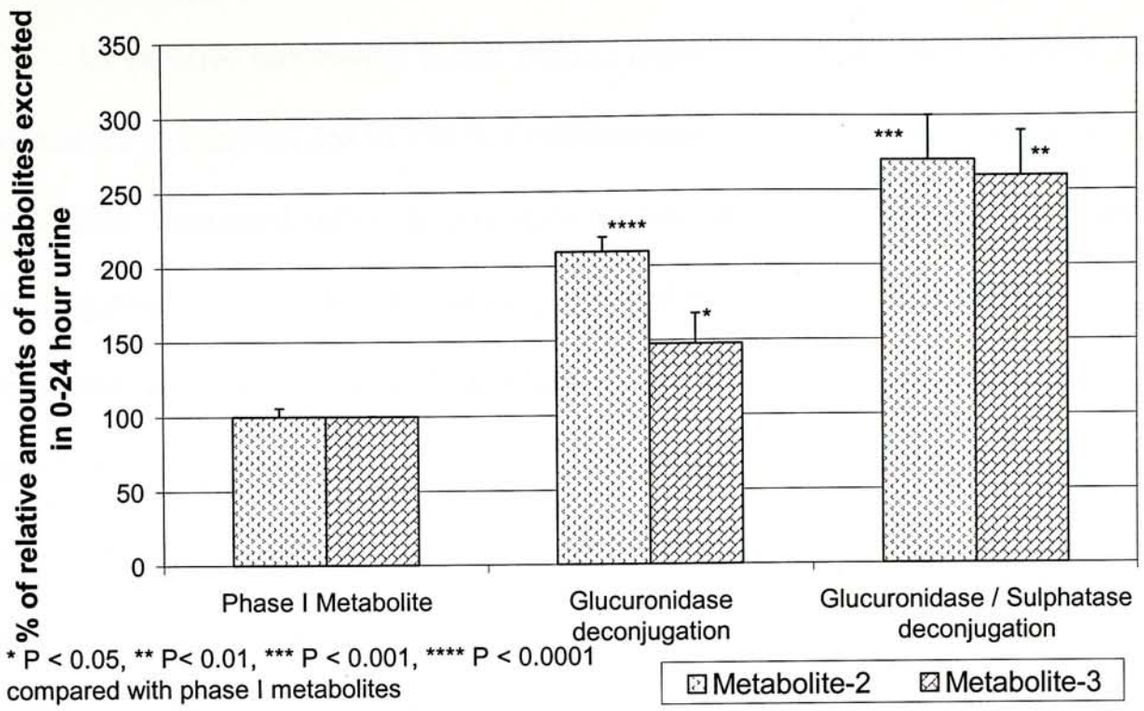

Figure 3.4.28 Metabolite-2 and metabolite-3 excreted from 0-24 hour urine of the phenobarbitone pretreated rats administered with *p*-Cl AAP (80 mg/kg, i.p.). (n = 5)

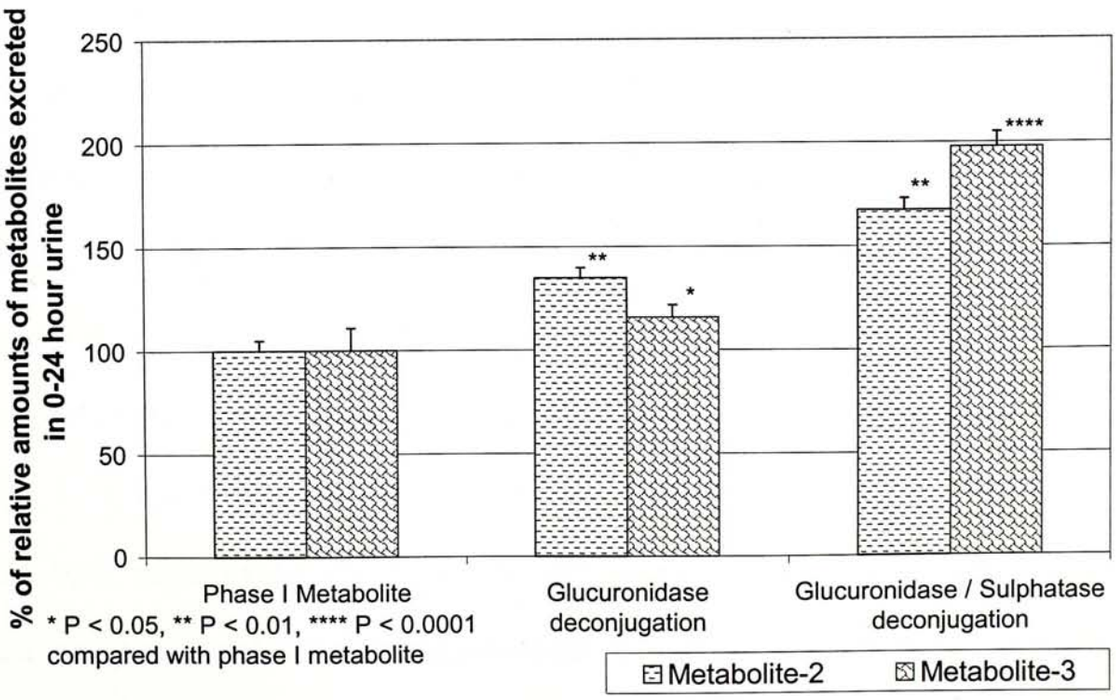

Figure 3.4.29 Metabolite-2 and metabolite-3 excreted from 0-24 hour urine of the non-phenobarbitone pretreated rats administered with *p*-Cl AAP (80 mg/kg, i.p.). (n = 5)

All putative metabolites found without enzymatic deconjugation were phase I metabolites and normalised to 100 % (as mentioned in section 2.5.6). The amount of metabolites measured after deconjugation was compared with those without deconjugation. For the phenobarbitone pretreated rats, after β-glucuronidase and β-glucuronidase / arylsulphatase deconjugation, the relative amounts of metabolite-2 were 209.3 ± 9.9 % and 270.3 ± 29.8 %, respectively. For the non-phenobarbitone pretreated rats, they were 146.8 ± 9.6 % and 183.3 ± 13.9 %, respectively. Hence, the relative amounts of phase I, glucuronide and sulphate conjugates of metabolite-2 for the phenobarbitone pretreated rats were 1 : 1 : 0.6, respectively. For the non-phenobarbitone pretreated rats, they were 1 : 0.47 : 0.36, respectively. It showed that metabolite-2 formed phase I, and both glucuronide and sulphate conjugates during the metabolism of *p*-Cl AAP.

In the case of metabolite-3, in phenobarbitone pretreated rats, the relative amounts after β-glucuronidase deconjugation and β-glucuronidase / aryl sulphatase deconjugation were 147.6 ± 20.3 % and 259.7 ± 30.3 %, respectively. For the non-phenobarbitone pretreated rats, they were 141.5 ± 6.7 % and 233.5 ± 8.7 %, respectively. Hence, the relative amounts of metabolite-3 in the forms of phase I, glucuronide and sulphate conjugates, for the phenobarbitone pretreated rats, were 1 : 0.48 : 1.12, respectively. For the non-phenobarbitone pretreated rats, they were 1 : 0.42 : 0.92, respectively. The relatively large amount of sulphate conjugate resulted when compared with those of glucuronide conjugate, showed that metabolite-3 displayed a much greater tendency to undergo sulphate conjugation than glucuronide conjugation.

The comparison of urinary excretion of metabolite-2 and metabolite-3 between the phenobarbitone and non-phenobarbitone pretreated rats is shown in Tables 3.4.5 and 3.4.6, and Figures 3.4.30 and 3.4.31.

Table 3.4.5 Comparison of urinary excretion (0-24 hour) of metabolite-2 between phenobarbitone and non-phenobarbitone pretreated rats administered with *p*-Cl AAP (80 mg/kg, i.p.) (n = 5)

	Non-phenobarbitone pretreated rats	Phenobarbitone pretreated rats
Phase I metabolite	100 ± 5.8 %	62.6 ± 4.1 %
Glucuronide conjugate	100 ± 17.5 %	166.0 ± 5.0 %
Sulphate conjugate	100 ± 25.8 %	225.1 ± 69.8 %

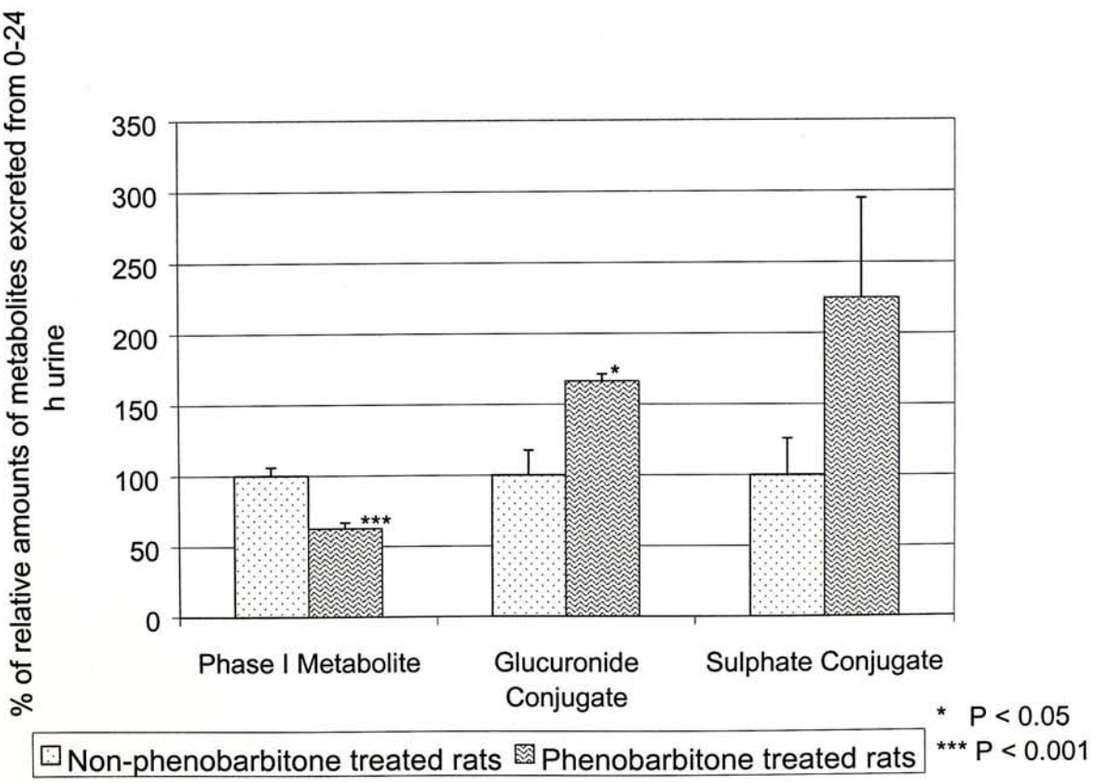

Figure 3.4.30 Comparison of urinary excretion (0-24 hour) of metabolite-2 between non-phenobarbitone and phenobarbitone pretreated rats administered with *p*-Cl AAP (80 mg/kg, i.p.) (n = 5).

Table 3.4.6 Comparison of urinary excretion (0-24 hour) of metabolite-3 between phenobarbitone and non-phenobarbitone pretreated rats administered with *p*-Cl AAP (80 mg/kg, i.p.) (n = 5)

	Non-phenobarbitone pretreated rats	Phenobarbitone pretreated rats
Phase I metabolite	100 ± 10.1 %	95.2 ± 0.3 %
Glucuronide conjugate	100 ± 11.7 %	126.9 ± 53.7 %
Sulphate conjugate	100 ± 8.9 %	124.3 ± 23.0 %

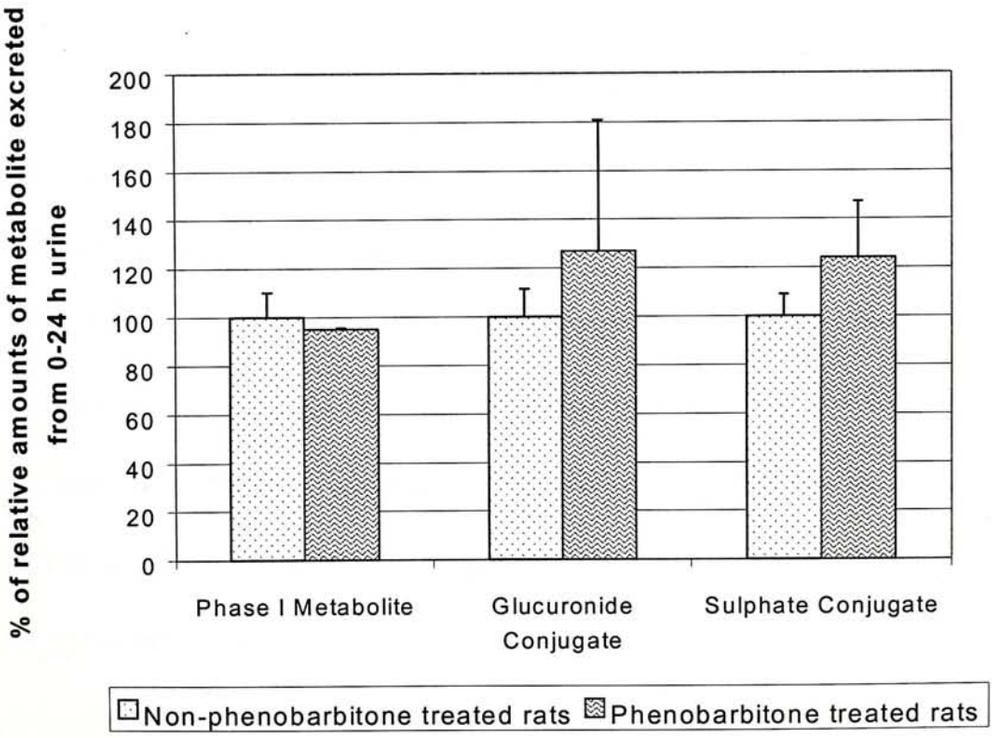

Figure 3.4.31 Comparison of urinary excretion (0-24 hour) of metabolite-3 between non-phenobarbitone and phenobarbitone pretreated rats administered with *p*-Cl AAP (80 mg/kg, i.p.) (n = 5).

When the amounts of metabolite-2 and its conjugates excreted from the non-phenobarbitone pretreated rats are set at 100 %, those excreted from phenobarbitone pretreated rats can be directly compared. After phenobarbitone pretreatment, the amount of the phase I metabolite significantly decreased ($P < 0.001$) (from 100 ± 5.8 % to 62.6 ± 4.1 %) while the amounts of glucuronide and sulphate conjugates of metabolite-2 excreted markedly increased (from 100 ± 17.5 % and 100 ± 25.8 % to 166 ± 5.0 % and 225.1 ± 69.8 %, respectively). A statistically significant increase in excretion ($P < 0.05$) was observed in the case of glucuronide conjugate (by 66 %). The amount of sulphate conjugate also increased (by 125 %). However, no statistically significant difference ($P > 0.05$) was obtained for sulphate conjugate, which might be due to relatively higher inter subject variations with the small number of animals examined ($n = 5$). Metabolite-2 exists in both phase I and phase II forms and several enzymes involved in the formation of metabolite-2. Phenobarbitone is cytochrome P450 enzyme inducer (Gibson and Skett, 1994). Metabolism of *p*-Cl AAP to metabolite-2 in phase I form is mediated by cytochrome P450 enzyme system which, might be the rate determining step for metabolism of the parent drug. Once phase I metabolite-2 is formed, it might quickly undergo phase II metabolism. Hence, more glucuronide and sulphate conjugates of metabolite-2 were found in the urine of phenobarbitone pretreated rats.

For the metabolite-3 of *p*-Cl AAP, similar comparison was made as with the studies on metabolite-2, i.e. treating the amount of metabolite-3 in non-phenobarbitone pretreatment as 100 %. Regarding phase I metabolite, the relative amount of metabolite-3 in phenobarbitone pretreated rat was 95.2 ± 0.3 %. This was approximately the same in amount as in non-phenobarbitone pretreated rats.

For the glucuronide and sulphate conjugates, the relative amount for phenobarbitone pretreated rats was 126.9 ± 53.7 % and 124.3 ± 23.0 % respectively. Only slight increases in the amounts of both conjugates with about 27 and 24 % were observed. This suggest phenobarbitone has no or very weak effect on the metabolism of *p*-Cl AAP to metabolite-3.

It was found that only after the deconjugation of the rat urine samples could metabolite-1, -4 and -5 be detected, indicating that these three metabolites were present as phase II conjugates only. The relative amounts of these three metabolites in phenobarbitone and non-phenobarbitone pretreatment are shown in Tables 3.4.7 and 3.4.8, and Figures 3.4.32 and 3.4.33.

Table 3.4.7 Phase II metabolites-1, -4 & -5 excreted from 0-24 hour urine of phenobarbitone pretreated rats administered with *p*-Cl AAP (80 mg/kg, i.p.). (n = 5)

Type of deconjugation	Metabolite-1	Metabolite-4	Metabolite-5
β-glucuronidase	100 ± 11.3 %	100 ± 7.3 %	100 ± 10.2 %
β-glucuronidase/aryl sulphatase	148.9 ± 11.3 %	354.9 ± 67.3 %	202.4 ± 15.2 %

Table 3.4.8 Phase II metabolites-1, -4 & -5 excreted from 0-24 hour urine of non-phenobarbitone pretreated rats administered with *p*-Cl AAP (80 mg/kg, i.p.). (n = 5)

Type of deconjugation	Metabolite-1	Metabolite-4	Metabolite-5
β-glucuronidase	100 ± 15.1 %	100 ± 30.7 %	100 ± 27 %
β-glucuronidase/aryl sulphatase	144.4 ± 18.0 %	298.7 ± 27.5 %	394.7 ± 144.7 %

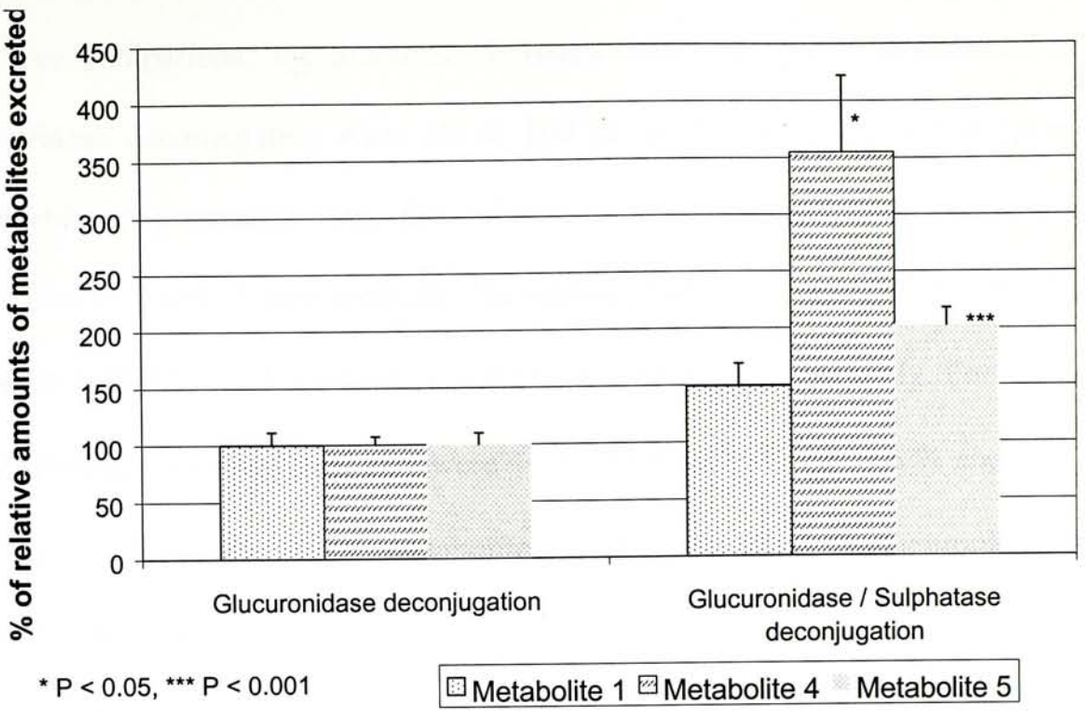

Figure 3.4.32 Phase II metabolite-1, -4 & -5 excreted from 0-24 hour urine of phenobarbitone pretreated rats administered with *p*-Cl AAP (80 mg/kg, i.p.). (n = 5)

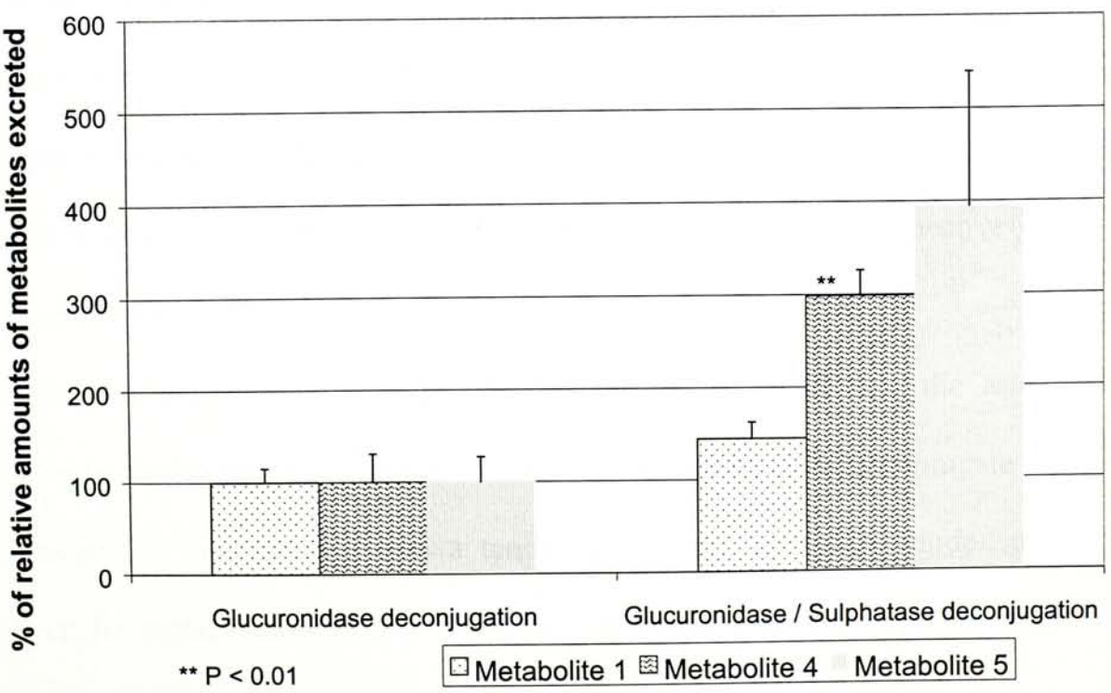

Figure 3.4.33 Phase II metabolite-1, -4 & -5 excreted from 0-24 hour urine of non-phenobarbitone pretreated rats administered with *p*-Cl AAP (80 mg/kg, i.p.). (n = 5)

For comparison, the amounts of metabolite-1, -4 and -5 determined after glucuronidase deconjugation were set at 100 % as described in section 2.4.6. In phenobarbitone pretreated rats, the relative amounts of sulphate conjugate of metabolites-1, -4 and -5 measured after the aryl-sulphatase deconjugation, were found to be 48.9 ± 19.8 %, 254.9 ± 67.3 % and 102.4 ± 15.2 %, respectively. For the non-phenobarbitone pretreated rats, they were 44.4 ± 18.0 %, 198.7 ± 27.5 % and 294.7 ± 144.7 %, respectively. Both metabolites-4 and -5, after β-glucuronidase/aryl sulphatase deconjugation, showed a significant increase compared with those subjected only to β-glucuronidase deconjugation ($P < 0.05$) in the phenobarbitone pretreated rats (Table 3.4.7), whereas in non-phenobarbitone pretreated rats, only metabolite-4 gave a significant increase ($P < 0.01$). Even though other metabolites in the different pretreatment groups did not show any statistically significant difference, a marked increase in the amount of metabolites was still observed after β-glucuronidase / aryl sulphatase deconjugation. The ratio of glucuronide to sulphate conjugate of metabolites-1, -4, and -5 were 1 : 0.49, 1 : 2.5 and 1 : 1, respectively for the phenobarbitone pretreated rats, and 1 : 0.44, 1 : 2 and 1 : 2.9, respectively for the non-phenobarbitone pretreated rats.

In the phenobarbitone pretreated rats, it was found that the amount of glucuronide conjugate of metabolite-1 differed from the sulphate conjugate by two-fold, suggesting metabolite-1 had a tendency to form the glucuronide conjugate. However, for metabolite-4, nearly 72 % was converted to the sulphate conjugate. For metabolite-5, the ratio of both glucuronide and sulphate conjugates was 1 : 1, indicating an equal preference for the formation of each conjugate.

In the non-phenobarbitone pretreated rats, the sulphate conjugate formed was 31 % for metabolite-1 and nearly 66 % for metabolite-4. These results were comparable to those obtained for phenobarbitone-pretreated rats, in that more glucuronide was present for metabolite-1, while sulphate conjugate was predominant for metabolite-4. Whereas, for metabolite-5, the glucuronide constituted nearly 75 % of the total amount of the metabolites, which was different from that obtained for phenobarbitone pretreated rats.

The comparison of urinary excretion of phase II metabolite-1, -4 and -5 between phenobarbitone and non-phenobarbitone pretreated rats is shown in Table 3.4.9 and Figure 3.4.34.

Table 3.4.9 Comparison of urinary excretion (0-24 hour) of phase II metabolite-1, -4 and -5 between phenobarbitone and non-phenobarbitone pretreated rats administered with *p*-Cl AAP (80 mg/kg, i.p.). (n = 5)

	Metabolite	Non-phenobarbitone pretreated rats	Phenobarbitone pretreated rats
Glucuronide Conjugate	1	100 ± 15.1 %	87.2 ± 9.9 %
	4	100 ± 30.7 %	123.7 ± 9.0 %
	5	100 ± 27.0 %	257.5 ± 26.3 %
Sulphate Conjugate	1	100 ± 40.2 %	210.2 ± 108.0 %
	4	100 ± 17.0 %	141.8 ± 28.3 %
	5	100 ± 41.0 %	116.2 ± 9.5 %

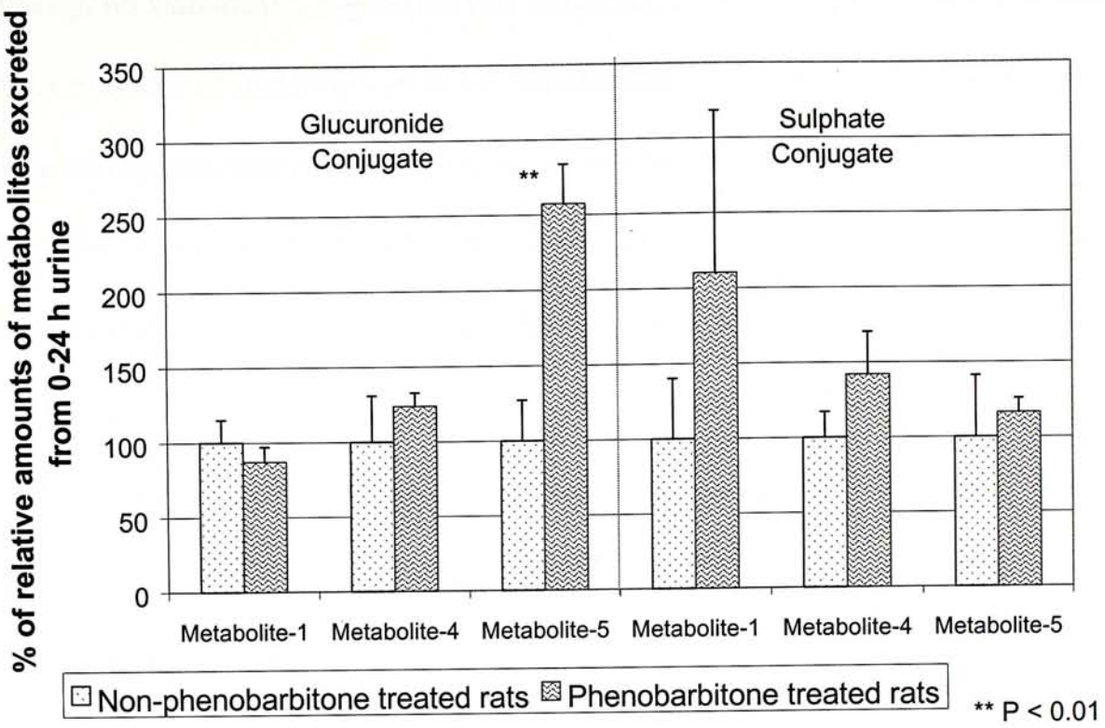

Figure 3.4.34 Comparison of urinary excretion (0-24 hour) of phase II metabolite-1, -4 and -5 between phenobarbitone and non-phenobarbitone pretreated rats administered with *p*-Cl AAP (80 mg/kg, i.p.) (n = 5).

In considering the amounts of the metabolites found in non-phenobarbitone pretreated rats as 100 %, the relative amounts of metabolite-1 as glucuronide and sulphate conjugates in phenobarbitone pretreated rats could be determined, and these were found to be 87.2 ± 9.9 % and 210.2 ± 108.8 % (Table 3.4.9), respectively. This showed that phenobarbitone pretreatment did not affect glucuronide formation (statistically insignificant) of metabolite-1, however it significantly increased its sulphation to about 110 %.

For metabolite-4, the relative amounts of glucuronide and sulphate conjugates in phenobarbitone pretreated rats determined were 123.7 ± 9.0 % and 141.8 ± 28.3 % compared with those found for non-phenobarbitone pretreated rats.

Although no statistical significance was obtained, a marked increase in the amount of both conjugates of metabolite-4 in phenobarbitone pretreated rats was observed. The increase in the amount of these two conjugates was about 24 and 42 %, respectively.

For metabolite-5, the amounts of glucuronide and sulphate conjugates in the phenobarbitone pretreated group relative to those in the control group were 257.5 ± 26.3 % and 116.2 ± 9.5 %, respectively. A statistically significant increase by 158 % ($P < 0.01$) in the amount of glucuronide conjugate was found. However, there was only a slight (statistically insignificant) increase (by 16 %) in sulphate conjugate.

Phenobarbitone is an inducer for the phase I metabolizing enzyme system, cytochrome P450 monooxygenases (Waxman and Azaroff, 1992). It is also an inducer of many glucuronosyl transferases (Bock *et al.*, 1973; Lilienblum *et al.*, 1982; Watkins and Klaassen, 1982; Watanable and Matsui, 1984), involved in the metabolism of morphine, chloramphenicol and bilirubin. The results suggest phenobarbitone might enhance the activity of the enzymes, including UDP-glucuronosyl transferases, which are involved in the phase II metabolism of *p*-Cl AAP, especially for the glucuronidation of metabolites-2, -4 and -5.

As phenobarbitone also enhances the expression of hydroxysteroid sulphotransferase a (STa) (Werle *et al.*, 1993), it will therefore enhance the activity of sulphotransferase. It might also enhance the activity of the sulphotransferase involved in the sulphation of the metabolites-1, -2 and -4 but not for metabolite-3 and -5 of *p*-Cl AAP. Furthermore, sulphation of the metabolites may also be mediated by other sulphorylase enzymes, such as ATP-sulfurylase and APS-kinase, which might also be induced by phenobarbitone (although there is no previous report). As a result, a prominent increase in the excretion of glucuronide and/or sulphate conjugates of

metabolites-1, -2, -4 and -5 was observed after three days pretreatment of phenobarbitone.

In addition, phenobarbitone induces cytochrome P450 enzymes, thereby increasing the phase I metabolism of *p*-Cl AAP to yield more metabolites either in their phase I form or further biotransformed to their phase II forms. Hence, the total amount of the metabolite-1, -2, -4 and -5 present in rat urine increased in phenobarbitone pretreated rats.

It is interesting to note that metabolite-6 was only found after the β-glucuronidase / aryl sulphatase deconjugation of the rat urine samples but not after the β-glucuronidase deconjugation. This suggested that metabolite-6 formed only the sulphate conjugate. Furthermore, metabolite-6 was not found in non-deconjugation samples. This confirms metabolite-6 undergoes phase II metabolism but without appearing as any form of phase I metabolite in urine. A comparison of its relative amount in both phenobarbitone and non-phenobarbitone pretreatment is shown in Table 3.4.10 and Figure 3.4.35.

Table 3.4.10 Comparison of urinary excretion (0-24 hour) of phase II metabolite-6 between phenobarbitone and non-phenobarbitone pretreated rats with *p*-Cl AAP (80 mg/kg, i.p.). (n = 5)

	Non-phenobarbitone pretreated rats	Phenobarbitone pretreated rats
Sulphate Conjugate	100 ± 23.1 %	107.0 ± 36.9 %

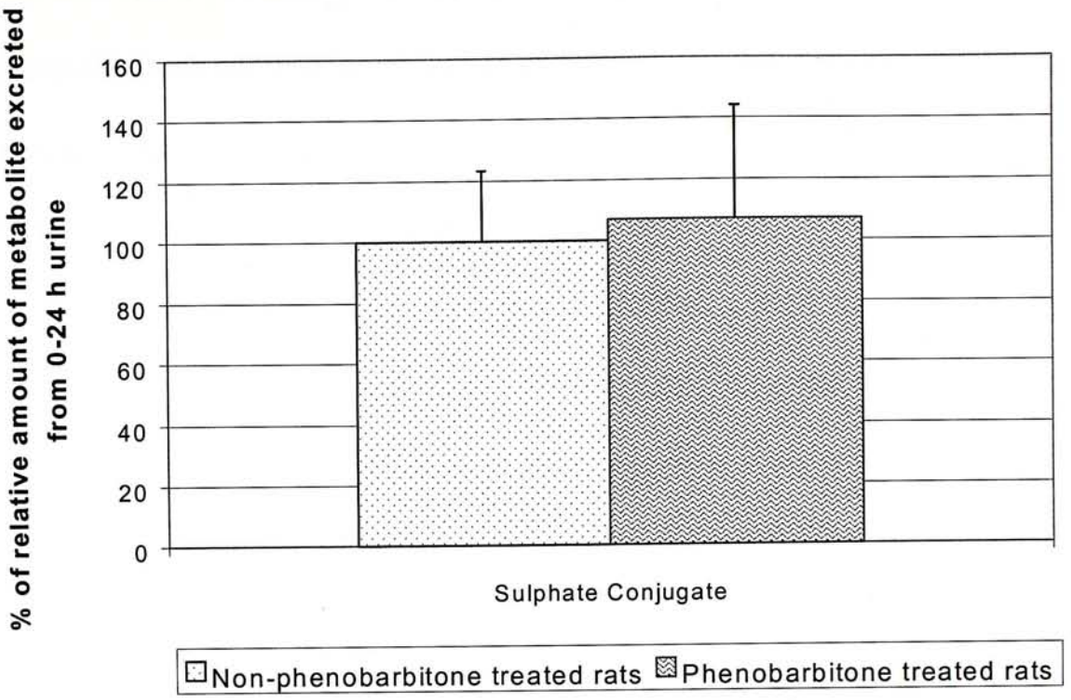

Figure 3.4.35 Comparison of urinary excretion (0-24 hour) of phase II metabolite-6 between phenobarbitone and non-phenobarbitone pretreated rats with *p*-Cl AAP (80 mg/kg, i.p.). (n = 5)

The relative amount of metabolite-6 in urine obtained from non-phenobarbitone pretreated rats was treated as 100 %, and the relative amount in phenobarbitone pretreated rats was 107.0 ± 36.9 %. No significant difference between two groups was found which suggests phenobarbitone had no effect on metabolite-6 of *p*-Cl AAP, as the enzymes involved were not induced by phenobarbitone.

Six metabolites of *p*-Cl AAP were excreted in rat urine, of which metabolites-2 and -3 were found to undergo both phase I and phase II metabolism. The remaining metabolites appeared to undergo phase II metabolism only. Both glucuronide and sulphate conjugates were formed for all except metabolite-6, which yielded the sulphate conjugate only. In the phenobarbitone pretreated rats, metabolites-1, -2, -4

and -5 showed a prominent increase in urinary excretion. From these metabolites, only metabolite-2 showed an increase in the amount of glucuronide and sulphate conjugates; the other metabolites exhibited an increased in the amount of either glucuronide conjugate or sulphate conjugate.

In the quantitation of some of the metabolites, a high standard deviation was observed. This might be due to a fluctuation in the physiological state of different rats, hence affecting the enzyme activities of those enzymes involved in metabolism of *p*-Cl AAP. As a result, the relative amount of the metabolites determined might vary. Furthermore, due to the unavailability of authentic standards, the assays used for the quantitation of the metabolites of *p*-Cl AAP could not be fully validated. However, this study has provided a preliminary quantitative assay for the metabolites and the determination of their relative amounts excreted from urine. This may also contribute to the observed higher standard deviations.

Chapter Four

Conclusion

In conclusion, the physicochemical properties of five structurally related aminoalkylpyridines (*p*-F, *p*-Cl, *p*-Br, *p*-CH_3, and *m*-CF_3 AAPs) have been investigated. These include partition coefficient (K^o_w), aqueous solubility at various temperatures, enthalpy of solution (ΔH^s), the melting point (T_m) and enthalpy and entropy of fusion (ΔH^f and ΔS^f). The K^o_w of the *p*-F, *p*-Cl, *p*-Br, and *p*-CH_3 AAPs were statistically indistinguishable within experimental errors while the K^o_w of *m*-CF_3 AAP was significantly lower than the other AAPs, which may be related to the increased ionization of the *m*-CF_3 substituted aniline leading to increased partition of the compound into the aqueous phase. The solubilities of AAPs in water increased with an increase in temperature and depended on the substituent on the benzene ring of AAPs (in the order: *p*-F > *p*-CH_3 > *p*-Cl > *p*-Br > *m*-CF_3). The thermogravimetric analysis and DSC revealed that AAPs do not contain any solvent of crystallization and are relatively thermostable.

A simple, sensitive and specific HPLC assay has been developed and validated for *p*-Cl AAP in rat blood and urine. The assay was reproducible with overall intra- and inter-day variations of less than 13 % and 18 %. The accuracy of the developed assay was acceptable with a range of about 83 to 98 % for blood and 86 to 99 % for urine samples. The extraction recovery of *p*-Cl AAP and limit of detection were 92 ± 3.0 % and 100 ng/ml, respectively (Lin. *et al.* 1998). This assay was used in the subsequent quantitation of *p*-Cl AAP in rat biofluids.

Preliminary pharmacokinetic studies were performed in the conscious rats after intravenous administration of *p*-Cl AAP. The half-life was 5.0 hours and the clearance was 1779.4 ml/hr. The volume of distribution was 12.71 L. The area under

curve (AUC) was 11.84 μg/ml·hr. The extensive extracellular distribution may be due to the high lipophilic property of this novel anticonvulsant.

Urinary metabolic studies were conducted in rats by administration of *p*-Cl AAP intraperitoneally and six novel metabolites were found. On-line HPLC analysis of the found metabolites enabled their tentative identification, and they were named as *N*-[4-(2-hydroxychlorophenyl)]-1-[4-(2,6-dihydroxypyridyl)]ethylamine (metabolite-1), *N*-[4-(chlorophenyl)]-1-hydroxy-1-[4-(pyridyl)]ethylamine (metabolite-2), 2-[4-(chlorophenyl)]amino-2-[4-(2,6-dihydroxypyridyl)]ethanoic acid (metabolite-3), *N*-[4-(chlorophenyl)]-1-[4-(pyridyl *N*-oxide)]ethylamine (metabolite-4), *N*-[4-(chlorophenyl)]-1-[4-(2-hydroxypyridyl)]ethylamine (metabolite-5) and 2-[4-(chlorophenyl)]amino-2-[(4-pyridyl)]ethanal (metabolite-6), respectively. All of them were shown to form glucuronide and sulphate conjugates except metabolite-6 which only formed sulphate conjugate. Metabolite-2 and -3 were excreted as both phase I and phase II forms, while the rests were as phase II metabolites. The metabolic pathway of the *p*-Cl AAP was proposed. Although β-amino alcohol was not directly found, amino aldehyde (metabolite-6) and amino acid (metabolite-3), the two metabolites using β-amino alcohol as a precursor during their formation, were identified. These metabolites might account for the anti-epileptic effect of the *p*-Cl AAP.

The urinary excretion of the intact *p*-Cl AAP collected in 0 - 24 hours was found to be 0.28 ± 0.07% and 0.18 ± 0.002% of the dosed amount in the phenobarbitone and non-phenobarbitone pretreated rats. Trace amounts of the parent drug found in urine may be due to extensive metabolism and / or retention of *p*-Cl AAP inside the body.

Since authentic standards for the metabolites were not available, only relative amounts of the metabolites could be determined. Comparison between the phenobarbitone and non-phenobarbitone pretreated rats showed that the overall amounts of metabolites were all increased by phenobarbitone pretreatment except for metabolite-3 and -6. Furthermore, a significant increase in the amount of glucuronide was only seen for metabolites-2, -4 and -5, while a marked increase in sulphate conjugation was only observed for metabolite-1, -2 and -4. This suggests that different enzymes are involved in the whole metabolic profile of *p*-Cl AAP, and phenobarbitone induces some of these enzymes.

The studies described in this thesis have helped to shed some light on the metabolic pathway of aminoalkylpyridines, which is crucial for understanding the mechanism of action and potential toxicity of this new class of anticonvulsant. This information may also aid in the rational design of more effective and safer anticonvulsants for the treatment of epilepsy, and provide a rational basis for using these drugs as probes for studying the basic mechanisms of epileptogenesis and epilepsy.

References

Alexander K.S., Laprade B., Mauger J.W., and Paruta A.N., (1978). *J. Pharm. Sci.*, **67**, 624.

Andreasen P.B., Froland A., Skovsted L., Anderson S. Aa., Hauge M., (1973). *Acta Medica Scandinavia.* **193**, 561-564.

Bartoszyk G.D., Meyerson N., Reimann W., Satzinger G., and von Hodenberg A., (1986). Gabapentin. In: Current Problems in Epilepsy: *New Anticonvulsant Drugs* (eds BS Meldrum and R.J., Porter), pp. 147-164. John Libbey, London.

Baumel I.P., Gallagher B.B., DiMicco J., and Goico H., (1973). *J. Pharmacol. Exp. Ther.* **186**, 305.

Beckett A.H., Shenoy E.V.B., (1973). *J. Pharm. Pharmacol.* **25**, 793-799.

Bock K.W., Frohling W., Remmer H., Rexer IS., (1973). *Biochim Biophys Acta.* **327**, 46-56.

Brennan R.W., Dehejia H., Kutt H., Verebeley K., McDowell F., (1970). *Neurology* **20**, 687-693.

Brodie B.B., Gilette J.R., La Du B.N., (1958). *Ann. Rev. Biochem.* **27**, 427-454.

Buchthal F., Svensmark O., Schiller P.J., (1960). *Neurology.* **2**, 624-630.

Butler W.H., (1989) *Epilepsia* **30 (suppl. 3)**, 43-45.

Butler W.H., Ford G.P., and Newserne J.W., (1987). *Toxicol. Pathol.* **15**, 143-148.

Chapman A., Keane P.E., Meldrum B.S., Simiand J., and Vernieres J.C., (1982). *Prog. Neurobiol.* **19**, 315-359.

Christiansen J., Dam M., (1973). *Acta Neurologica Scandinavia* **49**, 543-546.

Deshmukh T.R. and Kadaba P.K., (1992). *Pharmaceutic. Res.*, **9**, S-109.

Deshmukh T.R and Kadaba P.K., (1993). *Med. Chem. Res.*, **3**, 223-232.

Dollimore D., *"Thermoanalytical Instrumentation," in Analytical Instrumentation Handbook*, Ewing G.W., Marcel Dekker, New York, 1990, 905-960.

Dunham N.W. and Miya T.S. (1957). *J. Am. Pharm. Assoc., Sci. Ed.*, **46**, 208.

Ferrendelli J.A., Holland K.D., McKeon A.C., and Covey D.F., (1989). *Epilepsia* **30**, 617-622.

Fleck C., Kabath P., Linstedt A., Linstedt U., Scharke U., and Braunlich H., (1991) *Exp. Path.* **43 (1-2)**, 75-87.

Gerber N., Weller W.L., Lynn R., Ragno R.E., Sweetman B.J., Bush M.T., (1971). *J. Pharm. Exp. Therapeutics*. **178**, 567-569.

Gibson G. G. and Skett P. (1994) *Introduction to Drug Metabolism (2nd edition)*. Blackie Academic & Professional, UK.

Gilman J.T., (1995). *Ann. Pharmacother*. **29**, 144-151.

Glaser, G.H., (1972). *In "Antiepileptic Drugs"* (D. M. Woodbury, J.K., Penry, and R.P. Schmidt, eds.), pp. 219-226. Raven, New York.

Godine Y., Heiner L., Mark J., Mandel P., (1969). *J. Neurochem*. **16**, 869-873.

Graham D.G., (1989). *Br. J. Clin. Pharmacol*. **27 (suppl.)**, 43-45.

Grant D.J.W., Mehdizadeh M., Chow A.H.L., and Fairbrother J.E., (1984). *Int. J. Pharm.*, **18**, 25.

Grant D.J.W., and Higuchi T., (1990). *Solubility Behavior of Organic Compounds, Vol. 21, Techniques of Chemistry* (W. H. Saunders Jr., series ed.), John Wiley and Sons, New York.

Gumbleton M., Nicholls P.J., and Taylor G., (1990). *Pharm. Res*. **7 (1)**, 41-45.

Handley R., and Stewart A.S.R., (1952). *Lancet* **1**, 742.

Hansen J.M., Kristensen M., Skovsted L., Christensen L.K., (1966). *Lancet* **2**, 265-266.

Harms P.G., and Ojeda S.R., (1974). *J. Appl. Physiol*. **36**, 391-392.

Hauptmann A., (1912). *Luminal bei Epilepsie. Munch. Med. Wochenschr*. **59**, 1907-1909.

Hayashi, T. (1952). *Jap. J. Physiol.*, **3**, 46-64.

Herbert B., Carl D., and Dudley H.W., (1967). *Mass Spectrometry of Organic Compounds*, Holden-Day. Inc., San Francisco.

Johnston, G.A.R. (1973). *Biochem. Pharmacol.*, **22**, 137-40.

Julien, R.M., and Hollister, R.P. (1975). *Adv. Neurol*. **11**, 263-276.

Jung M.T., Lippert B., Metcalf B.W., Bohlen P., and Schechter P.J., (1977). *J. Neurochem.* **29**, 797-802.

Kadaba P.K., (1984a). Triazolines XIII. *J. Pharm. Sci.* **73**, 850-852.

Kadaba P.K., Stanovnik B. and Tisler M. (1984b). Δ2-1,2,3,-triazoline. *Adv. Heterocyc. Chem.* **37**, 217-349.

Kadaba P.K. (1988). *J. Med. Chem.*, **31**, 196.

Kadaba P.K. (1990). *Drugs of the Future.* **15**, 1013-1024.

Kadaba P.K., Steveson P.J., Nnane I.P. and Damani L.A. (1996). *Bioorg. Med. Chem.*, **4(2)**, 165-178.

Kaplan S.A., (1972). *Drug Metab. Rev.*, **1**, 15.

Leach M.J., Marden C.M., and Miller A.A., (1986). *Epilepsia*, **27 (5)**, 490-497.

Lewin R.H., and Bleck B., (1977) *Epilepsia.* **18**, 237-242.

Lilienblum W., Walli A.K., Bock K.W. (1982). *Biochem Pharmacol.* **31**, 907-913.

Lin G., Nnane I.P., Damani L.A., Tse K.K., Chow A.H.L., and Kadaba P.K. (1998) *J. Pharm. Bio. Ana.* (in press)

Lippert B., Metcalf B.W., Jung M.J., and Casara P., (1977). *Eur. J. Biochem.*, **74**, 441-445.

Locock C., (1857). Discussion of paper by E.H. Sieveking. Analysis of 52 cases observed by the author. *Lancet* **1**, 527.

Loscher W., (1981). *Biochem. Pharm.* **30**, 1364-1366.

Loscher W., and Schmidt D., (1988). *Epilepsy Res.* **2**, 145-181.

MacDonald R.L., McLean M.J., (1982). *Epilepsia* **23 (Supp 1)**, S7-18.

McLean M.J., MacDonald R.L., (1981). *Society for Neuroscience Abstracts* **7**, 629.

McLean M.J., MacDonald R.L., (1982). *Neurology* **32**, A223.

Meldrum B.S., (1984). *Epilepsia* **25 (supp 2)**, S140-149.

Merritt H.H., Putman T.J., (1938). *Arch. Neurol. Psychiatry* **39**, 1003-1015.

Miller A.A., Wheatley P., Sawyer D.A., Baxter M.G., and Roth B., (1986). *Epilepsia*, **27(5)**, 483-489.

Nicklasson M., Brodin A., and Sundelöf L., (1982). *Acta Pharm. Suec.*, **19**, 109.

Poole C.F., and Schuette S.A. (1984). *Contemporary Practice of Chromatography*, Elsevier, Amsterdam, 459.

Porter R.J., Cereghino J.J., Gladding G.D., Hessie B.J., Kupferberg H.J., Scoville B. and White B.G., (1984). *Cleve. Clin. Q.*, **51**, 293-305.

Smith R.N., Hansch C., Ames M.M., (1975). *J. Pharm. Sci.* **64**, 599-606.

Stevenson P.J., Hauksdottir R., Kadaba P.K., and Damani L.A. (1990). *J. Chromatogr.* **533**, 248-254.

Stevenson P.J., Hamelijnck M.A.F., Kadaba P.K., and Damani L.A. (1991). *J. Chromatogr.* **563**, 419-426.

Stevenson P.J., 1994, *PhD. Thesis*, University of London. (Supervisor Dr. L.A. Damani).

Stone, W.E. and Javid, M.J. (1983). *Brain Res.*, **264**, 165-7.

Storch R., and Braunlich H. (1975). *Acta Biol. Med. Germanica.* **34 (3)**, 519-521.

Storch R., and Braunlich H. (1976). *Acta Biol. Med. Germanica.* **35 (10)**, 1365-1371.

Storch R., and Braunlich H. (1977). *Acta Biol. Med. Germanica.* **36 (2)**, 237-244.

Swinyard E.A., Woodhead J.H., White H.S., and Frankln M.R., (1989). *In Antiepileptic Drugs* (3rd ed.) by Levy R., Mattson R., Meldrum B., Penry J.K., and Dreifuss F.E., Raven Press, New York.

Swinyard E.A., Sofia R.D., and Kupferberg H.J., (1986). *Epilepsia*, **27**, 27-34.

Watanable HK., Matsui M. (1984). *Biochem J.* **222**, 321-326.

Watkins JB., Klaassen CD. (1982). *Drug Metab Dispos.* **10**, 590-594.

Waxman D.J., and Azaroff L. (1992) *Biochem. J.*, **281**, 577-792.

Werle S.G., Schwarz M., Glatt H. (1993). *Carcinogenesis.* **14 (11)**, 2267-70.

William D.H., Fleming I. (1987). *Spectroscopic methods in organic chemistry* (4th ed.) McGRAW-HILL Book Company (UK) Limited, London.

Wolff L., (1912) *Justus Liebigs Ann. Chem.* **394** 23, 59, 68.

Yamaoka Y., Roberts R.D., and Stella Y.J., (1983). *J. Pharm. Sci.*, **72**, 400-405.

Zweig G., and Sherma J. (1972), *Handbook of Chromatography*, CRC Press, Cleveland, OH. II, 191-254.

Appendix

Published Paper

Ge Lin, Ivo P. Nnane, Lyaquatali A. Damani, Kai K. Tse, Albert H. L. Chow and Pankaja K. Kadaba. (1998). *J. Pharm. Bio. Ana.* (in press).